Early Stages of Ageing in Al-Mg-Si Alloys

Early Stages of Ageing in Al-Mg-Si Alloys

By
Hossein Seyedrezai, B.Sc.

A Thesis
Submitted to the School of Graduate Studies
in Partial Fulfilment of the Requirements
for the Degree
Master of Applied Science

McMaster University

MASTER OF APPLIED SCIENCE (2007) McMaster University
(Department of Materials Science and Engineering) Hamilton, Ontario

TITLE: Early Stages of Ageing in Al-Mg-Si Alloys

AUTHOR: Hossein Seyedrezai, B.Sc.

SUPERVISOR: Dr. Hatem S. Zurob

NUMBER OF PAGES: x, 131

To my Mother and Father

Abstract

Natural ageing is known to have a negative effect on the formability and bake-hardening response of Al-Mg-Si alloys. This is attributed to the formation of Mg and Si clusters during natural ageing. The clustering process was the subject of many studies in the literature, however, the formation mechanism and kinetics of it, continues to be poorly understood. The aim of this project is to shed some light on the cluster formation mechanism and measure clustering kinetics at low temperatures. A series of electrical resistivity measurements, positron annihilation lifetime spectroscopy and hardness tests were performed on samples aged over the temperature range of -20 to 50°C following solution treatment at temperatures of 525 and 560°C . A very good correlation between the results of various techniques was observed. In addition, three different stages in the clustering process were detected. Not surprisingly it was found that the excess quenched-in vacancies are the key players in the cluster formation process. In the first stage, annihilation of near-sink vacancies occurs while other vacancies start to bind with solute atoms and form clusters. In the second stage, clustering continues to take place but its rate slows down since the effective diffusion coefficient of vacancies decreases as they bind with more solute. Finally the clustering process enters the third stage with much slower kinetics. Interestingly, positron annihilation lifetime also reaches a constant value at the beginning of stage III which suggests the stabilization of vacancies. Two hypothesis were then developed to explain the existence of stage III: one based on the immobilization of vacancies due to the increased binding with solute atoms and another one which considers the overlapping of solute diffusion profiles around the clusters.

Finally it was shown that the resistivity change in stage II can be used to find the activation energy of clustering which is calculated to be approximately 46 kJ/mol. This is very close to the migration energy of vacancies and Mg atoms. Thus it was concluded that migration of these species is the major rate controlling parameter for the clustering process.

Acknowledgements

First, I would like to thank my supervisor Dr. Hatem Zurob for his kind and continued aid during my Master's program which made the writing of this thesis possible. Also the McMaster Center for Automotive Materials is appreciated for providing the funding of this project.

As well, I would like to thank my family for their endless encouragement and warm support which helped me pass through my studies like any other stage of my life.

I am very grateful to Dr. Peter Mascher from the Department of Engineering Physics at McMaster University for helpful discussions and providing access to the positron annihilation lab. Mr. Dmytro Grebennikov is also acknowledged with gratitude for performing the positron experiments.

Dr. Warren Poole from the Department of Materials Engineering at the University of British Columbia is gratefully appreciated for kindly granting access to his electrical resistivity facilities.

I would also like to thank Dr. Shahrzad Esmaeili from the University of Waterloo and Dr. David Lloyd from Novelis Inc. for their very useful suggestions and discussions.

Finally, I would like to thank all my colleagues in JHE-A203/C for their support and friendly conversations which provided me with the energy to finish the writing of this thesis.

Table of Contents

List of Figures

List of Tables

Chapter 1

Introduction

1.1 Aluminum in Automotive Industry

In the recent years, great emphasis has been placed on improving the fuel efficiency of automobiles. The motives behind this include the ever-increasing price of gas and environmental concerns due to the emission of gasses responsible for global warming. One of the possible alternatives in achieving this goal is to decrease the weight of the automobile without sacrificing safety and performance. This can be done by using lighter alloys with the same or nearly the same properties. In outer autobody panels, 6xxx series aluminum alloys (Al-Mg-Si) seem to be a very good fit because they provide a very good strength due to their significant precipitation hardening and at the same time they have very good formability which is required for forming processes. One of the drawbacks of these alloys is the detrimental effect of natural ageing on subsequent heat treatments. There are many more advantages and disadvantages in use of these alloys which are the subject of following two sections.

1.1.1 Why use Aluminum?

There are various advantages in the use of the 6xxx series aluminum alloys for auto body panels:

- Its density is almost three times smaller than that of steel
- With proper heat treatment a reasonable strength can be achieved which will

result in a very good strength/density ratio

- It can provide very good ductility and formability
- It has very good corrosion resistance
- It is recyclable

1.1.2 What are the problems?

Similar to any other material, 6xxx series aluminum alloys also have their own disadvantages which includes:

- They are more expensive than steels.
- Natural ageing can have a negative effect on their subsequent heat treatments.
- Joining Aluminum with other materials can be a challenging task especially due to the galvanic corrosion and poor weldability.
- Although aluminum is relatively easy to recycle, its separation from other materials in a recycling plant might not be easy and impurities (especially Fe which is the most frequently used material in automobiles) can deteriorate the mechanical properties of aluminum.

The effect of natural ageing on subsequent ageing can be very important since it can easily cause the strength/density ratio of aluminum (after artificial ageing) to reach to small values and consequently, question the whole purpose of using aluminum rather than steels in the auto body panels. In addition to this, natural ageing can decrease the formability of an alloy by an unwanted and insufficient increase in strength. This can result in difficulties during stamping and forming of the sheets. Therefore many studies were devoted to this particular issue which will be discussed

extensively in chapter 2. In this chapter the general problem of natural ageing effect will be defined and then the key elements in solving that issue will be mentioned.

1.2 Natural Ageing and Paint Bake Cycle problem

Auto body panels need to be painted after they are formed. After painting, they will undergo a process which is called Paint Bake Cycle (PBC) and it is done in order to bake the paint. It simply consists of heating the parts at temperatures around 175-180°C and for about 30 minutes. For Al-Mg-Si alloys this is an ideal temperature range for precipitates to form. However if alloy has gone through a period of natural ageing at room temperature prior to the PBC, the potential increase in strength can not be achieved. Numerous studies have been done in this field to find:

- The mechanism responsible for this phenomenon (starting with Pashley et al. in 1966 to recent year such as Edwards et al. 1998 or various research by Murayama et al. in 1998, 1999 and 2001)
- Techniques to prevent this problem (see Yamada et al. 2000 and Birol 2005b for example)

It is well accepted that formation of small clusters is responsible for the negative effect of natural ageing on the mechanical properties of alloy after PBC and some of the possible solutions for solving this problem includes artificial ageing (for example Yamada et al. (2000) and Bryant (1999)) or pre-straining of alloy before natural ageing (for example see Birol (2005b). Section 2.4 in chapter 2 is devoted to the review of previous research done in these areas. For now it can be said that there are still some questions about the effect of natural ageing on the PBC response of Al-Mg-Si alloys which remains unanswered including:

- Details of the clustering process such as its kinetics and activation energy.
- The exact mechanism which will result in the negative effect of clusters on the subsequent heat treatments after natural ageing (such as PBC).

This research focuses on answering the first question. In chapter 2, the previous studies done in this area will be reviewed. Then the objectives of this project will be expressed and clarified in chapter 3. In the chapter 4, the experimental techniques used for achieving the project's goal, and the logic behind them will be discussed. The results of experiments and their discussion will be given in chapters 5 and 6 respectively. Finally, conclusion will be made and recommendations for the possible future work will be provided in chapters 7 and 8.

Chapter 2

Literature Review

2.1 Introduction

In this chapter, the results of previous studies on the natural ageing of Al-Mg-Si alloys are reviewed. This starts with an overview on the ageing sequence of 6xxx alloys in section 2.2. This is then followed by the discussion of the effect of low and intermediate temperature ageing on these alloys properties in section 2.3. Finally, in section 2.4, the paint bake cycle and the parameters affecting it are discussed.

2.2 Ageing Sequence in 6xxx Aluminum Alloys

It is generally accepted that the ageing process in Al-Mg-Si alloys is as follows: (Miao and Laughlin 1999)

α (sst) $\rightarrow$ GP Zones (clusters) $\rightarrow \beta'' \rightarrow \beta' \rightarrow \beta$ (Mg_2Si)

Edwards et al. (1998) suggested that this can be expressed in more details as:

α (sst) $\rightarrow$ individual clusters of Mg and Si $\rightarrow$ Co-clusters of Mg and Si $\rightarrow$ GP-zones $\rightarrow \beta'' \rightarrow \beta' \rightarrow \beta$ (Mg_2Si)

By using the Differential Scanning Calorimetry (DSC), Miao and Laughlin

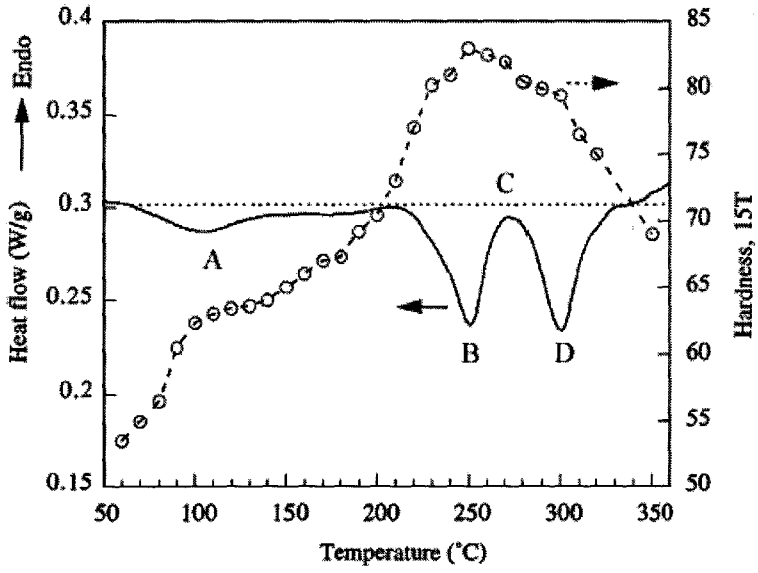

Figure 2.1: DSC and corresponding Hardness plots of an as-quenched AA6111 sample (Miao and Laughlin 2000a).

(2000a) showed that in the as-quenched sample at the very early stages of ageing, either GP-zones or clusters form. This can be proved by an increase in the hardness of sample and also by existence of an exothermic peak in the DSC graph. (Peak A in figure 2.1)

By continuing ageing, the next precipitates which will be formed would be β'' (peak B in figure 2.1) , β' (peak D in figure 2.1) and β (Mg_2Si) respectively.

The DSC curve shown in figure 2.1 is the most common one for 6xxx alloys however some researchers reported graphs which are slightly different from this. For example Dutta and Allen found an exothermic peak for β'' formation which was abnormally broad. They de-convoluted the peak into two separate peaks which after TEM analysis they were associated with GPI (GP-Zones) and GPII (β'') formations (Dutta and Allen 1991).

The maximum hardness in 6xxx alloys can be achieved by formation of β'' during short ageing times. Any further progress in precipitation, i.e. formation of

coarser β'' and later precipitates, will decrease the hardness.

Although this general ageing sequence is widely accepted, the details of the process (such as the effect of composition and ageing temperatire) are still not clearly understood. The effect of different ageing processes, such as natural and artificial ageing, will be discussed in section 2.3 while the effect of composition change is the subject of sections 2.2.5 and 2.2.6. The aim of this section is to provide extensive information about each of the precipitates which are formed during ageing of 6xxx series aluminum alloys.

2.2.1 GP Zones/Clusters

Clusters/GP-Zones are believed to form by ageing the Al-Mg-Si Alloy at low and intermediate temperatures. Figure 2.1 shows a DSC curve along with the corresponding hardness plot of an as-quenched Al-Mg-Si alloy. In this figure, an exothermic peak (denoted by A) at around 100°C is associated with formation of GP-Zones/Clusters (Miao and Laughlin 2000a). In the DSC curves which were obtained by Edwards et al. (1998), unlike the one shown in here, this peak is very broad and asymmetric. They suggested that this peak actually consists of two overlapping peaks of clusters and GP-zone formation.

The GP-Zones/Clusters are very small and for this reason they cannot be observed in the conventional TEM. Figure 2.2 shows the bright-field TEM image of a balanced Al-Mg-Si alloy which is naturally aged for 70 days. No evidence of any precipitates can be found in this picture (Murayama and Hono 1999).

Further research has been done on GP-zones/clusters. The conditions which each of these precipitates will form are different and will be discussed in section 2.3 extensively. In this section only the main characteristic properties of these are reviewed. As it was mentioned before no direct evidence of clusters/GP-zones can

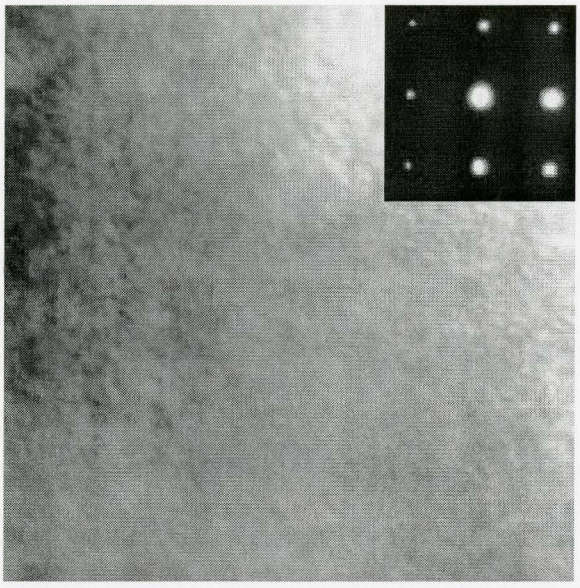

Figure 2.2: TEM bright field image and the corresponding [001] selected area diffraction patterns obtained from the Al-0.70Mg-0.33Si (balanced) alloy after natural ageing for 70 days (Murayama and Hono 1999).

be found using conventional TEM pictures in Al-Mg-Si alloys. This triggered further research on them by using the HRTEM in the recent years. Figure 2.3 shows the HRTEM image of a sample which was naturally aged for 70 days (figure 2.3.a) and a sample which was artificially aged at 70°C for 16 hours (figure 2.3.b). It is generally believed that the result of first treatment is formation of clusters while the second treatment will result in microstructure with GP-Zones (Murayama and Hono 1999). As it can be seen, clusters are still so small that they do not produce any contrast in HRTEM while the precipitates in Figure 2.3.b show small contrast. These precipitates are marked with arrows. It was shown in figure 2.2 that no contrast and streaks are observed in the conventional TEM image of this alloy and this means that these precipitates are fully coherent with the matrix. Thus, based on these observations and by using the DSC results (similar to figure 2.1) it can be concluded that the precipitates observed after 16 hours of ageing at 70°C are GP-zones (Dutta and Allen 1991 and Murayama and Hono 1999). It is important to mention that GP-zones in

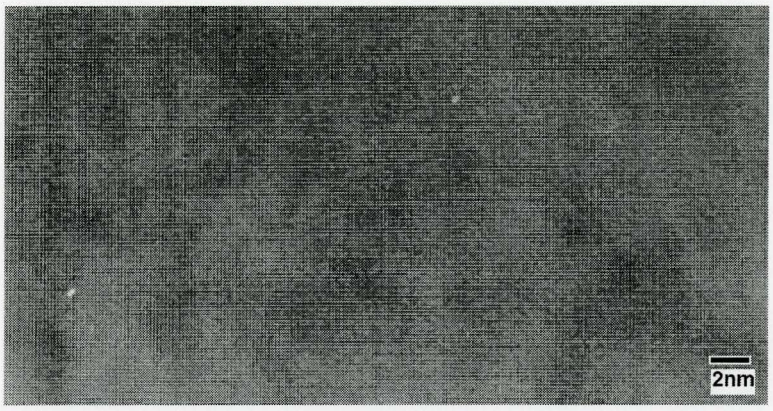

(a)

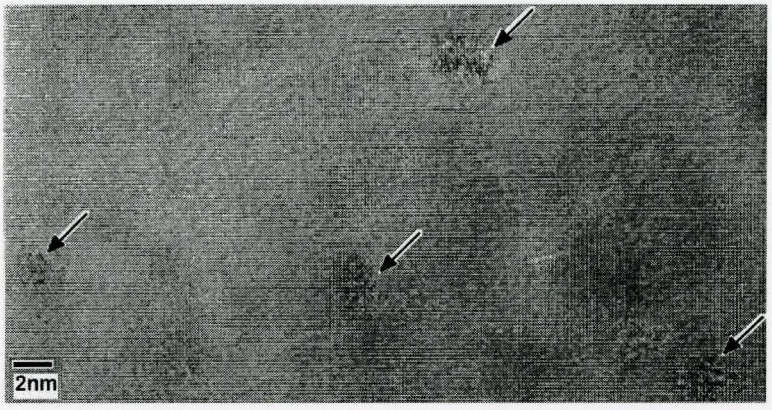

(b)

Figure 2.3: HRTEM images taken from the $[001]_{Al}$ zone axis of the Al-0.65Mg-0.70Si alloy after (a) Natural ageing for 70 days and (b) 70°C pre-ageing for 16 hours (Murayama and Hono 1999).

Al-Cu alloys have been found to produce streaks in the diffraction patterns (see Sato et al. 2003 or the review article by Polmear 2004), however in the case of Al-Mg-Si alloys clear streaking (along $[001]_{Al}$) was not generally observed by any researcher although some found signs of very diffuse and small streaks (for example see article by Sato et al. 2003). Edwards et al. (1998) suggested that this might be due to the fact that the atomic scattering factors of Al, Mg and Si are all very similar to each other.

Definition of clusters and GP-Zones in this project

In this project, clusters and GP-zones are treated differently, thus, in order to avoid any confusion, they will be defined in this section.

Clusters are zones in the matrix which simply have higher number of solute atoms (Mg and/or Si) compared to the random distribution of them in the matrix. They are very small and they do not produce any contrast even in HRTEM images. They do not have any distinct structure since they are not a phase.

GP-zones are similar to clusters, however, they have a structure although it is not resolved. They can be seen in the HRTEM images. Also some researchers (for example Sato et al. 2003) observed streaks in the SAD patterns due to their existence. Detailed information about GP-zones and clusters (including references) can be found in the paper by Esmaeili et al. (2003).

2.2.2 β'' Precipitates

β'' is the main strengthening phase in Al-Mg-Si alloys. It is formed by ageing at higher temperatures. The exothermic peak B at around 250°C in the DSC curve shown in figure 2.1 is associated with the formation of these precipitates (Miao and Laughlin 1999).

β'' is a needle-shaped precipitate which has a monoclinic structure and is oriented along $< 100 >$ of aluminum matrix (Andersen et al. 1998). The orientation relationship between these precipitates and the Aluminum matrix is believed to be $(001)_{Al}//(010)_{\beta''}$, $[311]_{Al}//[011]_{\beta''}$ (Edwards et al. 1998). In TEM pictures these needle shaped precipitates are identified by their circular end-on views and also the strain contrast around them when they are viewed face-on (Esmaeili et al. 2003). Figure 2.4 shows a TEM picture of β'' precipitates. This micrograph is taken from $[001]_{Al}$ zone axis. In the bright-field image (figure 2.4.a) the needles are shown as

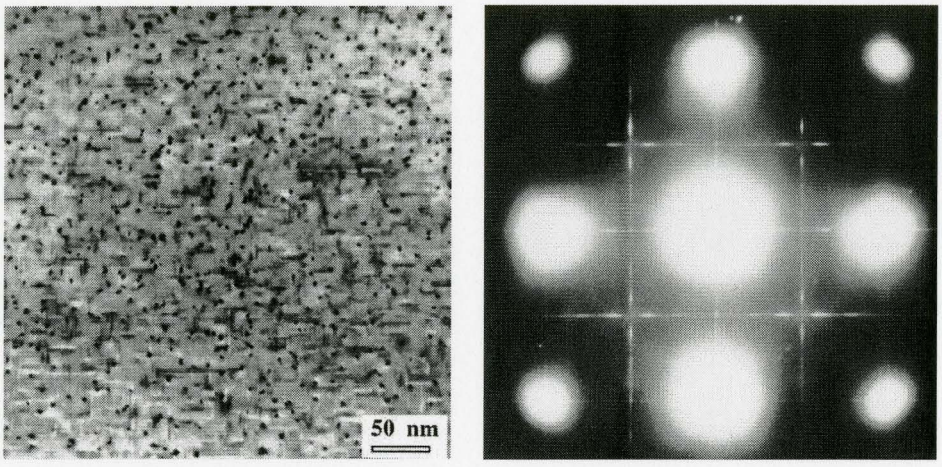

(a) (b)

Figure 2.4: Typical TEM micrograph of the β'' precipitates (a) bright field image (b) SAD pattern of the same area shown in a. Zone axis is $[001]_{Al}$ (Miao and Laughlin 2000b).

either lines (needle direction [100] or [010]) or circular dots (needle direction [001]). Also in the corresponding SAD pattern shown in figure 2.4.b, the streaks along [100] and [010] can be seen. This can prove that these precipitated are elongated along $< 100 >$ of aluminum matrix.

The exact composition of β'' precipitates is not clearly known. However various studies found the Mg:Si ratio. The EDS results of Maruyama et al. (1997) indicates Mg:Si ratios of 1.78 and 1.0 for Si-balanced and Si-excess alloy. Using Atom Probe technique, Edwards et al. (1998) found the ratio to be close to 1.2 for Si-excess alloy. All of these results were also confirmed by Murayama and Hono (1999) who found the Mg:Si ratio for balanced alloy and Si-excess alloy to be close to 2:1 and 1:1 respectively.

2.2.3 β' Precipitates

β' is the subsequent precipitate after β''. It offers less strengthening properties than β''. This can be clearly seen in hardness curve observed in figure 2.1.

These precipitates are in form of rods with circular cross section which are oriented along $< 100 >$ of aluminum matrix. Their crystallographic structure is believed to be hexagonal (Andersen et al. 1998). In the TEM bright-field image (figure 2.5) β' precipitates can be easily seen. They are reported to have a large length to diameter ratio and therefore they have a prominent shape effect which will result in clearly visible streaks along $< 001 >_{Al}$ in the SADP of the sample (figure 2.5). In addition to $< 001 >$ streaks, faint streaks through $< 002 >$ spots can also be seen. The intensity modulation of these streaks is very similar to that of hexagonal rod-shaped phases. These results along with the DSC results can confirm that the precipitates observed in figure 2.5 are indeed β' and they have a hexagonal structure (Dutta and Allen 1991).

By using x-ray microanalysis Lynch et al. (1982) found that for the Al-1.16wt.%Mg_2Si alloy, the mass ratio of Mg:Si is 1.73 which equals to atomic ratio of 1.99. However using EDS, Maruyama et al. (1997) found the Mg:Si ratio to be 1.75 and 1.21 for balanced and Si-excess alloys respectively. Note that some researchers (such as Edwards et al. 1998) argue that the presence of excess Si in the matrix will result in the formation of other precipitate designated as B' which is often mistaken with β' (Edwards et al. 1998). These precipitates have hexagonal structure with a = 0.104 nm, c = 0.405 nm and the Mg:Si ratio is found to be close to 1.15 using EDS, PEELS and APFIM (Edwards et al. 1996).

2.2.4 β Precipitates (Mg_2Si)

The β precipitates are the final stable precipitates in Al-Mg-Si alloys. They are formed during ageing at high temperature and for very long times, i.e. over-ageing. β precipitates are in the form of plates which are oriented along $< 100 >$ of aluminum matrix. They have the well known CaF_2 structure (Andersen et al. 1998)

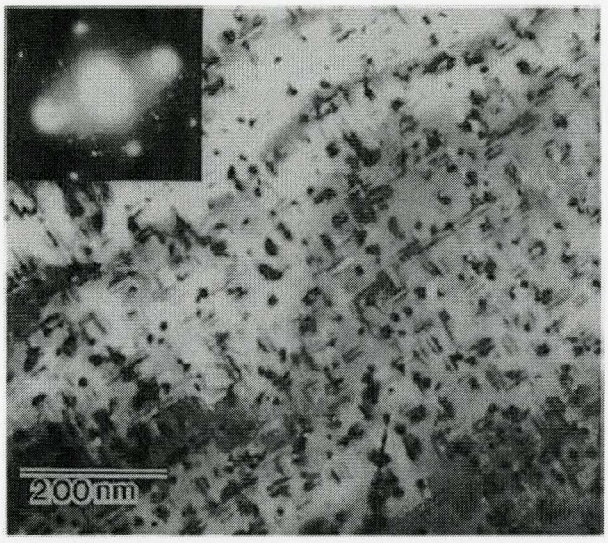

Figure 2.5: Bright-field TEM micrograph showing the rod-shaped β' precipitates and the corresponding SADP (Dutta and Allen 1991).

and according to Maruyama et al. (1997) their Mg:Si ratio is equal to 2.10 and 2.13 for balanced and Si-excess alloys respectively.

2.2.5 Effect of Cu Addition

Addition of Cu into Al-Mg-Si alloy can introduce new precipitates in the material. The precipitation sequence which could happen in these quaternary alloys can be summarized as (Miao and Laughlin 2000b):

Alloys with low Cu content: GP Zones (clusters) $\rightarrow \beta'' \rightarrow \beta' + Q' \rightarrow \beta$

Alloys with High Cu content: GP Zones (clusters) $\rightarrow \beta'' \rightarrow Q' \rightarrow$ Q

As it can been seen, by addition of copper, a different phase of Q and its precursor phase, Q', are appeared in the precipitation sequence. Q precipitates have Hexagonal structure with a=1.04nm and c=0.405nm (Miao and Laughlin 2000b). These precipitates are aligned along $< 100 >_{Al}$. Both Q and Q' are lath-shaped. They

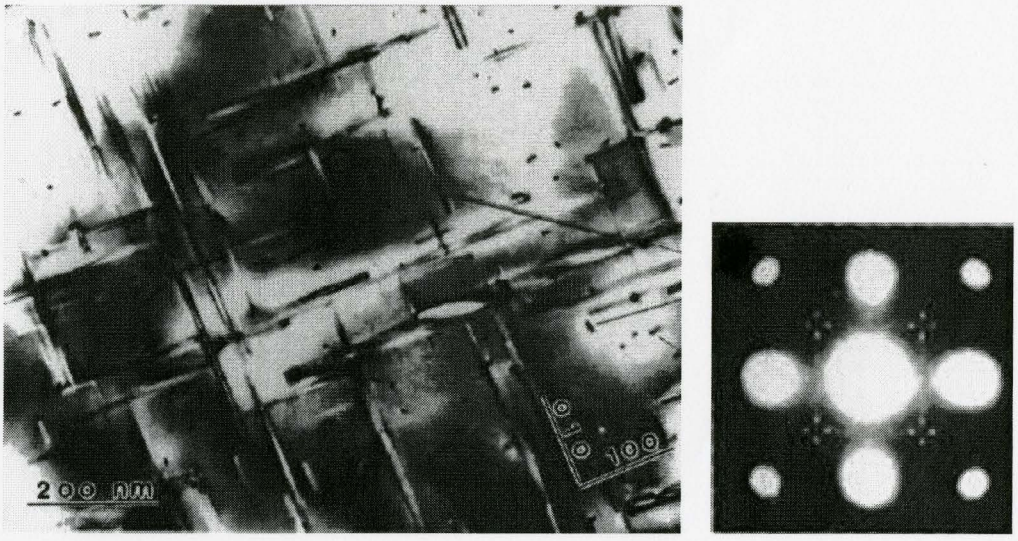

(a) (b)

Figure 2.6: (a) TEM Micrograph of the Q phase in Al-Mg-Si-Cu alloy and (b) the corresponding SADP (Chakrabarti and Laughlin 2004).

can be easily distinguished from needle/rod shaped β''/β' precipitates. Finally the orientation relationship with the matrix is: $[001]_{Al}//[0001]_{Q'}$ and $(020)_{Al}//(21\bar{3}0)_{Q'}$ (Chakrabarti and Laughlin 2004). Figure 2.6 shows a TEM micrograph of Q phase. Q' is found to have Mg:Al:Si:Cu of 6:4:6:1 (Matsuda et al. 2001) however the exact composition of Q phase is not clearly known. Some possible compositions include $Al_5Cu_2Mg_8Si_6$, $Al_4CuMg_5Si_4$, $Al_4Cu_2Mg_8Si_7$ and $Al_3Cu_2Mg_9Si_7$. (refer to article by Chakrabarti and Laughlin (2004) for complete details)

The sequence mentioned above is not always reported in the same way by other researchers. for example Esmaeili et al. (2003) found the coexistence of Q' and β'' precipitates in some of their samples. Honma et al. (2004) reported no sign of Q' precipitates after very long ageing times at 180°C , however, although significantly less in number density/volume fraction compared to β'' precipitates, Esmaeili et al. (2003) observed Q' in the same ageing temperature. This might be due to the extremely copper rich alloy used in the latter research. (0.70 wt.% for Esmaeili et al. compared

to 0.40wt.% of copper for Honma et al.)

Formation of Q' precipitate is always kinetically favorable over the competing phases however both Q and β precipitates are stable at temperatures below 300°C and therefore coexistence of Q' and β'' in low Cu content alloys is not very surprising (Miao and Laughlin 2000b).

Miao and Laughlin (2000b) found that the introduction of Cu in the alloy does not alter the characteristics of clusters/GP-Zones (at least in chemical way). This was proven by the 3D atom probe results which showed no correlation between Mg and Cu atoms while very strong correlation between Mg and Si was observed for the same alloy and with the same heat treatment (Murayama et al. 2001). Unlike the case of clusrers/GP-zones, Cu can alter β'' precipitates both chemically and structurally. It was shown by Miao and Laughlin (2000b) that for high copper content alloys, copper will be incorporated in the β'' precipitates and will also change the lattice parameters of mentioned precipitate.

It was shown by Esmaeili and Lloyd (2006) that addition of Cu to Al-Mg-Si alloys in moderate levels enhances the kinetics of precipitation only in the As-Quenched alloy, i.e. it does not affect the subsequent ageing of a pre-aged alloy. This is believed to be due to the enhancement in the nucleation process which was proven thermodynamically by the same authors (Esmaeili and Lloyd 2004) where it was shown that copper containing alloys have higher ΔG for nucleation of precipitates (or clusters) compared to non-copper containing alloy. The TEM results of Esmaeili and Lloyd (2006) also confirm this mechanism since the alloy with higher Cu content shows much denser and finer structure of β'' precipitates. The reason that Cu does not affect any subsequent ageing after pre-ageing is that in the pre-aged materials, unlike the as-quenched alloys, the process of precipitation during ageing happens by growth of already present precipitates rather that nucleation of new ones (Esmaeili

and Lloyd 2006).

Further discussion about this topic is not within the scope of this thesis and interested readers are refereed to the very good article by Chakrabarti and Laughlin (2004) for more details.

2.2.6 Effect of Excess Si

It is generally believed that excess Si in the composition of Al-Mg-Si alloys affects the formation kinetics, characteristics (e.g. composition) and thermodynamics (e.g. Driving force) of clusters and other precipitates, however, it does not change the nature and sequence of ageing in these alloys (Maruyama et al. 1997, Ceresara et al. 1970 and Maruyama et al. 1997). It was shown by Ceresara et al. (1970) that excess Si in the composition of Al-Mg-Si alloy enhances the kinetics of clustering and the density of zones. As it can be seen in figure 2.7, the alloy with excess Si in composition has much denser precipitate structure after ageing treatment compared to the balanced alloy. Si excess reduces the solubility of Mg_2Si and at the same time it increases the degree of matrix supersaturation. Ceresara et al. concluded that based on the basic concepts of precipitation, this will result in a higher density of zones which are also finer in size when the excess Si increases. They proved this for the case of artificial ageing at 175°C where higher concentration of excess Si resulted in much finer and denser structure of β'' precipitates (Ceresara et al. 1970).

Murayama and Hono (1999) showed that the atomic ratios of Mg to Si in co-clusters, GP-zones and β'' precipitates in an excess Si alloy (Al-0.65Mg-0.7Si wt. %) were always close to 1:1. However in the balanced alloy this ratio was closer to 2:1. This theory becomes more legitimate by considering the fact that in the short and intermediate ageing times, no evidence of individual Si precipitates is found. Consequently when the alloy has larger concentration of Si, the Mg:Si ratio should

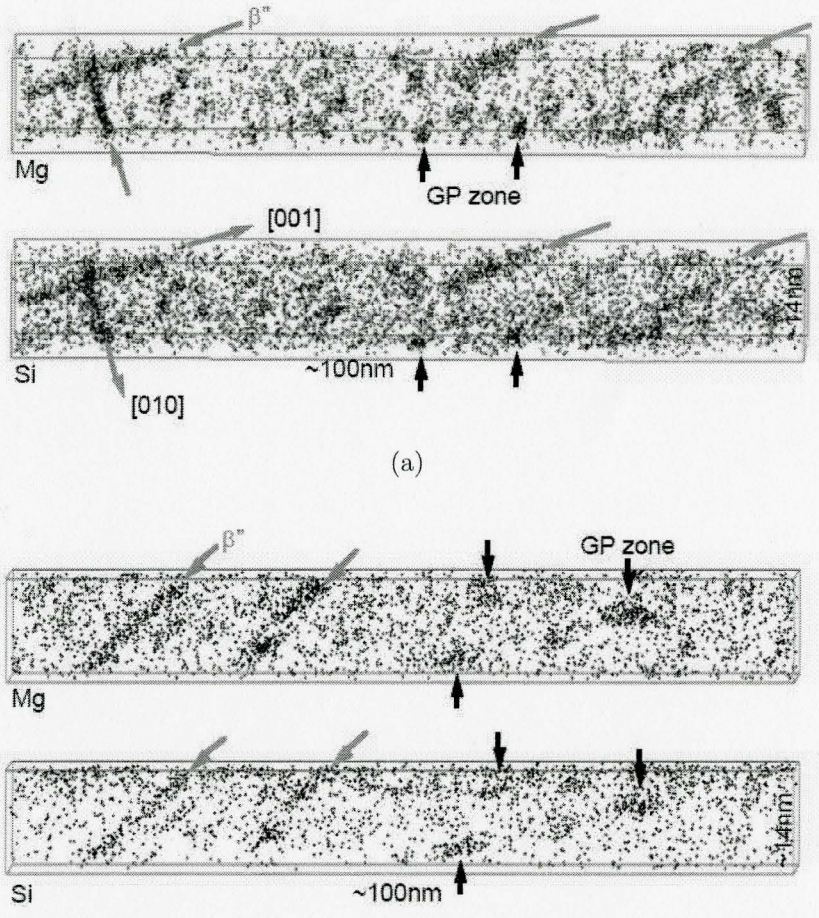

Figure 2.7: 3DAP elemental mapping of (a) Al-0.65Mg-0.70Si (Si-excess) alloy and (b) Al-0.70Mg-0.33Si (balanced) alloy which were aged at 175°C for 10 hours immediately after pre-ageing at 70°C for 16 hours (Murayama and Hono 1999).

become smaller than that of the balanced Si alloy (Maruyama et al. 1997). However, since the stable final precipitate in these alloys is Mg_2Si, it makes sense that as precipitation process progresses, the Mg to Si ratio in the excess-Si alloy gets closer to the equilibrium value of 2:1. This means that by the end of the ageing process, a Si-Rich precipitate should form. Indeed, Edwards et al. (1998) reported the formation of other Si-rich precipitate (B′) in addition to β'. Also Matsuda et al. (1994) found evidence of the Si-rich precipitates presence in the over-aged conditions.

Note that the direct relationship between Si concentration and the Mg:Si ratio in precipitates/zones, demonstrates another fact about the role of Si in the precipitation process, which is: densities of clusters, GP-zones and β'' precipitates are all determined by available number of Si atoms rather than Mg atoms (Murayama and Hono 1999). Thus the higher number density of these precipitates/zones in excess Si alloy is explainable.

2.3 Ageing of Al-Mg-Si Alloys

Ageing can have different effects on the properties of 6xxx aluminum alloys. This depends on type of ageing, i.e. natural ageing, artificial ageing or combination of these two. In this research natural ageing is defined as ageing at temperatures below 50°C, e.g. room temperature ageing while artificial ageing is any ageing which occurs as temperatures above 50°C.

The effect of natural ageing (or ageing at low temperature) on Al-Mg-Si alloys has been a subject of controversies due to its very complex effect on the microstructure of these materials. In this section, some of the previous studies on natural and artificial ageing of 6xxx alloys are reviewed.

2.3.1 As-Quenched Properties

Using the atom probe technique, the concentration depth profile of samples can be identified. An example of such study on as-quenched Al-Mg-Si alloy is shown in figure 2.8.a. What these diagrams show is the number of detected solute atoms vs. total number of detected atoms. Consequently the slope of these diagrams is equal to the concentration of each solute atom (Murayama et al. 1998). The Mg diagram clearly shows sudden jumps in the concentration of Mg which corresponds

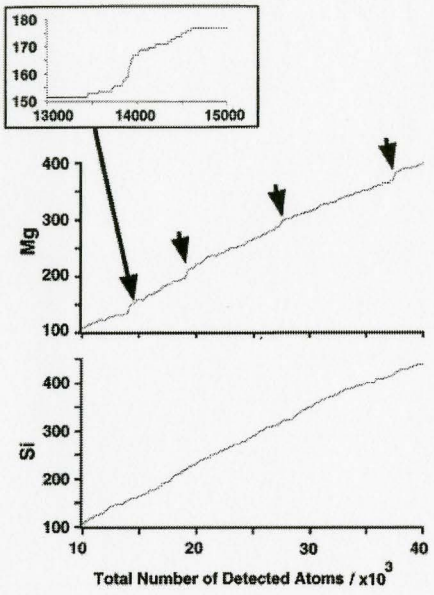

(a)

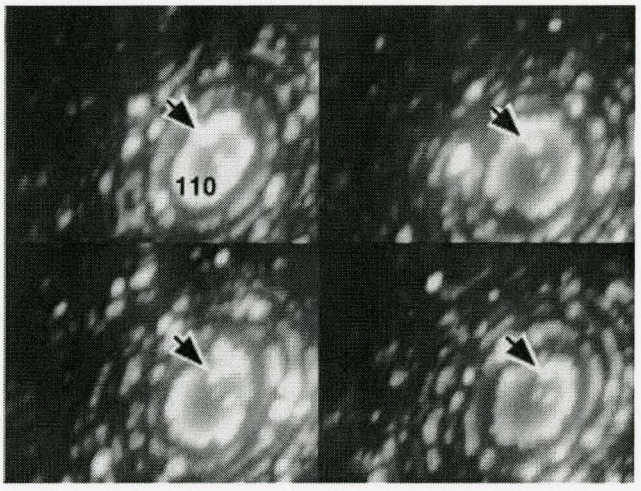

(b)

Figure 2.8: (a) Integrated concentration depth profile of the As-Quenched Al-0.65Mg-0.76Si alloy. Notice the jumps in the Mg concentration plot. (b) Layer by layer FIM images of $(011)_{Al}$ planes of Al-0.65Mg-0.76Si alloy. Bright spots correspond to Si atoms (Murayama et al. 1998).

to existence of Mg clusters. The same result can not be concluded from the Si diagram, however Field Ion Microscopy (FIM) images of $(001)_{Al}$ planes of the same sample shows signs of Si clustering (figure 2.8.b). These images where taken from a sequence of $(011)_{Al}$ layers of the same sample used in figure 2.8.a. In these pictures, bright spots correspond to Si atoms. As it can be seen the three spots marked by black arrows exist in all of these consecutive layers. Therefore it can be concluded that Si clustering also happens in the as-quenched state of the sample (Murayama et al. 1998).

2.3.2 Natural (Low Temperature) Ageing

Figure 2.9 shows the DSC curves for AA6111 alloy with various ageing conditions. From this figure it is obvious that in all samples which have gone through a

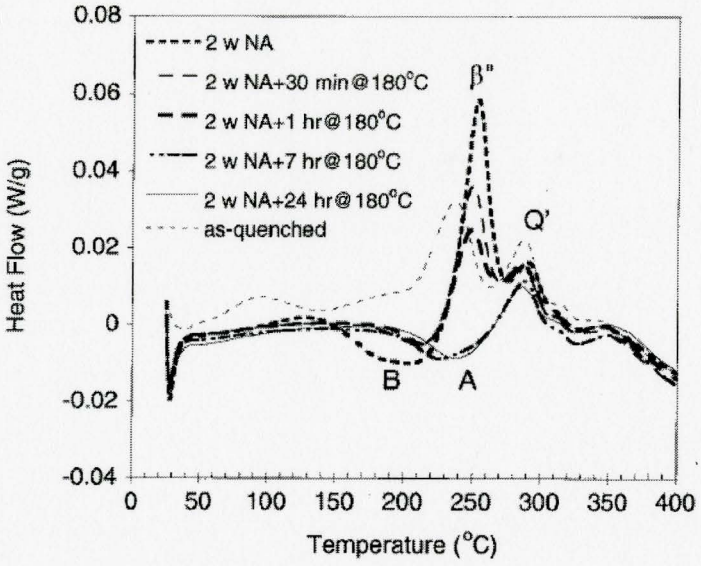

Figure 2.9: DSC curves of solution treated, 2-weeks naturally aged and two-steps aged (NA+ageing at 180°C for different times) samples (Esmaeili et al. 2003).

period of natural ageing, no trace of clusters and/or GP-zones formation peaks can be found while a broad exothermic peak associated with cluster formation exists in the case of solution treated sample. Also in this figure and in the case of naturally aged material, the broad endothermic peak (B) can be seen which is attributed to clusters dissolution (Esmaeili et al. 2003). In agreement with most other recent studies, this suggests that during natural ageing, small clusters have been formed.

If the samples are aged at room temperature and for a long time, using integrated depth profile technique (discussed before in section 2.3.1), it can be shown that in addition to the individual clusters of Mg and Si atoms, co-clusters of them can also be found (Murayama et al. 1998). The integrated concentration depth profile of Al-0.65Mg-0.76Si after natural ageing has been shown in figure 2.10. Similar to figure 2.8.a, arrows show clusters of individual atoms. In addition to individual clusters of Mg and Si however, in this figure, co clusters of these atoms can also be found (shaded area). The co-clusters are formed due to the high tendency of Si and Mg atoms to

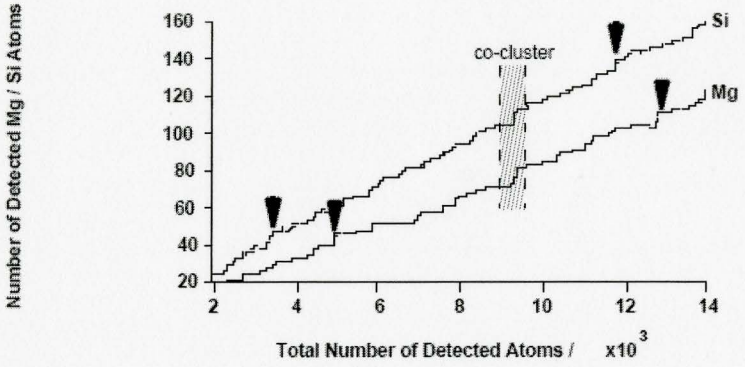

Figure 2.10: Integrated concentration depth profile of Al-0.65Mg-0.76Si alloy Naturally aged for 70 days (Adopted from Murayama and Hono 1999).

aggregate. This can be proved by using contingency tables technique (Murayama et al. 1998). Note that the same research showed no evidence of co-clusters in the as-quenched state of alloy.

The findings of Murayama et al. have been confirmed by other researchers. For example, Edwards et al. (1998) showed in their atom probe results that there are three types of clusters present in the early stages of ageing: cluster of individual Mg atoms, clusters of individual Si atoms and co-clusters of both Mg and Si atoms. Their research also indicated that these clusters are not forming simultaneously. At very beginning of the process, individual clusters are formed. This will be followed by formation of co-clusters at the longer ageing times. This clearly rejects the mechanism suggested by various researchers (such as Dutta and Allen 1991) that during natural ageing only individual clusters of Si are formed.

In their paper, Doan et al. suggested the formation of vacancy clusters prior to solute clusters (Doan et al. 2000). This is based on the DSC results that they obtained from an as-quenched Al-0.58Si-0.98Mg-0.33Cu (wt.%) alloy which also included impurities of iron and chromium. They observed three exothermic peaks prior the endothermic clusters dissolution peak. These peaks are centered at 373, 415 and

465°C. They calculated the activation energy for the first peak to be 79kJ/mole. This is significantly smaller than the diffusion activation energy of Mg and Si however it is close to the activation energy of vacancies migration. Therefore they concluded that this peak corresponds to formation of vacancy cluster. The other two exothermic peaks were claimed to be due to "formation of Silicon and/or Magnesium clusters or some other unknown phase" (Doan et al. 2000). The latter conclusion might be true based on the findings of Edwards et al. (1998) however the former claim needs to be considered with extra care since no other evidence of such finding has been reported in literature for Al-Mg-Si alloys, although this was mentioned for the case of Al-Si alloys (Ozawa and Kimura 1971) and pure Aluminum (Panseri et al. 1963). The very high binding energy between Mg and vacancies, results in the formation of Mg clusters during quenching (see previous section and discussion about Al-Mg binary alloys in following paragraphs) and since the number of these atoms in the matrix is larger than that of vacancies, as a hypothesis, existence of Mg in matrix might stop vacancy clusters from forming. This needs more detailed study to be clearly understood.

To investigate the process of clustering further, it is required to review the cluster formation in binary Al-Mg and Al-Si alloys. This will be done in the following paragraphs:

The case of binary Al-Mg alloys has been well studied in the literature. Figure 2.11 shows the resistivity results obtained from isochronal annealing of different Al-Mg alloys (Panseri et al. 1963). In this experiment, samples are kept at each temperature for 2 minutes and then the temperature is increased. As it can be seen, for the case of pure aluminum, only decrease in resistivity (in 2 steps) is observed. This is attributed to elimination of the non-equilibrium quenched-in vacancies. In the first step (which is slightly below room temperature), vacancies are condensed into the planar dislocation loops available in the matrix (Panseri et al. 1963). This is verified

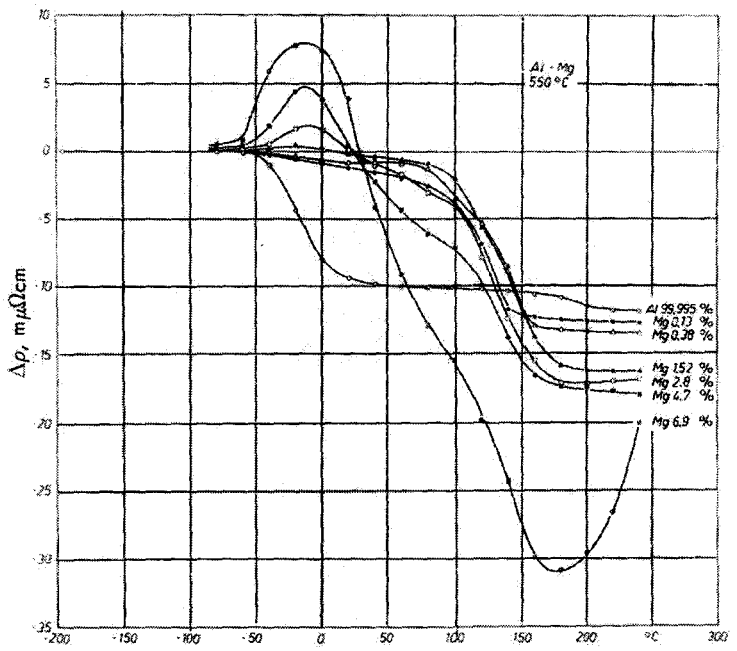

Figure 2.11: The electrical resistivity evolution during isochronal annealing of different Al-Mg alloys (Panseri et al. 1963).

by various researchers TEM results (Hirsch et al. 1958 and Kuhlmann-Wilsdorf and Wilsdorf 1960). The second step (which happens at temperature above 150°C) is believed to be due to the elimination of vacancies by the mechanism of dislocation loops climb (Federighi 1959 and Silcox and Whelan 1960).

The effect of small magnesium additions (less than 1.5wt.%) to the matrix can be observed clearly in figure 2.11. The initial decrease (due to formation of vacancy loops), observed in case of pure Al, is disappeared here. In addition to that, the second decrease in resistivity is now happening at temperatures above 130°C and it is different from that of pure aluminum. These observations suggest that a strong binding energy exists between magnesium atoms and vacancies which will lead to the retainment of the quenched-in vacancies in the matrix in temperature of up to about 100°C (Panseri et al. 1963). The nature of this strong interaction between vacancies and Mg atoms can be attributed to the fact that existence of vacancies around Mg

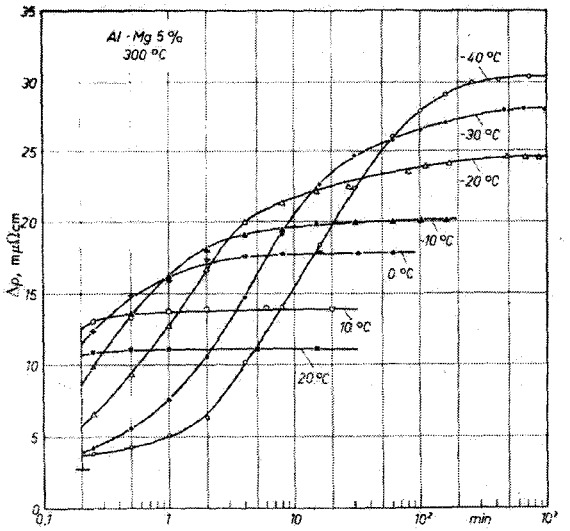

Figure 2.12: The Electrical resistivity evolution of Al-5wt.%Mg alloy during isothermal ageing at various temperatures (Panseri et al. 1963).

atoms (which are larger than Al atoms) can reduce the surrounding strain energy significantly. These Mg-vacancy pairs can move inside the matrix at low temperatures (Panseri et al. 1963).

In the case of concentrated Al-Mg alloys (with Mg>1.5 wt.%) an increase in resistivity is observed at relatively low temperatures where the decrease was detected in the case of pure Aluminum. This is attributed to the clustering of Mg atoms which also happens very fast. This could be due to the strong interaction between vacancies and Mg atoms which results in the entrapment of all vacancies (or more correctly Mg-vacancy pairs) after few jumps. This is confirmed by the results of isothermal resistivity measurements shown in figure 2.12 where the resistivity values reach the saturation level after a relatively short time. Further clustering is only possible by evaporation of vacancies from zones and into the matrix, which is an extremely slow process. (Panseri et al. 1963)

Finally before proceeding to binary Al-Si alloys it is worth mentioning that the process of cluster reversion in Al-Mg alloys starts happening as temperature is

increased (see figure 2.11) which results in a decrease in the resistivity. This continues until finally at temperatures above 100°C a sharp decrease (similar to that of pure Al) happens in the resistivity. Note that at intermediate temperatures (below 100°C) although vacancies evaporate from zones into the matrix (due to clusters reversion), since the strong interaction between Mg and vacancies still exists, the final elimination of extra quenched-in vacancies can happens only at temperatures above 100°C. It should be mentioned that the very sharp fall in the resistivity of Al-6.9wt.%Mg is attributed to the precipitation of Mg (Panseri et al. 1963) and should not be confused with the clusters behavior.

The other possible important conclusion from figure 2.11 is that the movement of Mg atoms in Al-Mg alloys happens by means of vacancies since the increase in resistivity (due to clustering) occurs at the same temperature range that the decrease in resistivity (due to vacancies migration and elimination) was observed in the pure Aluminum (Panseri et al. 1963).

Now the clustering in Al-Si binary alloys will be examined. The DSC results from Al-Si alloys shows no exothermic peak at the early stages of precipitation (Gupta and Lloyd 1992). This could mean that the Si-clusters might have been formed either during or immediately after quenching (Edwards et al. 1998). The high resolution TEM micrographs taken form as-quenched solution treated Al-1.2wt%Si alloy seems to be in agreement with this (Nakagawa et al. 2005). As it can be seen in figure 2.13.a, in the low magnification picture, a dislocation loop along with microscopic patches can be observed. The high resolution micrograph of the same area which is shown in figure 2.13.b reveals that in all patches, a small area of dark contrast parallel to $\{111\}_{matrix}$ and of size of less than 5nm exists. Since the size of these small patches increases with time and also no GP-Zone streaks were observed in the SADP patterns, Nakagawa et al. (2005) then concluded that these patches are the clusters of Si. As it

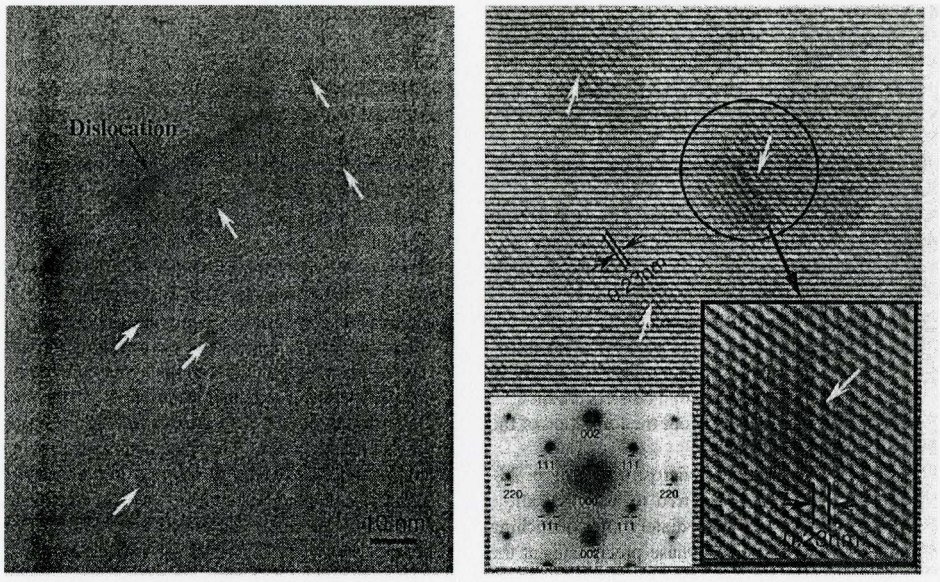

(a) (b)

Figure 2.13: TEM micrographs of Al-1.2wt.%Si sample quenched form 853K to 273K. (a) Low resolution. Notice the dark patches marked with white arrows along with the dislocation line. (b) High resolution picture of the same spot shown in a. The dark contrast might be related to the existence of Si cluster (Nakagawa et al. 2005).

was mentioned earlier, the DSC curve for this alloy doesn't show any exothermic peak related to clustering of Si atoms (Gupta and Lloyd 1992). Based on the results of Hornbogen et al. (1992), Starink and Zahra (1997) and Van Rooyen and Mittemeijer (1989), Zhen and Kang concluded that the non-appearance of Si clusters formation peak in the DSC curves of Al-Si alloys is not because of the rapid formation of these clusters but it is due to the low heat effect of Si clustering (Zhen and Kang 1998). Their main alibi for this claim was the obvious increase in hardness of these alloys during natural ageing in the research results of Hornbogen et al. (1992). To support this theory further, the following discussion seems necessary.

The relation between solute atom flux (J_i) and the gradient of vacancy concentration (∇C_V) is given by: (Howard and Lidiard, 1965)

$$J_i = \frac{Na_0^2 C_{vi} \nabla C_V (w_1 + 7k_1/2) + C_{it}(-w_1 + 13k_1/2)}{3(w_1 + w_2 + 7k_1/2)(C_{it} - C_{vi})^2} \tag{2.1}$$

where N is the number of lattice sites per unit volume, a_o is the lattice constant, C_{vi} is the concentration of solute-vacancy pairs, C_{it} is the atomic concentration of solute atoms, w_1 is the frequency for a vacancy to rotate around the paired solute atom, w_2 is the frequency of vacancy and solute atom exchange and k_1 is the frequency for a vacancy-solute atom to break. Generally C_{vi} is much smaller than C_{it} in aluminum alloys. Therefore, if w_1 is less than $13k_1/2$ (weak binding), solute atoms flow in the opposite direction of the vacancy flux. In the opposite case where w_1 is greater than $13k_1/2$ (tight binding), the solute atoms flow is in direction of vacancy flux (Ozawa and Kimura 1971). Ozawa and Kimura did the calculations for Al-Si alloys and they found that in these alloys, w_1 is greater than $13k_1/2$. This lead to a conclusion that silicon atoms flow in the same direction with vacancies. They then both condense on the dislocation loops (which are already present in the sample after quenching). The process of vacancy clustering happens very fast, e.g. just after 15 sec (at 273K) from quenching.[1] These clusters are very stable due to adsorption of Si atoms to vacancies since this reduces the mobility of vacancies (Ozawa and Kimura 1971). Using electrical resistivity measurements, El Sayed and Kovacs (1974) proved in their research that after the stage of vacancy-Si binding, only pairs are moving within the matrix. Clusters of Si atoms will continue their growth in the next stages of ageing (which includes disappearance of dislocation loops).

The mechanism of Al-Si precipitation is studied extensively by various researchers and since detailed knowledge of this procedure is not within the scope of this project, enthusiastic readers are referred to the related publications (Ozawa and

[1] Although this time is very short, it is still enough for silicon atoms to cluster on dislocation loops. In pure aluminum, dislocation loop growth and shrinkage happens much faster because vacancies are not bonded to Si atoms and consequently they are not slowed down (Ozawa and Kimura 1971).

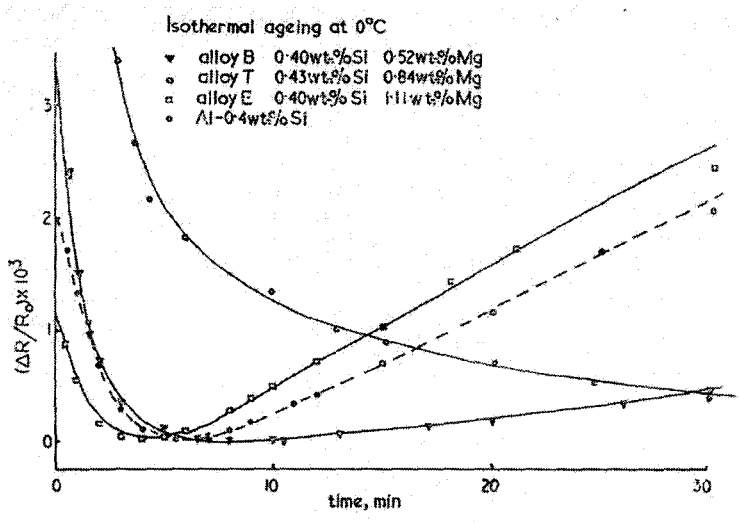

Figure 2.14: Effect of Mg concentration on the resistivity of Al-Mg-Si alloys during ageing at 0°C (Chatterjee and Entwistle 1973).

Kimura 1971, and El Sayed and Kovacs 1974).

Now the process of clustering in ternary Al-Mg-Si alloys can be better understood. Figure 2.14 shows the results of electrical resistivity measurements on four different alloys during isothermal ageing at 0°C. It seems that the resistivity curve consists of two components. The shorter component (which appears in case of both ternary and binary Al-Si alloys) is believed to be due to the clustering of Si atoms since it exists for sample with and without Mg. The reason for the fall is the vacancy aggregation and also migration of Si atoms from matrix (Chatterjee and Entwistle 1973). As it was discussed previously, this clustering happens heterogeneously on vacancy clusters (Ozawa and Kimura 1970). The second component of resistivity is the increasing part which since it is only present in Mg containing alloys, it is believed to be due to clustering of Mg atoms. This theory is strengthened by the fact that alloys with higher concentration of Mg have larger resistivity increase (Chatterjee and Entwistle 1973).

Panseri and Federighi (1966) showed that the electrical resistivity of samples

during ageing increases in two steps: a "fast" stage and a "slow" one. This can be explained based on the model proposed by Federighi and Thomas (1962). This model suggests that the interaction between vacancies and clusters depend on the binding energy between these two. Using this, Panseri and Federighi (1966) suggested that the change of resistivity increase rate is because of the vacancies entrapment in the clusters after they have brought solute atoms to clusters. This is due to the very high interaction between vacancies and clusters. Finally after a very short period of time, the rate of resistivity increase drops rapidly, i.e. the "slow" stage starts, because all vacancies are trapped thus they are virtually eliminated from the matrix. After this point the reaction rate will be controlled by the low concentration of free vacancies still present in the matrix (Panseri and Federighi 1966).

Dutta and Allen (1991) and Yamada et al. (2000) proposed that during natural ageing only clusters of Si form. As it was mentioned earlier, the DSC curves for Al-Si alloys does not show any exothermic peak for Si cluster formation (Gupta and Lloyd 1992). In contrast in DSC analysis of Al-Mg-Si alloys, Miao and Laughlin (2000a) observed a distinct exothermic peak which they related it to the cluster formation (see figure 2.1). So this clearly shows that in addition to Si clustering, another phenomenon is also happening. Edwards et al. (1998) suggested that based on the Al-Si, Al-Mg and Al-Mg-Si alloys ageing results plus the atom probe data, first individual clusters of Mg and Si atoms form. This is then followed by formation of co-clusters (see figure 2.15). They believe that formation of co-cluster is possible only by dissolution of Mg clusters and then movement of these atoms toward Si atoms.

Perhaps one of the most comprehensive studies which have been done on clustering so far is the one performed by Kovacs et al. (1972). In this research, they performed a series of iso-thermal ageing treatments in the temperature range of -40 to 200°C. They measured the electrical resistivity evolution during these ageing

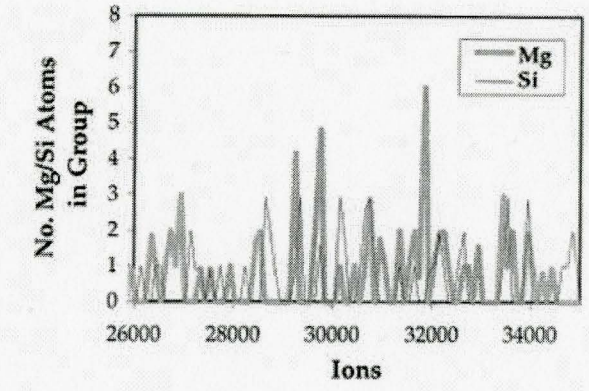

(a)

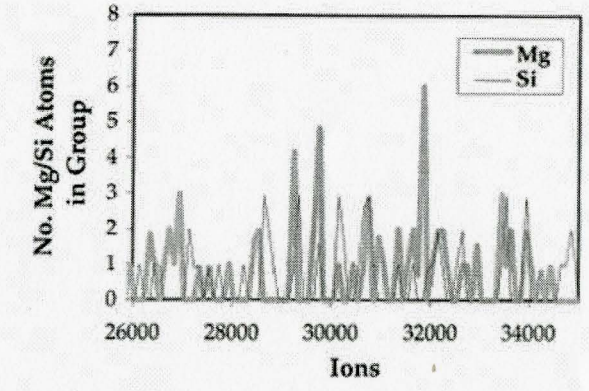

(b)

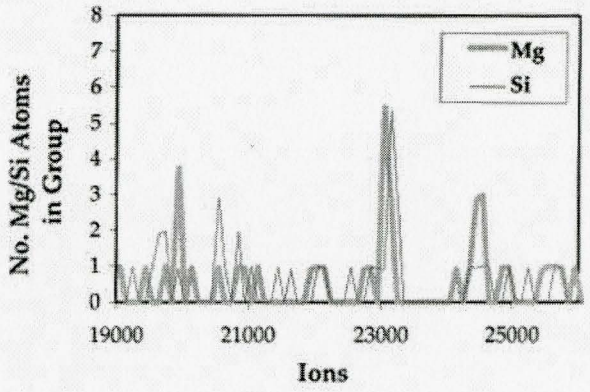

(c)

Figure 2.15: Section of APFIM concentration profile of an AA6061 specimen which has been heated to the temperature right before the first exothermic peak observed in DSC curves (associated with the cluster formation). Evidences of Mg, Si clusters and co-clusters of them can be observed in (a), (b) and (c) respectively (Edwards et al. 1998).

processes. The results which are shown in figure 2.16 are very interesting: Different stages of clustering can be observed. The number of stages, however, depends on the ageing temperature. At very low temperatures (below -20°C), only a decrease in the electrical resistivity was observed. This is then followed by a constat resistivity value. At temperature between -20 to 15°C an increase in resistivity after the initial drop can be found. At temperatures higher than 15°C and lower than 120°C, the initial drop was not observed any more and only increase in resistivity was seen. Above 120°C the resistivity decrease is observed after a period of increase. Kovacs et al. suggested that similar to Al-Si alloys, the initial drop in the resistivity (which happens only at very low temperatures) is due to the formation of Si clusters. Note that the resistivity of material is a multi-factor parameter which depends on the formation of clusters, changes in the concentration of solute atoms and the behavior of vacancies during ageing. The second stage (the increase in resistivity), they suggested that, is due to precipitation of Mg and Si atoms on the Si clusters formed during the first stage. The possible mechanism for third stage (saturation of resistivity) could be due to the decrease in concentration of Mg to a certain critical value. Finally for the final drop in resistivity they suggested that if the temperature is high enough, then the nuclei of Mg_2Si (or more correctly β'') starts to form which will result in the decrease of resistivity (Kovacs et al. 1972).

Studies of Gaber et al. (2004) showed that the kinetics of Mg and Si co-clustering during the natural ageing is controlled by "migration of silicon atoms and coalescence with Mg atoms". This conclusion was made based on the calculated activation energy for clustering of Mg and Si atoms which was equal to 53.5 kJ/mol. The diffusion energy of Si in Al is equals to 124 kJ/mol and the vacancy formation energy is equals to 71.3 kJ/mol so the migration energy of Si atoms in Aluminum can be calculated as 52.7 kJ/mol which is very close to the value of clustering activation

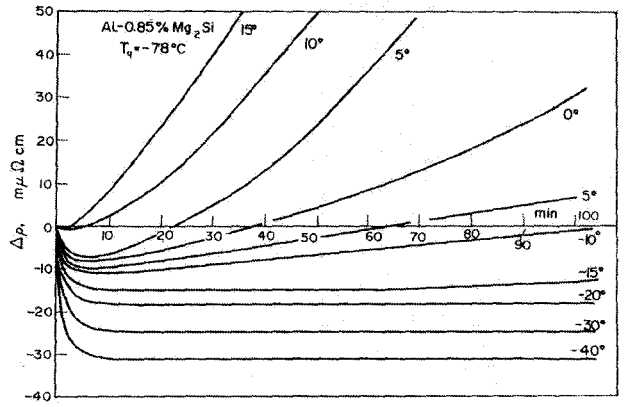

(a)

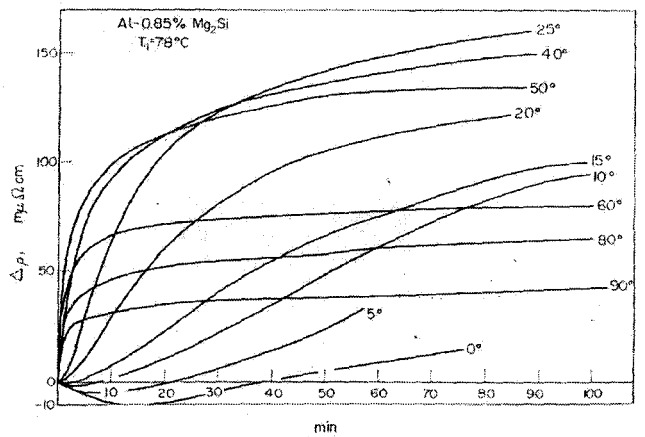

(b)

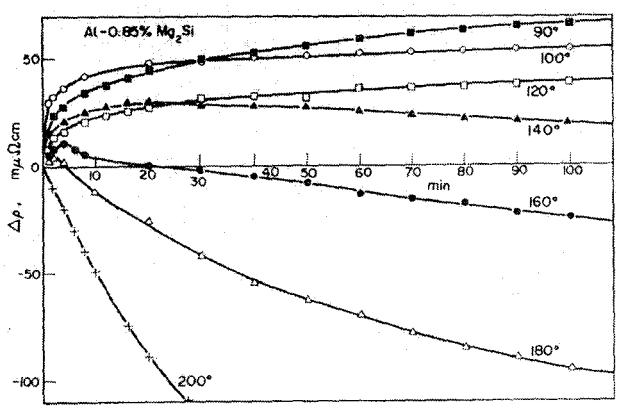

(c)

Figure 2.16: Electrical resistivity evolution of an Al-0.85% Mg_2Si alloy during ageing at various temperatures. (a) and (b) Samples are quenched to -78°C and (c) samples are quenched to the RT. (Kovacs et al. 1972)

energy. However this might not be necessarily true since this energy is also very close to the 58.4kJ/mol of the vacancies migration energy (see table A.3).

It was shown by Esmaeili et al. that the first 24 hours period of natural ageing has the highest effect on Al-Mg-Si alloys. In other words natural ageing beyond a day has a very little effect on solute concentration and also on the changes in free energy associated with solute supper saturation. (Esmaeili et al. 2005)

2.3.3 Artificial Ageing

Artificial ageing in this thesis is defined as ageing at temperatures above 50°C and usually below 120°C. This type of ageing is believed to form different types of precipitates/zone in terms of stability at higher temperatures.

The resistivity evolution versus time for various artificial ageing temperatures is shown in figure 2.17. As it can be seen for low temperature ageing (i.e. 20 and 60°C) the resistivity increases with time. However for higher ageing temperatures, resistivity first increases and then starts to decrease as ageing proceeds. Note that the amount of resistivity increase is temperature dependent, meaning that the lower the ageing temperature, the higher the increase will be (Esmaeili et al. 2000).

Yamada et al. showed that if the ageing of Al-Mg-Si alloy is carried out at temperatures above 50°C, a different type of zones will form. They define them as "Mg/Si/Vacancy clusters" (Yamada et al. 2000). However as it was mentioned earlier in this thesis (and in agreement with most other literature), these zones are defined as GP-zones. Yamada et al. proved that these GP-zones (which will also form during two-step quenching from solution treatment temperature) are different from those formed during ageing at lower temperatures since the exothermic peak produced by them in the DSC analysis is at different temperatures. In the case of GP zones the peak is between 348 and 423K while this is around room temperature for the case

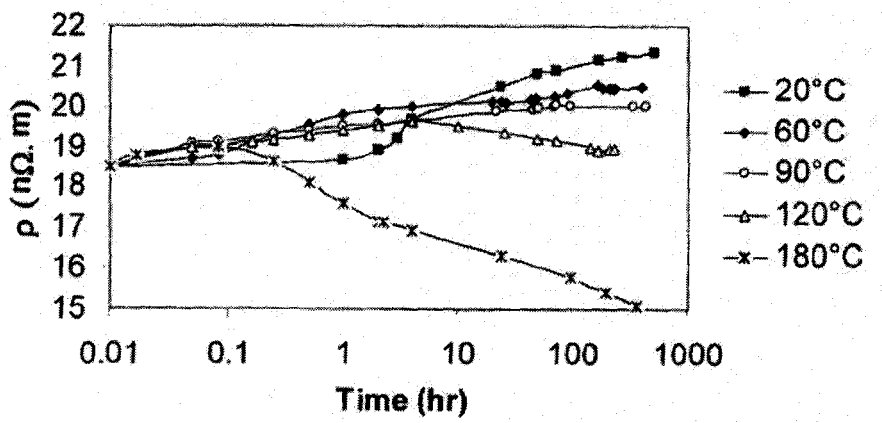

Figure 2.17: Resistivity evolution with ageing time for water quenched AA6111 samples during ageing at various temperatures (Esmaeili et al. 2000).

natural ageing clusters (Yamada et al. 2000). This theory was also supported by Dutta and Allen (1991). In addition to this Dutta and Allen (1991) also suggested the competitive nature between formation of these two zones, i.e. formation of one zone (e.g. clusters) suppresses the formation of the other zone (e.g. GP-zones). The results of Zhen and Kang (1997) also confirms that pre-ageing at higher temperatures, effectively suppresses the clustering process at lower temperatures.

The main feature of GP-zones is that they will act as the nucleation site for β'' in further steps of ageing at higher temperature, e.g. Paint Bake Cycle (Yamada et al. 2000). This will be discussed in more details in section 2.4.3.

Before proceeding to the next section, it would be useful to mention the effect of quenching rate on the ageing behavior. As it can be seen in figure 2.18, slower quenching rates, e.g. oil quenching (OQ) rather than water quenching (WQ), will result in lower value of electrical resistivity but the general ageing behavior remains almost unchanged. There are two possible reasons for this phenomenon; first, slower

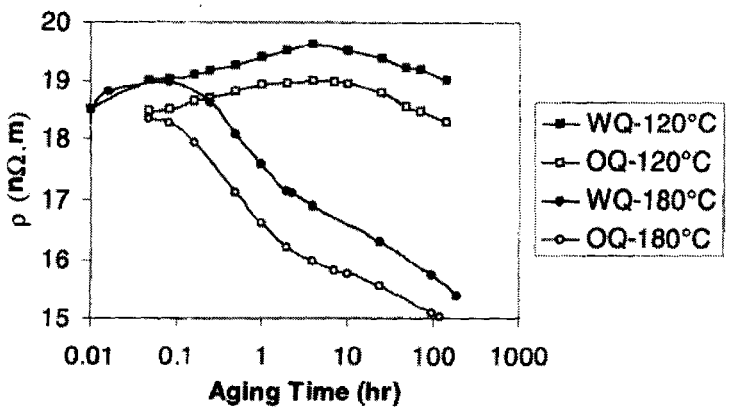

Figure 2.18: Effect of the quenching rate on the ageing behavior of an AA6111 alloy (Esmaeili et al. 2000).

quenching rate results in the greater vacancy loss during quenching and second, grain boundary precipitation happens during oil quenching which will deplete the matrix from solute atoms. Both of these result in lower resistivity level for the OQ samples (Esmaeili et al. 2000).

2.4 Paint Bake Cycle (PBC)

Paint bake cycle is a process in which the aluminum sheets are heated at 170-180°C for 20-30 minutes. There are different reasons for such a process which includes: providing paint curing and in the case of aluminum alloys, precipitation hardening of material (Esmaeili et al. 2003).

Typically during ageing of Al-Mg-Si alloy without any prior ageing history other than the solution treatment process, two different precipitates are formed (during ageing at times which are not very long). These precipitates are GP-zones and β''. If there is an addition of Cu in matrix, as it was discussed in section 2.2.5, Q' precipitates might also form (Esmaeili et al. 2003). Figure 2.19 shows evolution of these precipitates during ageing of the Al-Mg-Si-Cu alloy (AA6111) without any prior

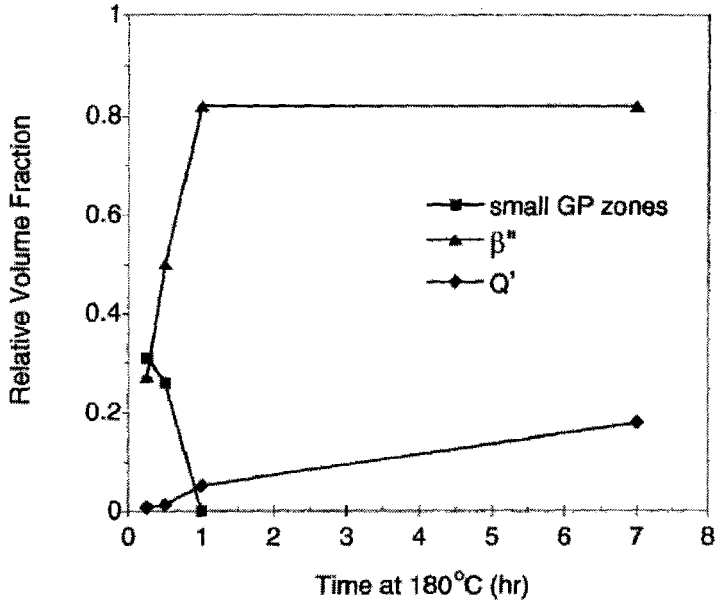

Figure 2.19: Evolution of different precipitates during 180°C ageing of an Al-0.79Mg-0.60Si-0.70Cu alloy without a prior ageing history . (Esmaeili et al. 2003)

ageing history, at 180°C.

2.4.1 Paint Bake Response (PBR)

The Paint Bake Response (PBR) can be defined as the increase in yield strength of Al-Mg-Si alloy after the paint bake cycle (Bryant 1999).

Different pre-ageing treatments have different effects on PBR. It is well accepted in literature that natural ageing has an adverse effect on PBR by decreasing the maximum achievable strength of aluminum sheet after short ageing times during paint bake cycle. As it can be seen in Figure 2.20, although the initial hardness of naturally aged sample (dotted line) is higher than that of the as-quenched sample (solid line), the hardness of naturally aged material is always (expect at very long ageing times) lower than that of as-quenched material.

It is generally believed that artificial ageing has a beneficial effect on PBR

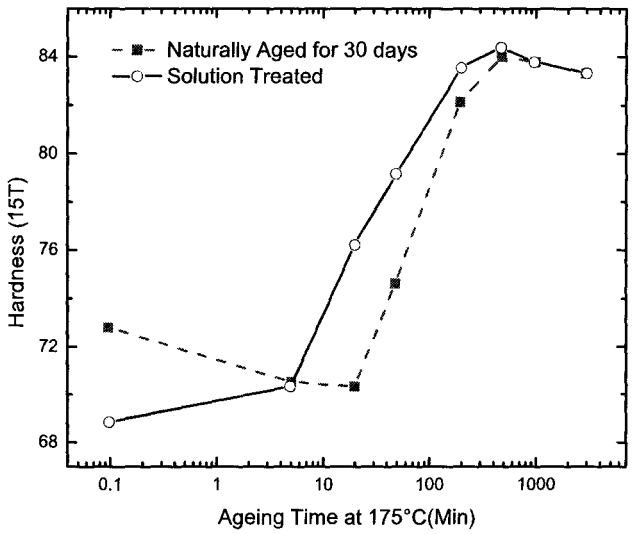

Figure 2.20: Hardness evolution during ageing at 175°C in sample (a) Without natural ageing history (b) with 30 days of natural ageing (Adopted from Miao and Laughlin 1999).

(Birol 2005a). This means that if the 6xxx aluminum sheet undergoes an artificial ageing treatment prior to the natural ageing and bake hardening, the adverse effect of natural ageing can be minimized.

The effect of different pre-ageing treatments on PBR and the mechanisms which they can modify the PBR are the subject of discussion in the following two sections.

2.4.2 Effect of Natural Ageing on PBR

It was mentioned in section 2.4.1, that natural ageing is generally believed to have a negative effect on the PBR. Figure 2.21 shows the evolution of yield stress during ageing of the 6111 aluminum alloy at 180°C. As it can be seen in this figure, after 1 hour of ageing (which is even more than conventional PBC times), the increase in strength of a naturally aged material is only 30% of the potential increase for T4

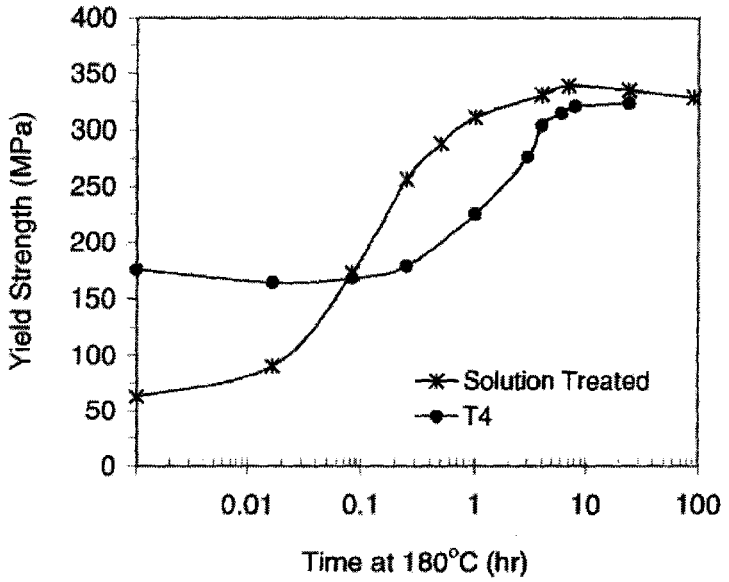

Figure 2.21: Evolution of yield strength during ageing at 180°C (typical PBR temperature) for solution treated sample and T4, 1-year naturally aged sample (Esmaeili et al. 2003).

material at 180°C ageing temperature. Also this increase is much lower than that of a solution treated sample without prior ageing history (Esmaeili et al. 2003). The same research shows that the total number density and volume density of precipitates after a period of natural ageing which is followed by PBC (with different times) are considerably lower than the case of the sample which PBC is done right after solution treatment (Esmaeili et al. 2003).

It was discussed extensively in section 2.3.2 that natural ageing of Al-Mg-Si alloys results in formation of very small Mg and Si clusters after very short ageing times (less than 24 hours). So the difference in microstructure of naturally aged sample and solution treated one should play an important role in the adverse PBR of naturally aged material. The presence of naturally aged clusters changes the subsequent precipitation processes and their kinetics in different ways (especially for the case β''): first, as clustering proceeds the degree of supersaturation of solute atoms in the matrix is decreased and this will result in smaller driving force for nucleation of

further precipitates. It is evident from the DSC curves shown in Figure 2.9, the yield strength drop shown in Figure 2.21 and the hardness drop in figure 2.20 that these clusters must first dissolve in the matrix at the beginning of PBC. This is possibly because of their size which is smaller than the critical size (r_c) above which they are stable due to the capillary effects (Murayama and Hono 1999). It was shown by Esmaeili et al. (2003) that the cluster dissolution process is a very slow one. Consequently the number density of precipitates will become significantly lower than the solution treated samples.

The dissolution of clusters also leads to a decrease in the number of quenched-in vacancies to the equilibrium value at the PBC temperature. According to findings of Panseri et al. (1963) (shown in figure 2.11) vacancies annihilate at temperatures above 100°C regardless of their binding properties with solute atoms. Consequently the kinetics of precipitation at higher temperatures will slow down (Murayama and Hono 1999). The Esmaeili mechanism seems to be in agreement with many other researchers results (for example Zhen and Kang 1997). This slow process can also contribute to the slow nucleation rate of β'' (or Q') precipitates thus the second effect of natural ageing clusters on PBR is based on the concepts of nucleation and growth. It was shown in the same research by Esmaeili et al. (2003) that the number density of precipitates in the naturally aged material is considerably smaller than that of the solution treated sample. This will result in growth of smaller number of precipitates (Esmaeili et al. 2003) with the slower kinetics (due to the lower concentration of vacancies) and therefore inferior paint bake response of the naturally aged material compared to the solution treated one.

2.4.3 Effect of Artificial (pre-)ageing on PBR

It is well accepted that pre-ageing prior to the paint bake cycle improves the PBR (just to name a few: Yamada et al. 2000, Zhen and Kang 1997, Murayama and Hono 1999). The mechanisms which have been suggested for the positive effect of pre-ageing are however very different from author to author and sometimes they contradict each other. In this section the most important ones will be discussed.

Various researchers suggested that there is a temperature range in which the artificial ageing prior the PBC is effective in suppressing the negative effect of natural ageing on PBR. This is because the "thermal stability of coherent precipitates depends on their size due to the capillary effect" and therefore GP zones formed at higher temperatures are more stable than the clusters that are formed at lower temperatures (Murayama and Hono 1999). Yamada et al. (2000) estimated the temperature range at which the clusters/GP-Zones formed during pre-ageing are stable at higher temperatures to be between 50°C and 150°C.

Zhen and Kang (1997) proposed that pre-ageing at high temperatures significantly suppresses the formation of clusters during the natural ageing period after pre-ageing and prior to PBC. According to Dutta and Allen (1991) this might be due to the competitive nature of clusters and GP-zones formation.

Using DSC, TEM and atom probe techniques Bryant suggested that after artificial ageing of Al-Mg-Si alloy, GP-zones are formed (Bryant 1999). This result is also confirmed by other researchers (for example Murayama and Hono 1999). This is explainable by the concepts of vacancies and solute atoms supersaturation. At high temperatures of solution treatment the concentration of vacancies is much higher than low temperatures. Therefore upon quenching, there is not enough time for them to return to equilibrium values and these extra vacancies will be retained in the matrix (Silcox and Whelan 1960). Now if the material is placed at suitable temperature, it

is possible that due to the high binding energies between solute atoms and vacancies, small clusters form. If the temperature is high enough (above a critical value) these clusters become stable in size. The model proposed by Bryant (1999) argues that pre-ageing at temperature above this critical temperature biases the formation of zones which he called them "disordered clusters". Other researchers however called these zones GP-zones and in this thesis as well, the same designation is used. Birol and Karlik (2005) proposed that by formation of the stable GP-zones during artificial ageing, if the sample is naturally aged at low temperature prior to the PBC, cluster formation will be suppressed. This is due to the consumption of Mg and Si atoms during the formation of GP-zones and consequently lower driving force available for further clustering at low temperatures. The next step which is the microstructure evolution during PBC after artificial ageing and its mechanism however, is somewhat controversial among researchers:

Bryant (1999) suggested that during the artificial ageing at higher temperatures (e.g. PBC), GP-zones undergo a partial dissolution. This results in a high concentration of solute atoms in the matrix and also transient flux of vacancies which were trapped inside clusters. However as it was mentioned earlier this is not the same accepted mechanism among other researchers. For example Murayama and Hono (1999) suggested that at the PBC temperature, only clusters smaller than critical size r_c (or simply the ones that are formed at lower temperature) are dissolved in the matrix and the more stable clusters (i.e. GP-Zones) can either transform directly to β'' or act as a nuclei for them. This theory seems more acceptable since many DSC results showed no sign of an endothermic peak for GP-zones dissolution (for example Miao and Laughlin 2000a). Note that based on the DSC results and TEM micrographs, Bryant (1999) suggested that after the partial dissolution of GP-zones, an intermediate meta-stable phase which does not have characteristics of either GP-

zones or β'' will form. The formation of an intermediate meta-stable phase was also mentioned by Miao and Laughlin (2000b) and Chakrabarti et al. (1998) although they did not observe any evidence showing the dissolution of GP-zones prior to its formation.

Before proceeding to the next section it is worth mentioning that sequential quenching can also have the same effect on the PBR as artificial ageing (Yamada et al. 2000). This is due to the loss of the excess vacancies during slower quenching and consequently delayed formation of clusters during natural ageing (Yamada et al. 2000).

2.4.4 Effect of Pre-straining on PBR

One of the techniques which is found to minimize the effect of natural ageing on PBC is pre-straining. Figure 2.22 shows the change in hardness of samples with various amounts of pre-straining and a week of natural ageing prior and after PBC. As it can be seen, pre-straining results in appreciable improvement of PBR. Birol (2005b) showed that by pre-straining the Al-Mg-Si alloy prior to natural ageing, the clustering can be greatly suppressed (although it is not entirely stopped). This can be explained by the concepts of dislocations and excess quenched-in vacancies. When the material is deformed, high number of dislocations are introduced in the alloy. They can then act as annihilation sites for excess vacancies. So before a remarkable progress can be made in formation of clusters, most of the vacancies disappear from the matrix and therefore cluster formation during natural ageing is suppressed (Birol 2005b).

The DSC curves for AA6016 alloys with various pre-straining amounts prior to a week of natural ageing are shown in figure 2.23. As it can be seen, the exothermic peak for natural ageing clusters formation is not present in any of these curves,

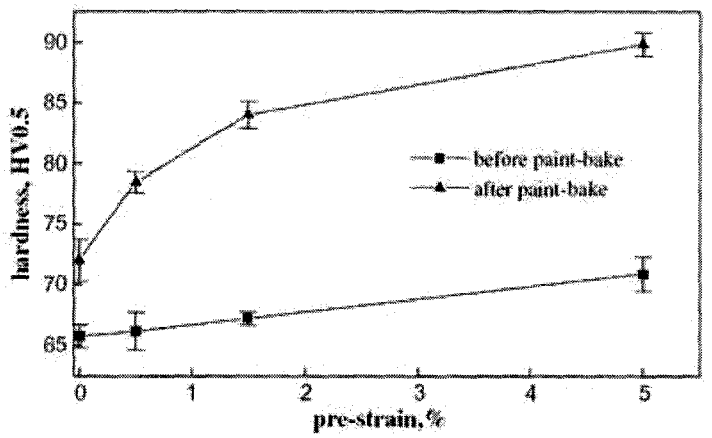

Figure 2.22: Change in hardness of one-week naturally aged AA6016 with various amounts of pre-straining prior to and after the PBC (Birol 2005b).

however, the endothermic dissolution peak is shifted to lower temperatures and also the peak height is decreased when the values of pre-straining is increased. Also notice the small broad exothermic peak in pre-strained specimens before the β'' peak. From this figure it can be concluded that: (a) clustering happens even in pre-strained specimen however in a very limited amount. (b) From the smaller endothermic peak of cluster dissolution plus the smaller β'' peak which is also at lower temperature it can be concluded that clustering is very limited in the material with larger pre-strain. (c) The small broad exothermic observed at around 150°C peak could be attributed to the formation of GP zones. Considering points (a), (b) and (c), Birol (2005b) suggested that not only pre-straining dislocations can suppress clustering but it can also provide heterogenous nucleation sites for GP-zones which can then grow and convert to β'' directly without dissolution.

Although pre-straining could be beneficial to PBR of Al-Mg-Si alloys, however it can increase the strength of alloy prior to the PBC too and therefore can cause problems in forming (e.g. stamping) of the material due to its lower formability (Birol 2005b).

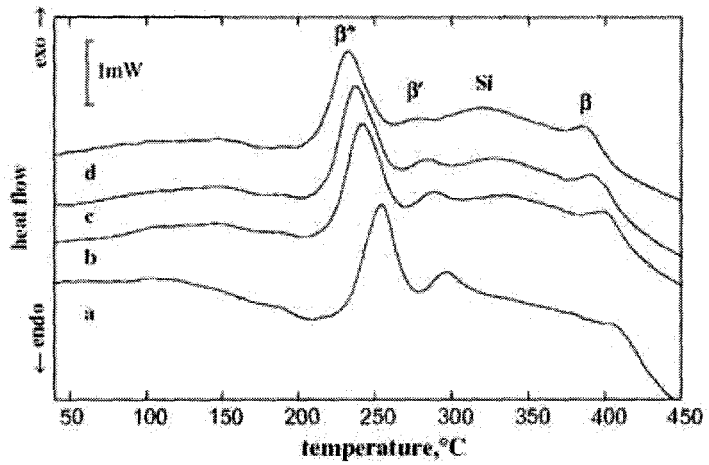

Figure 2.23: DSC curves of one-week naturally aged AA6016 prior to and after the PBC with (a) no pre-strain (b) 0.5% pre-strain (c) 1.5% pre-strain and (d) 5% pre-strain (Birol 2005b).

2.4.5 Effect of Copper / Excess Si on PBR

It is generally accepted that addition of Cu to the Al-Mg-Si alloys will improve their paint bake response. This is shown in figure 2.24. One of the possible reasons for this is that the addition of Cu results in the formation of Q and Q' precipitates at high temperatures (including PBC) and therefore can improve the PBR of the alloy (Chakrabarti et al. 1998). However this mechanism is rejected by Murayama et al. (2001). They proposed that Q' can only form during long ageing times and 20-30 minutes of PBC is not enough for these precipitates to form. Other suggested mechanisms for the positive effect of Cu on PBR (see Murayama et al. 2001 for full details) includes the decrease in solubility limit of Mg_2Si by Cu addition and subsequent increase of supersaturation of this phase (Collins 1958) or reduced migration rate of Mg and Si by introduction of Cu in the alloy and therefore suppression of the cluster formation at room temperature (Chatterjee and Entwistle 1973).

Esmaeili and Lloyd suggested that addition of copper to the Al-Mg-Si alloy only improves the nucleation of precipitates (or zones) and does not affect the growth

process. Therefore, in the Cu containing alloy, where the initial number of precipitates are higher during pre-ageing (see section 2.2.5), the microstructure becomes finer and denser after a period of artificial ageing (e.g. PBC) compared to non-Cu containing alloys (Esmaeili and Lloyd 2006).

The positron annihilation lifetime results of Honma et al. 2004 showed that addition of copper to the alloy, with the same composition of other alloying elements, results in a very fast recovery of quench-in vacancies (Honma et al. 2004). This improves the PBR of the Cu containing alloy because it suppresses the clustering process. The Doppler broadening results of the same research showed no sign of the characteristic Copper curve and therefore it was suggested that vacancies are not bound to Cu atoms so the very rapid recovery of vacancies is not due to the vacancy-Cu complex (Honma et al. 2004). Further study is required to find the reason behind this phenomenon.

The effect of Si on PBR can be clearly observed in figure 2.25. As it was shown in this figure, in samples with excess Si and for the identical heat treatment, the density of particles is higher and the microstructure also seems finer. It was discussed earlier in section 2.2.6 that the concentration of Si determines the density of co-clusters, GP-zones and β'' (Murayama and Hono 1999). Therefore, at any given ageing condition, the more the Si content of matrix, the denser the hardening precipitates/zones will become. The microstructure of alloy after natural ageing in both balanced and Si-excess alloys consist of small clusters (Murayama et al. 1998) which need to be dissolved in the matrix during PBC. However in alloys with excess Si, the higher number of Si atoms also results in a denser microstructure after PBC since the number of Si atoms controls the density of particles and consequently Si-excess alloy will have a better PBR. More studies are required to clarify this mechanism.

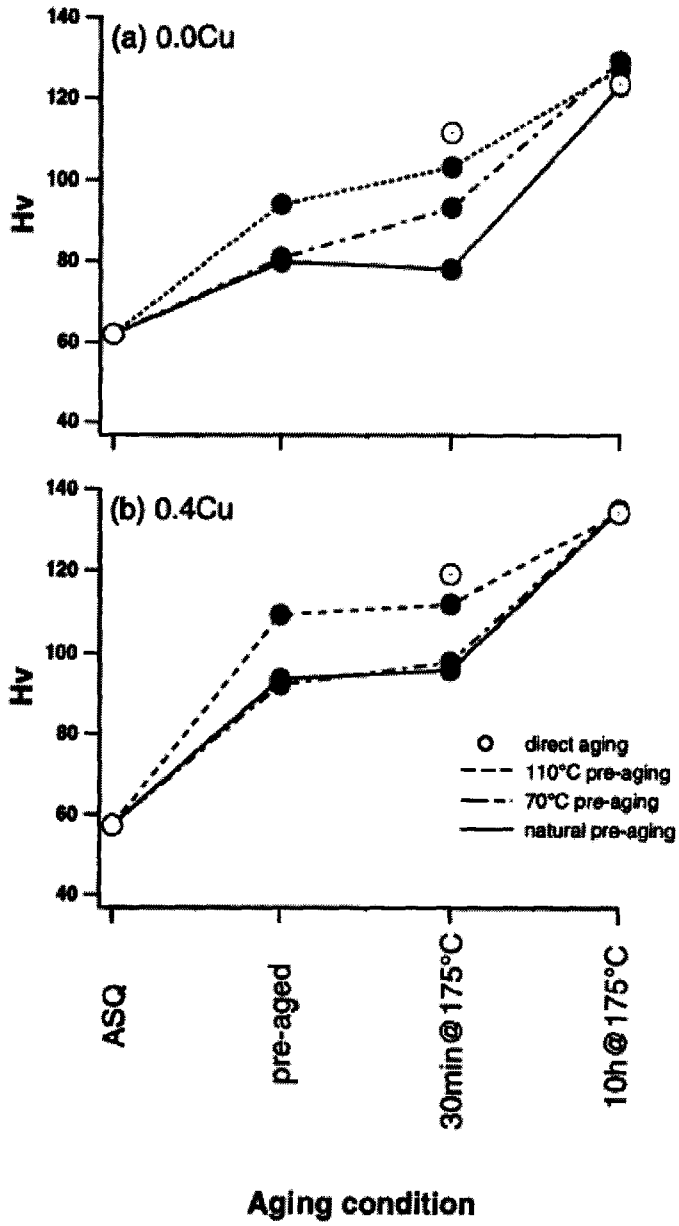

Figure 2.24: Hardness evolution of samples with (a) no copper and (b) 0.4 wt.% copper after various ageing treatments (Murayama et al. 2001).

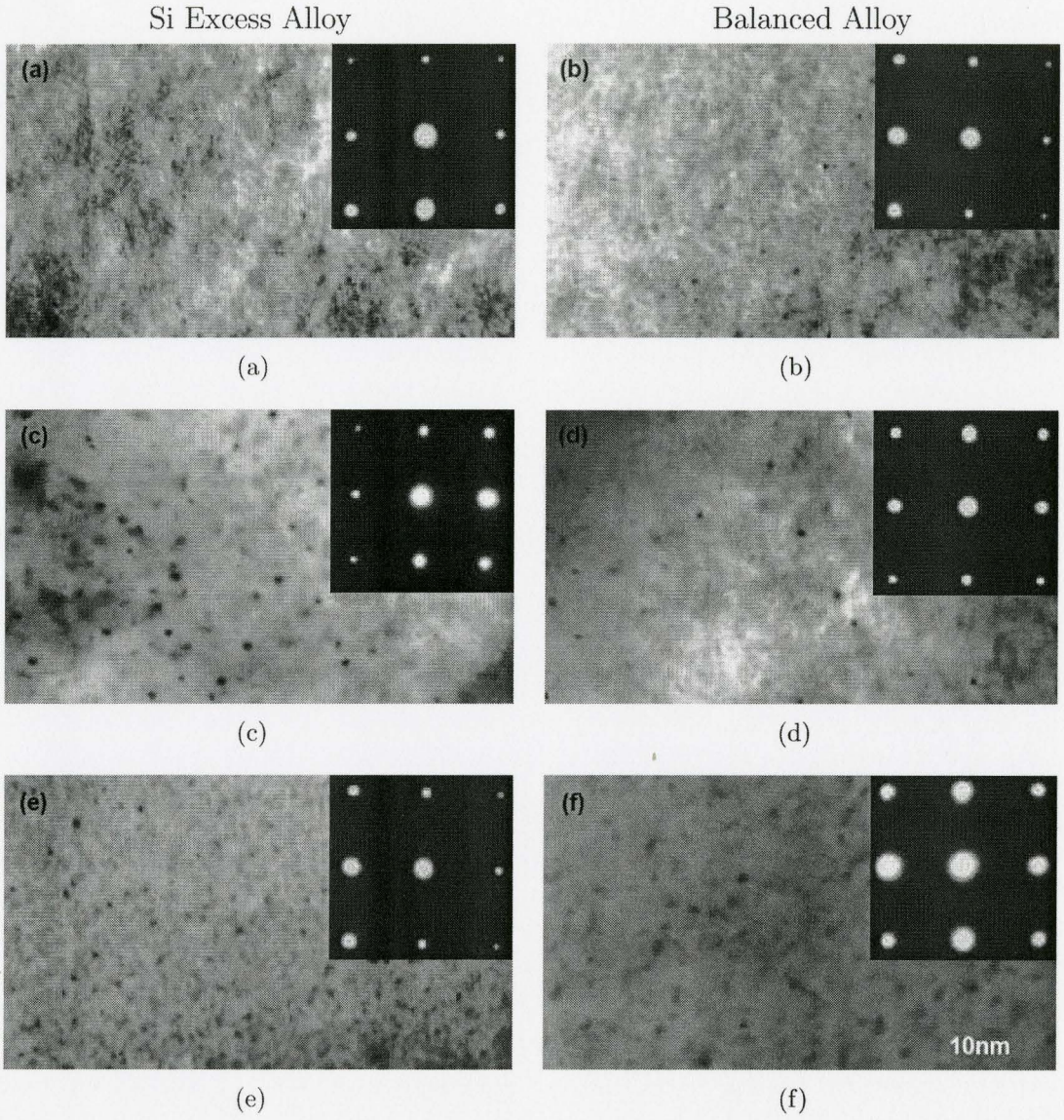

Figure 2.25: TEM micrographs of two Al-Mg-Si alloys. (a), (c) and (e) with Excess Si, (b), (d) and (f) with Balanced Si. The top row ((a) and (b)) are for samples which were naturally aged for 70 days and then subjected to ageing at 175°C for 30 minutes. The middle row is for samples directly subjected to PBC treatment after solution treatment and without a period of natural ageing. The bottom row is for samples pre-aged at 70°C for 16 hours and then subjected to the same PBC treatment as (a) and (b) (Murayama and Hono 1999).

2.5 Overview of The Experimental Techniques

In this section an overview of the experimental techniques used in the clustering studies plus a short theoretical background about them will be provided.

2.5.1 Electrical Resistivity Measurements

Electrical resistivity measurements is one of the most popular methods in precipitation studies. This could be due to the extreme sensitivity of this technique to microstructural changes. However this sensitivity could be problematic in some cases since the interpretation of the complex multi-factor resistivity signal is not always straightforward and needs at least one other type of experiment to complement the data.

In this section, the basic concepts of the electrical resistivity measurements are briefly discussed.

Essentially the electrical resistivity signal is due to the various electron scattering events which are happening inside the material. There are many scattering sites in the specimen including: phonon vibrations, chemical impurities (alloying atoms) and crystal imperfections such as vacancies, dislocations and grain boundaries (Rossiter 1991 and Fickett 1971).

The resistivity of the sample can be determined by passing a current i into the specimen with cross section A and measuring the voltage drop along the length l:

$$\rho = (v/i).(A/l) \tag{2.2}$$

This can be simplified further into:

$$\rho = r.(A/l) \tag{2.3}$$

where r is the resistance of the material. Microscopically, resistivity can be determined using the classic Drude formula: (Rossiter 1991)

$$\rho = \frac{m}{ne^2\tau} \tag{2.4}$$

where n is number of electrons (with mass of m and charge of e) per unit volume . τ is the mean free time of collision and is related to the conduction mean free path (Λ) with the following formula: (Rossiter 1991)

$$\Lambda = v_f\tau \tag{2.5}$$

where v_f is the electrons velocity at the Fermi level. Raeisinia et al. (2006) suggested that if the scattering center spacing is in the order of the mean free path of scattering, the contribution of that center cannot be neglected while in the case of great difference between these two distances, the scattering effect of that center can be ignored. In a very simple analysis using equations 2.4 and 2.5, Raeisinia and Poole (2006) calculated the conduction mean free spacing of AA6111 alloy to be approximately 25nm. If the precipitate size is in the order of 10nm, it was shown that precipitates account for 15-25% of total resistivity. This value decrease to 10-15% and below 5% for the case of precipitates in the order of 10-100nm and over 1000nm respectively (Raeisinia et al. 2006).

The electrical resistivity of the material can be simply described by Matthiessen's Law. This formula is used to describe the effect of solute atoms (Raeisinia et al. 2006) and can be described as: (Rossiter 1991)

$$\rho_{tot}(T) = \rho_0 + \rho_h(T) \tag{2.6}$$

where ρ_0 is the temperature independent residual resistivity and $\rho_h(T)$ is the temper-

ature dependant resistivity of pure host at temperature T. This is however, a very general formula and the resistivity analysis of solute atoms and precipitates are often much more complex. In order to include the effect of these factors equation 2.6 can be modified to (Raeisinia et al. 2006):

$$\rho_{tot}(T) = \rho_{pure}(T) + \sum_i \rho_i C_i + \rho_{ppt} \tag{2.7}$$

where the $\sum_i \rho_i C_i$ part takes into account the contribution of solute atoms by fraction summation of each solute's resistivity factor and the ρ_{ppt} part takes into account the effect of precipitates. The temperature dependent part includes the phonon vibrations scattering and therefore increases rapidly by increasing the temperature. Indeed, Fickett indicated that at near room temperature, the phonon scattering will become the dominant contributor to the resistivity value of alloy (Fickett 1971).

Another way of describing the effect of different factors on resistivity is by introduction of the scattering center resistivity coefficient (Raeisinia and Poole 2006). The first comprehensive review based on this concept was done by Fickett (1971). In this approach, the effect of each scattering center, on the overall resistivity of specimen, is described by a coefficient. Some of these coefficients which are of importance in aluminum alloys are listed in table 2.1. It is important to keep in mind that these values are not very accurate since various uncertainties are involved in the sample preparation and microstructure characterization techniques and this limits the accuracy of measurements (Raeisinia and Poole 2006).

2.5.2 Mechanical Testing

Mechanical testing is the easiest and fastest way to observe the macroscopic effects of the precipitation process. Despite its simplicity, it can provide an exten-

Table 2.1: Resistivity coefficients at room temperature

Scattering Center	Resistivity Coefficient		Variable
Phonons	0.1*	$n\Omega\text{m.K}^{-1}$	Temperature
Grain Boundaries	$1E-7$†	$n\Omega m^2$	Grain Boundaries per unit Volume
Dislocations	$3E-16$†	$n\Omega m^3$	Density
Vacancies	26 ± 5†	$n\Omega m.at\%^{-1}$	Concentration
Interstitial Atoms	10*	$n\Omega m.at\%^{-1}$	Concentration
Substitutional Atoms	$2-80$*	$n\Omega m.at\%^{-1}$	Concentration

* Raeisinia and Poole 2006

† Fickett 1971

sive amount of information about the material. This is why it is the most common technique in the precipitation research and has been used in almost all studies done in this field. Generally, in mechanical testing, the interaction between dislocations and various obstacles can be observed. In the simplest manner, the yield stress of the alloy can be related to microstructure using the following formula: (Esmaeili et al. 2003a)

$$\sigma_{ys} = \sigma_i + \sigma_{ss} + \sigma_{ppt} \tag{2.8}$$

where σ_{ys}, σ_i, σ_{ss} and σ_{ppt} are yield stress, intrinsic strength, solid solution strengthening and precipitation strengthening factors respectively.

In the case of the ageing process, the only changing variables during the experiment (which has an effect on mechanical properties of the material) are the precipitates/zones type and concentration of solute atoms. This changes the σ_{ss} and σ_{ppt} in equation 2.8.

During clustering, the only factor in σ_{ppt} part is the clusters contribution. There are two different approaches to model the hardening effect of clusters: Friedel's statistical approach (Esmaeili et al. 2003b and Esmaeili et al. 2003a) and the "Mod-

ulus Hardening" approach (Starink et al. 2004 and Starink et al. 2005). In this thesis the former method (Friedel's) is used.

In the Friedel's model, the hardening effect of an obstacle is decribed by (Esmaeili et al. 2003b):

$$\sigma_{ppt} = \frac{M.F}{b.L} \tag{2.9}$$

where: M is the Taylor's factor, b is the magnitude of Burger's vector and L is the effective distance between obstacles. The Obstacle strength (F) in this formula is the maximum interaction force between an obstacle and a dislocation. Both F and L change with time as ageing proceeds. An obstacle is defined as "strong" if the dislocation breaking angle is smaller than 120°and it is "weak" if this angle is larger than 120°. Due to the extreme small size of clusters, they can be considered as weak obstacles (Esmaeili et al. 2003a).

For aluminum alloys with the precipitates directed along $< 100 >_{Al}$ direction (for example β'', β' and β in Al-Mg-Si Alloys), Nie et al. (1996) calculated L to be equal to:

$$L_{Strong} = (\frac{2\pi}{f})^{1/2}.r \tag{2.10}$$

where f is the volume fraction and r is the radius of precipitates.

For clusters, which are considered as weak obstacles, the effective obstacle spacing is equal to (Esmaeili et al. 2003b):

$$L_{Weak} = (\frac{\sqrt{3}\Gamma}{F})^{1/2}.L_{Strong} \tag{2.11}$$

where Γ is the line tension of dislocations ($\sim Gb^2/2$). Now using equations 2.11 and 2.10, the effective distance between weak obstacles (clusters) can be calculated as:

$$L_{Weak} = (\frac{2\sqrt{3}\pi\Gamma}{Ff})^{1/2}.L \tag{2.12}$$

It is easier to write the formulas based on the relative (normalized) values of f and F:

$$f_r = \frac{f}{f_{peak}} \tag{2.13}$$

$$F_r = \frac{F}{F_{peak}} \tag{2.14}$$

Finally using equations 2.9, 2.12, 2.13 and 2.14, the contribution of clusters to the overall strength of an Al-Mg-Si alloy can be calculated as:

$$\sigma_{cluster} = \frac{M.F_{peak}^{3/2} f_{peak}^{1/2}}{b.(2\sqrt{3}\pi)^{1/2}\Gamma^{1/2} r_{peak}^{3/2}}.r^{1/2} f_r^{1/2} = C'_{cluster}(r_{cluster} f_{r.cluster})^{1/2} \tag{2.15}$$

To simplify equation 2.15 even further, an average value for $r_{cluster}$ can be taken and it can be assumed that it is constant in equation 2.15 (Esmaeili et al. 2003a). Note that this is a rough estimation of the clusters strengthening effect and it predicts higher/lower values for smaller/larger clusters. Based on this, equation 2.15 can be summarized into:

$$\sigma_{cluster} = C_{cluster}.(f_{r.cluster})^{1/2} \tag{2.16}$$

From equation 2.16, it is expected that cluster formation increases the hardness of Al-Mg-Si. The degree of it, however, depends on the kinetics of clustering which is expressed by $f_{r.cluster}$.

The other approach in calculating the hardening contribution of clusters is by

considering their "Modulus Hardening" effect. The most comprehensive modeling using this approach has been done by Starink et al. (2004) and (2005). The assumption here is that clusters do not have any internal order, structure and specific shape and consequently, order strengthening and stacking fault hardening can be ignored. Since there is also no interface defined between clusters and the matrix, the chemical hardening can also be neglected. However the modulus hardening, due to the difference between the modulus of the matrix and clusters, is significant and can be calculated as (Starink et al. 2005):

$$\Delta\tau_{cluster} = \frac{\Delta\mu}{4\pi\sqrt{2}} f_{cluster}^{1/2} \tag{2.17}$$

where $\Delta\mu$ is the difference between the modulus of matrix and clusters which can be expressed by (modified from Starink et al. 2005):

$$\Delta\mu = x_{Mg}\mu_{Mg} + x_{Si}\mu_{Si} + x_{Al}\mu_{Al} \tag{2.18}$$

The problem is to defined the exact composition of clusters. As it was mentioned earlier in chapter 2, this is not simple due to the experimental errors and also the evolution of Mg:Si ratio in the clusters during ageing. This is why this approach is not used in this project.

2.5.3 Positron Annihilation

The positrons are defined as Anti-Particles of the electrons. They can be obtained from the β^+-decay of radioactive isotopes (Krause-Rehberg and Leipner 1999). The most popular source for production of positrons in labs is the ^{22}Na source. The formation of positrons in this material is accompanied by simultaneous emission of γ-ray with energy of 1.27MeV according to the following two decay reactions:

$$^{22}Na \rightarrow ^{22} Ne + \beta^{+} + \nu \ (neutrino) \tag{2.19}$$

$$^{22}Na \rightarrow ^{22} Ne + \gamma \ (1.28MeV) \tag{2.20}$$

The simultaneous emission of this characteristic γ-ray with positron can be used as a mean of marking the birth of positrons (Buck et al. 1979).

As positrons travel inside the metal matrix, they lose energy through ionization and excitation of atoms, excitation of plasmon and also by formation of phonon and electron-hole pairs (Meyendorf et al. 2004). Positrons diffuse inside the matrix in distances in the order of 100nm before they encounter an electron and finally annihilate (thermalization distance). The annihilation of positrons results in emission of mostly two γ rays (photons) with the energies of 511keV (Krause-Rehberg and Leipner 1999). This can be used as the end-mark of the positron life inside the matrix. During this mass-energy transformation, the energy, momentum and spin is conserved. Since energetic positrons are rapidly thermalized after entering the matrix, if they are not bound to electrons, it can be concluded that the initial state of the system (matrix with many electrons) controls the characteristics of the annihilation process almost entirely. This provides us with a tool to study the material by using careful measurements of time and momentum of annihilation (Buck et al. 1979). The former measurement (time) is the basis of positron annihilation lifetime spectroscopy (PALS). In this method, the 1.28MeV and 0.511MeV gamma rays are used to calculate the lifetime of the positron inside the matrix. The momentum analysis of the annihilation process includes measurement of two different parameters: the angle between the two annihilation γ-rays and the energy difference between them. The latter is the basis of angular correlation measurements while the former is used in Doppler Broadening Spectroscopy (DBS). Figure 2.26 shows the schematic of the annihilation process, its characteristics and techniques of studying it.

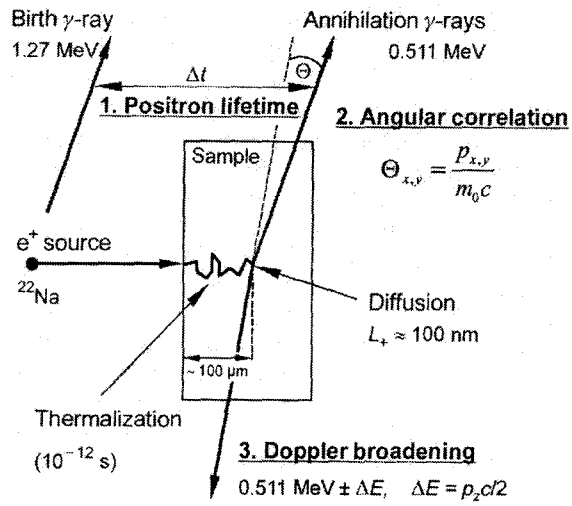

Figure 2.26: Schematic of the positron annihilation process inside the matrix (Krause-Rehberg and Leipner 1999).

From these three techniques, the lifetime measurement was chosen in this project for studying the process of clustering. In order to understand the results of this technique, a brief introduction is required which is the subject of the next section.

Positron Lifetime Spectroscopy (PALS)

Since the positrons are anti-particles of electrons, their lifetime must depend on the density of electrons. Therefore any phenomenon that can change the electron density can change the positron survival probability around it. At the same time, other factors also control the probability of positron distribution. For example positrons are strongly repelled by the ion cores and the potential energy of positron is smallest in the interstices of the lattice. The ion cores have an extended field of repulsion which defines the probability of the positron occupying positions (Seeger 1973).

The simplest defect in metals is the mono-vacancy. The existence of vacancy first decreases the effect of ion-cores repulsion since the core of the atom is removed

from the vacancy site. At the same the valance electrons around the removed atom must redistribute themselves by screening along the vacancy and this decreases the electron density at the vacancy site. This results in a longer lifetime of the positrons at the vacancy sites. Consequently in the case of metals with wide ion cores and large valency (such as Aluminum), the trapping of positron in the vacancy is favored compared to the bulk of the material. This will result in a longer lifetime of the positron at vacancy sites. Note that in the case of narrow ion core metals with small valency (Z=1) (such as alkali metals), the increasing effect of vacancies on lifetime might not be as strong as it was for the case of other metals (Seeger 1973).

Other types of defects can also change the positron lifetime, for example dislocations, grain boundaries, voids and surfaces (Buck et al. 1979). In general, when k different types of defects (with lifetime τ_i and intensity I_i of the ith one) are present in the matrix, the decay spectrum of positrons can be expressed by (Krause-Rehberg and Leipner 1999):

$$D(t) = \sum_{i=1}^{k+1} I_i exp(-\frac{t}{\tau_i}) \tag{2.21}$$

Note that in case of perfect-lattice metals, only the bulk lifetime of the matrix (τ_b) can be detected. The positron lifetime spectra, $N(t)$, is the absolute value of the time derivative of $D(t)$ which is: (Krause-Rehberg and Leipner 1999)

$$N(t) = \sum_{i=1}^{k+1} \frac{I_i}{\tau_i} exp(-\frac{t}{\tau_i}) \tag{2.22}$$

The bulk and mono-vacancy lifetimes of Aluminum, Magnesium and Silicon are listed in table 2.2.

The general idea behind the positron annihilation lifetime spectroscopy is the use of the positron birth γ-ray (with energy of 1.28MeV) and annihilation γ-rays

Table 2.2: Positron Lifetime in Al, Mg and Si

Material	τ_{Bulk} (psec)	$\tau_{Mono-vacancy}$ (psec)	Reference
Aluminum	163	244	Sterne and Kaiser (1991)
Magnesium	235	255	Manninen et al. (1975)
Silicon	218	270	Krause-Rehberg and Leipner (1999)

(each with energy of approximately 0.511 MeV) to find the positron lifetime. It was discussed earlier that the time delay between emission of these two photons can be related to the lifetime of positrons. Note that the thermalization process (e.g. excitation of phonon or plasmon by positrons) happens very quickly and within few picoseconds. This time is very small and is not comparable to positron lifetime which is typically in the order of few hundred picoseconds. Therefore in positron lifetime analysis the thermalization time is usually neglected.

In this technique, the ^{22}Na source is sandwiched between two identical samples with a minimum thickness of 1mm each. The source should be weak enough to ensure that only one positron enters and remains inside the sample at a given time before annihilation happens (Krause-Rehberg and Leipner 1999). At the same time it should be strong enough to provide a good counting rate however it should not be very strong since it reduces the signal to noise ratio. A value of 10-20μCi is often selected (Buck et al. 1979). A pair of detectors are placed around the sample-source sandwich to detect the γ-rays. The γ-rays are converted to analog electric pulses using these scintillator-Photomultiplier detectors. These electric pulses are then processed by discriminators which their output start and stop a time-to-amplitude convertor (TAC). The amplitude of this electronic stop watch is proportional to the time difference between 1.28MeV and 0.511MeV gamma rays which itself is related to the lifetime of positrons. Each annihilation event is then recorded into a single channel

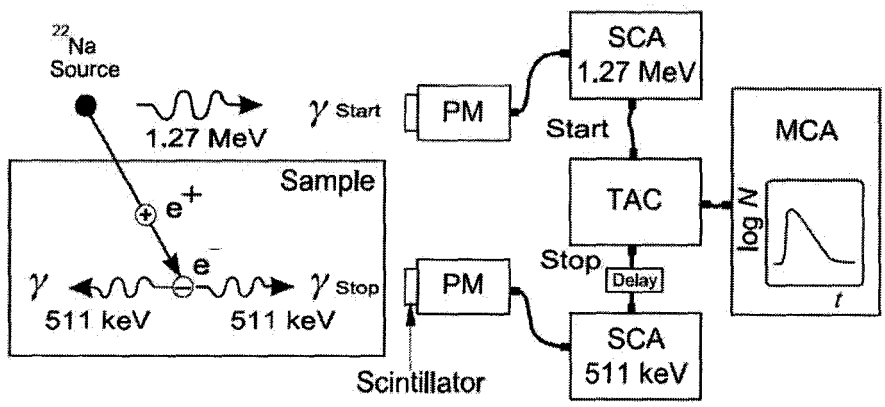

Figure 2.27: Schematic of a fast-fast PALS setup (Krause-Rehberg and Leipner 1999).

of a multi-channel analyzer. The channel number acts as the time scale. The end result is the plot of number of counts per channel number (time) (Krause-Rehberg and Leipner 1999).

If the time measurements are performed at the same time as the energy selections (using a fast differential discriminator), then the setup is called fast-fast setup, otherwise it is called fast-slow (Krause-Rehberg and Leipner 1999). The schematic of a fast-fast setup is shown in figure 2.27.

The rest of the analysis is pure mathematics. First the background is removed. Then the annihilation of positrons inside the source (2-15% of total annihilated positron depending of the source foil thickness) is calculated and removed. Finally a model spectrum with a given number of components and resolution function is used to perform a least square fitting of the experimental data. There are various parameters to be fitted which can be categorized into linear (such as intensities and background) and non-linear (such as lifetimes) ones. The fitting of each group of parameters is done independently. There are number of computer programs available for fitting based on the Gauss-Newton non-linear routine such as LIFSPECFIT, POSITRONFIT or PATFIT (Krause-Rehberg and Leipner 1999).

Chapter 3

Research Objectives

As it was mentioned in the previous chapter, it seems that any attempt towards solving the problem of the negative effect of natural ageing on the paint bake response (PBR) in Al-Mg-Si alloys, requires a clear understanding of the whole clustering process. However, earlier studies failed to fulfill this goal completely. This is why this research is focused only on the cluster formation while other aspects of PBR such as improving it by various techniques is not considered here. Thus the objectives of this project can be summarized into the followings:

- Investigate the low temperature ageing of Al-Mg-Si alloys (from -20 to 50°C) in order to complement previous high temperature studies.
- Find the role of vacancies in the cluster formation process.
- Find the kinetics of clustering.
- Find the activation energy of clustering and from that identify the controlling parameter of the whole process.
- Suggest a general model for the clustering process.

Chapter 4

Experimental Method

4.1 Introduction

In this chapter, the experimental procedures required for achieving the project objectives are discussed. First, in section 4.2, the composition of the alloy used in this research and the reason behind choosing it is mentioned. Then details about the heat treatment processes will be given in section 4.3. Finally the experimental techniques will be discussed in section 4.4.

4.2 Alloy Composition

The alloy which was chosen for this research was a member of the 6xxx series aluminum alloys. The selection was done based on the following criteria:

- The alloy should be copper free. This was the first and most important criterion in the selection process. The reason for this was to avoid the complex effects of copper on the ageing sequence and kinetics (see section 2.2.5 for full details).
- The alloy should be similar to other alloys which were previously studied in the literature.
- The alloy should be clean. Meaning that the impurity content (such as Fe, Mn, Cr, etc...) should be as small as possible.

- The alloy should have a large temperature range for the solution treatment process.

Not all of the conditions above can be satisfied simultaneously, for example due to the industry demand, the choice of copper-free 6xxx alloy is very limited since copper provides better mechanical properties of the material. The impurity content also is not always very low. So a compromise should be made in the process of alloy selection. Based on the above criteria and available commercial alloys, a material with the following composition was chosen:

Table 4.1: Chemical composition of the alloy used in this research. (in wt.%)

Mg	Si	Cu	Fe	Al
0.46	1.05	0	0.14	rest

4.3 Heat Treatment

The heat treatment of this alloy is a combination of solution treatment and ageing processes. First the samples are heated to the solution treatment temperature and then they are water quenched. This is then followed by the ageing process at various low temperatures for short and long times.

The samples were designated as XXX.YY where XXX is the solution treatment temperature and YY is the ageing temperature.

Solution Treatment:

Two different solution treatment temperatures were chosen according to the chemical composition of alloy and using the Thermo-Calc software with the

database provided by ALCAN Inc. These temperatures are selected based on the solidus temperature (~588°C) and the Mg_2Si dissolution temperature (~519°C).

The reason behind choosing two different ageing temperatures is to provide two different concentrations of vacancies in the matrix and therefore investigate the effect of vacancies on the clustering process.

Based on the above discussion, 525 and 560°C with holding times of 15 and 10 minutes respectively are chosen as solution treatment temperatures. The gap between these two temperatures is large enough to produce considerable difference in concentration of vacancies in the matrix. To illustrate this point further, simple theoretical calculations will be made in the following paragraphs.

The equilibrium concentration of vacancies can be calculated using following formula: (Cahn and Haasen 1983)

$$c_v^{eq} = \exp(\Delta S_v^f / k_B) \exp(-\Delta H_v^f / k_B T) \tag{4.1}$$

where ΔS_v^f and ΔH_v^f are the entropy and enthalpy of vacancy formation respectively. k_B is the Boltzman's constant. Now using equation 4.1 and ΔH_v^f of 65.68 kJ/mol (table A.2) the ratio between equilibrium concentration of vacancies at 560 to 525°C can be found:

$$c_{v.560}^{eq} / c_{v.525}^{eq} \simeq 1.52 \tag{4.2}$$

So the choice of 525 and 560°C for solution treatment will provide difference of almost 50% in total vacancy concentration.

Quenching:

The quenching of samples should be fast enough to avoid considerable vacancy loss during the process. The easiest way to achieve this is by using water at ambient temperature as the quenching medium.

Ageing:

As it was mentioned earlier in the objectives (chapter 3), the concept of this research is the study of low temperature ageing, which based on the data available in the literature, will result in formation of clusters. Most of the previous studies indicated that ageing below 50°C can ensure formation of clusters rather than GP zones (see Yamada et al. 2000 for example). Therefore ageing was performed at -20, 0, Room temperature and 50°C for short (0-300 minutes) and long (5 hours to 7 days) durations.

Transition Time Considerations:

In order to stop any unwanted ageing of the samples, all specimens were immersed in the liquid nitrogen prior to any experiment or ageing. This is especially critical for the case 0 and -20°C samples.

4.4 Experimental Techniques

There are various techniques which can be used in order to investigate the precipitation processes. However, not all of these are applicable to the study of clusters. The extremely small size of these zones along with the lack of any interface with the matrix[1] makes the direct observation of clusters almost impossible. Conse-

[1]Clusters are essentially parts of a matrix which have a higher concentration of solutes than the rest of it.

quently, The focus will be placed on other techniques which can give indirect evidence of clustering.

The electrical resistivity measurements is the classical technique to study precipitation therefore it is also used in this project to analyze the clustering phenomenon. However, the resistivity signal provides information about various microstructural changes during ageing (such as vacancies, solute atoms and actual clusters) and consequently in order to interpret the results of this technique, other types of analysis are often required to complement the data. This is why the positron annihilation lifetime spectroscopy (PALS) was chosen to provide information about vacancies during the clustering process. PALS is not a new technique in physics, however, the application of it in the study of clustering is very new. There are limited number of publications in this area including Reich et al. 2001, Buck et al. 1979 and Dupasquier et al. 2004.

Finally, hardness testing was performed on all samples since it can demonstrate the actual effect of clustering at the macroscopic level. The advantage of this technique is its simplicity and ability to provide data required for detailed simulations. There are other types of experiments which have been used before to study precipitation and clustering, e.g. DSC, TEM and 3DAP, however for the reasons which will be mentioned later in section 4.4.4, they were not utilized in this research.

Figure 4.1 shows the schematics of experimental procedures and research objectives. The general overview of the experimental method used in this project is given in table 4.2.

4.4.1 Electrical Resistivity Measurements

The theory behind this technique was given earlier in section 2.5.1, chapter 2. The electrical resistivity measurements were performed at the University of British

Table 4.2: Summary of the experimental techniques

Technique	Features	Procedures	Results
Electrical Resistivity	Most sensitive	At the liquid N_2 temperature	Clustering can be observed indirectly
	Easy to perform	100 mm × 10 mm × 1 mm samples	Signal is due to the contribution of clusters, solute atoms and vacancies
		Pre-treated samples	Clustering Mechanism cannot be identified by using only this technique
			It is possible to find clustering activation energy
Positron Annihilation	Very sensitive	100 mm × 10 mm × 1 mm samples	Vacancies effects can be seen
	Rarely used in precipitation and clustering studies of metallic systems	The lifetime technique is used	Signal is due to the contribution of vacancies
	Sensitive to vacancies (their number and surrounding) Not easy to analyze	Pre-treated samples	Can be combined with electrical resistivity results to identify the mechanism of clustering
Hardness/Tensile	Very Simple	According to ASTM E8M-04 for tensile and ASTM E18-07 for macro-hardness measurements	Gives an overall view of clustering
	Quick to analyze	In-Situ Samples for hardness and pre-aged for tensile tests	Can complement the results of other techniques

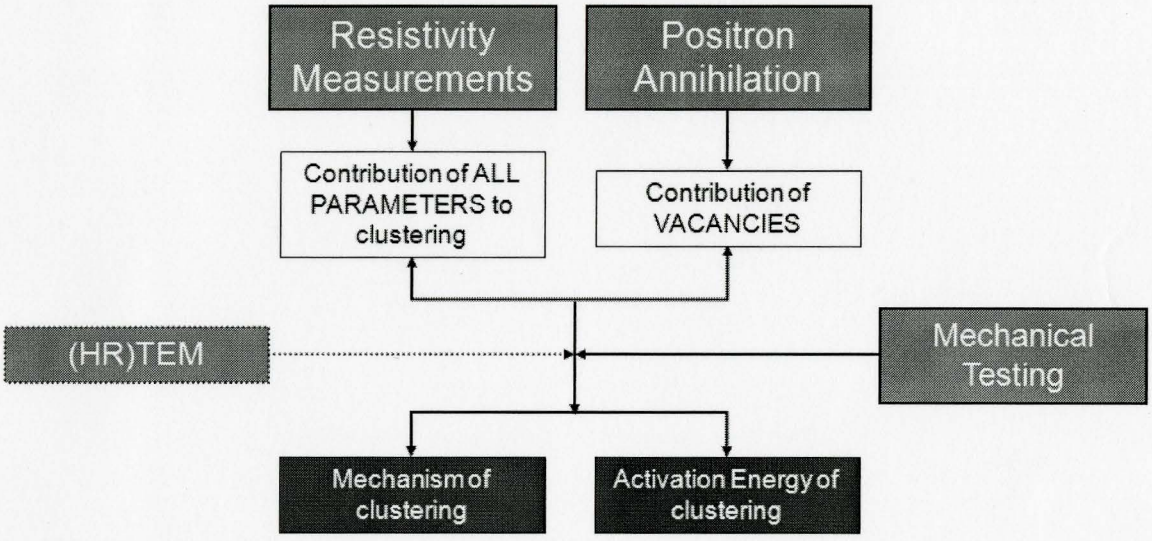

Figure 4.1: Schematic of the experimental procedures

Columbia using a custom made four point probe system by passing the current of 21mA through 100 mm × 10 mm × 1 mm samples. Using a systematic calibration procedure, this sample size gave the smallest error (Esmaeili et al. 2005) while at the same time it provided a signal which is strong enough for the clusters to be detected.

The samples were pre-treated at various ageing conditions (see section 4.3) and then kept inside the liquid nitrogen prior to the resistivity measurements to avoid further ageing. All experiments were performed by immersion of the setup in the liquid nitrogen (77K) to minimize the phonon scattering effect which is extremely large at room temperature and consequently makes the measurement of the clustering signal at RT impossible.

For each series of samples solution treated at the same temperature, the values of resistivities are normalized to the resistivity of the as-quenched RT sample according to the following formula. The choice of the RT sample was arbitrary and other samples could have been used in this process.

$$\rho_{norm.i} = \rho_i * (\frac{\rho_{AQ.RT}}{\rho_{AQ.i}}) \tag{4.3}$$

where $\rho_{norm.i}$ is the normalized resistivity of ρ_i, $\rho_{AQ.RT}$ is the as-quenched resistivity of RT sample and $\rho_{AQ.i}$ is the as-quenched resistivity of sample i.

4.4.2 Mechanical Testing

There are various mechanical tests available which can be used in the precipitation studies including: the Hardness, Tensile, Stress relaxation and strain rate sensitivity measurements. In this project only hardness and tensile tests are used mainly due to their simplicity and time and temperatures sensitivity of samples. Also because of the pronounced Portevin Le-Chatelier (PLC) and dynamic ageing effects in aluminum alloys (especially Mg containing ones such as 6xxx series alloys), the signal due to the cluster formation would become buried under the background noise of the stress relaxation and strain rate sensitivity tests. The solution to this problem is to perform the test at low temperatures (such as 77K), however, the facilities required for these experiments were not available during the period of this project and consequently they were not utilized.

Hardness Test

The hardness test is the simplest and quickest mechanical test available. However, despite its simplicity, it can give a very good and precise overview of the precipitation process. A very good advantage of hardness test is the possibility of using the in-situ samples. This means that measurements of samples can be done while they are being aged. A series of Macro-hardness tests were performed on all 8 samples with ageing history according to section 4.3. All measurements are done according to ASTM E18-07 standard. The indentor used was standard Rockwell 1/8" ball with

the load of 60 Kg (Rockwell H scale). For each point, at least 6 measurements were taken and the average was found. All tests were performed at room temperature and for the shortest possible time in order to minimize the unwanted ageing of the samples.

Tensile test

The sole purpose of the tensile test in this project is to provide the relationship between hardness results (HRH scale) and the yield stress values. Therefore tensile tests were only performed on samples which were solution treated at 560°C and then aged at room temperature. For other samples, the same formula which was found for 560.RT samples was used to convert hardness values (in HRH) to yield stress (in MPa).

Samples with the gage length of 25mm, width of 6mm and thickness of 1mm were chosen according to the ASTM E8M-04 standard. The crosshead speed was 1 $mm.min^{-1}$ which is equal to a strain rate of 6.6×10^{-4} sec^{-1}. The 0.2% proof stress technique was used to find the yield stress of the material.

4.4.3 Positron Annihilation

In this project, a fast-fast setup is used. The source was ^{22}Na with the strength of 20 μCi. All experiments are done at very low temperatures (Below -50°C) by purging the detection chamber with Argon gas. A minimum of 10^6 counts were detected for each measurements. The PATFIT routine (Kirkegaard et al. 1989) was chosen for the fitting procedure. For each sample, a 3-lifetimes fitting was performed and the average lifetime is then calculated.

4.4.4 Techniques which are not used/applicable

Perhaps one of the best techniques to study clusters is the Atom Probe. It can provide valuable information about the nature of clusters (or other precipitates) such as their chemical composition. In addition to this, in combination with the contingency data analysis, it can provide evidence of clusters and co-cluster existence in the alloy (for example see figures 2.7, 2.8.a and 2.10). Despite the powerful capabilities of AP, it was not utilized in this project simply due to lack of access to the facilities. However, the composition of alloy used here is very similar to ones which have been already investigated using AP in the literature.

Transmission Electron Microscopy (TEM) is another powerful technique in precipitation studies, however due to the extreme small size of clusters, their coherency with the matrix, the small strain field around them and also closeness of the atomic numbers of Mg, Al and Si, TEM cannot show any sign of the clusters (see figures 2.2 and 2.3.a).

X-Ray Diffraction is another possible technique to analyze precipitates, however, since clusters do not have any structure or internal order different from that of the matrix (refer to section 2.2.1 in chapter 2 for more details), it is impossible to use x-ray diffraction technique to analyze them.

Other techniques such as DSC, strain rate sensitivity and stress relaxation were also available and they were used before in the clustering studies, however, they were not utilized in this research either due to their complexity (the latter two, see section 4.4.2) or availability of extensive data about them in the literature (DSC).

Chapter 5

Results

5.1 Introduction

In this chapter, the results of the various experiments discussed in chapter 4 are shown. Discussion of these results will be given in chapter 6

5.2 Hardness Tests

The hardness test results are shown in figures 5.1 to 5.4. There are two groups of graphs: first, results of short term ageing (up to 300 minutes) in linear scale and second, results of ageing up to a week in logarithmic scale (long term). As it can be seen, Hardness increases very rapidly with time at the beginning of ageing and then the rate of the hardness increase, slows down considerably. The detailed discussion of these results will be given in chapter 6, section 6.2.1.

5.3 Tensile Tests

Tensile tests were performed only on 560.RT samples which were aged for up to 300 minutes. Ageing times are chosen to be synchronized with the hardness measurements of the same samples. The evolution of yield stress (0.2% proof stress) versus time is shown in figure 5.5.

By plotting Hardness values versus yield stress of samples with the same ageing

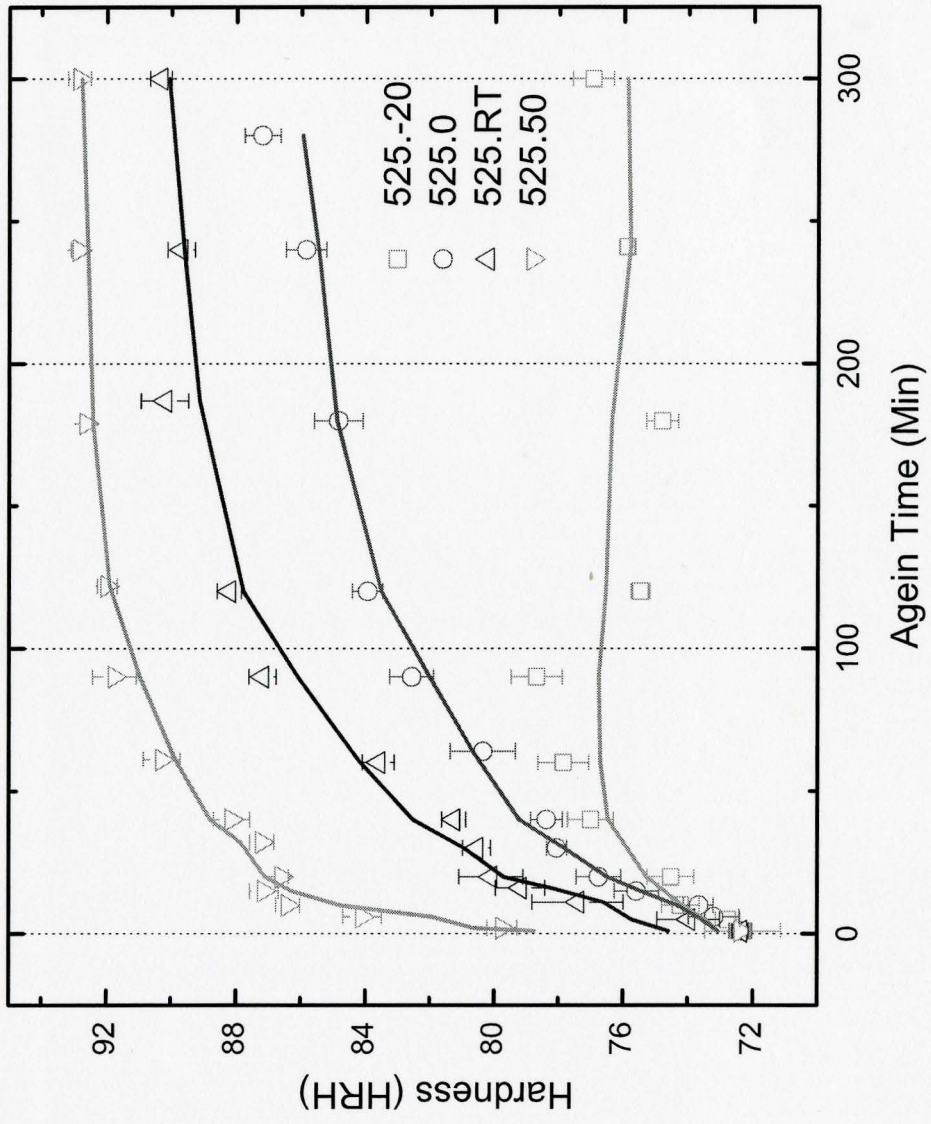

Figure 5.1: Hardness evolution of 525°C samples during short ageing times. Note that X axis is in the linear scale.

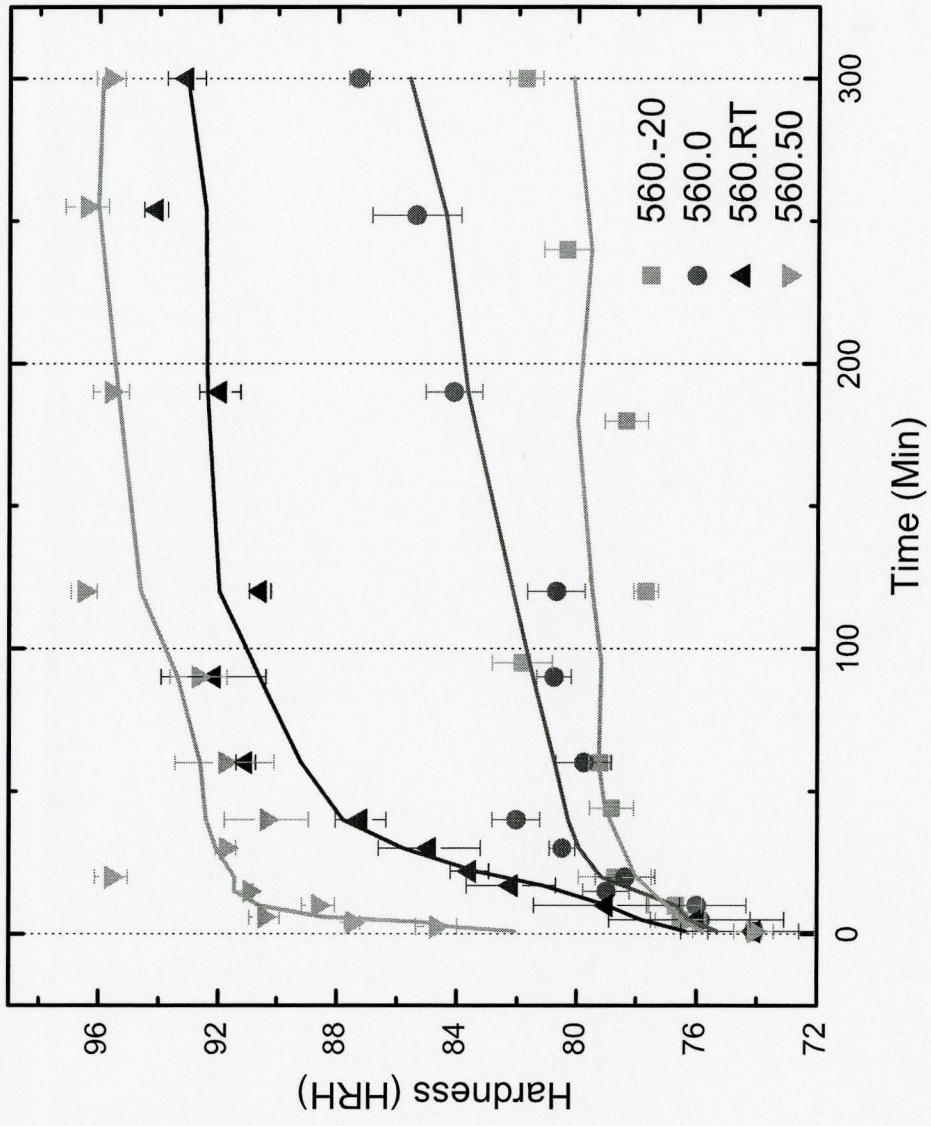

Figure 5.2: Hardness evolution of 560°C samples during short ageing times. Note that X axis is in the linear scale.

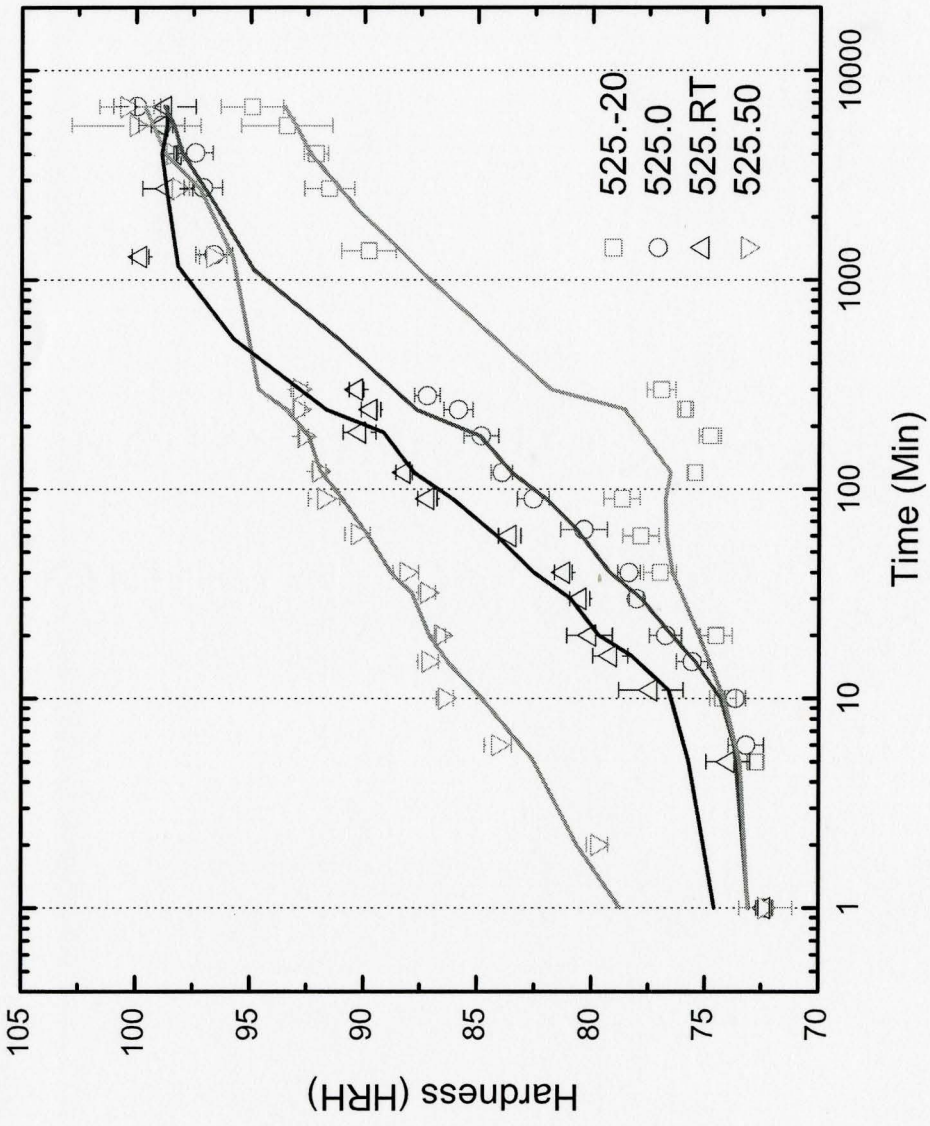

Figure 5.3: Hardness evolution of 525°C samples during long ageing times. Note that X axis is in the logarithmic scale.

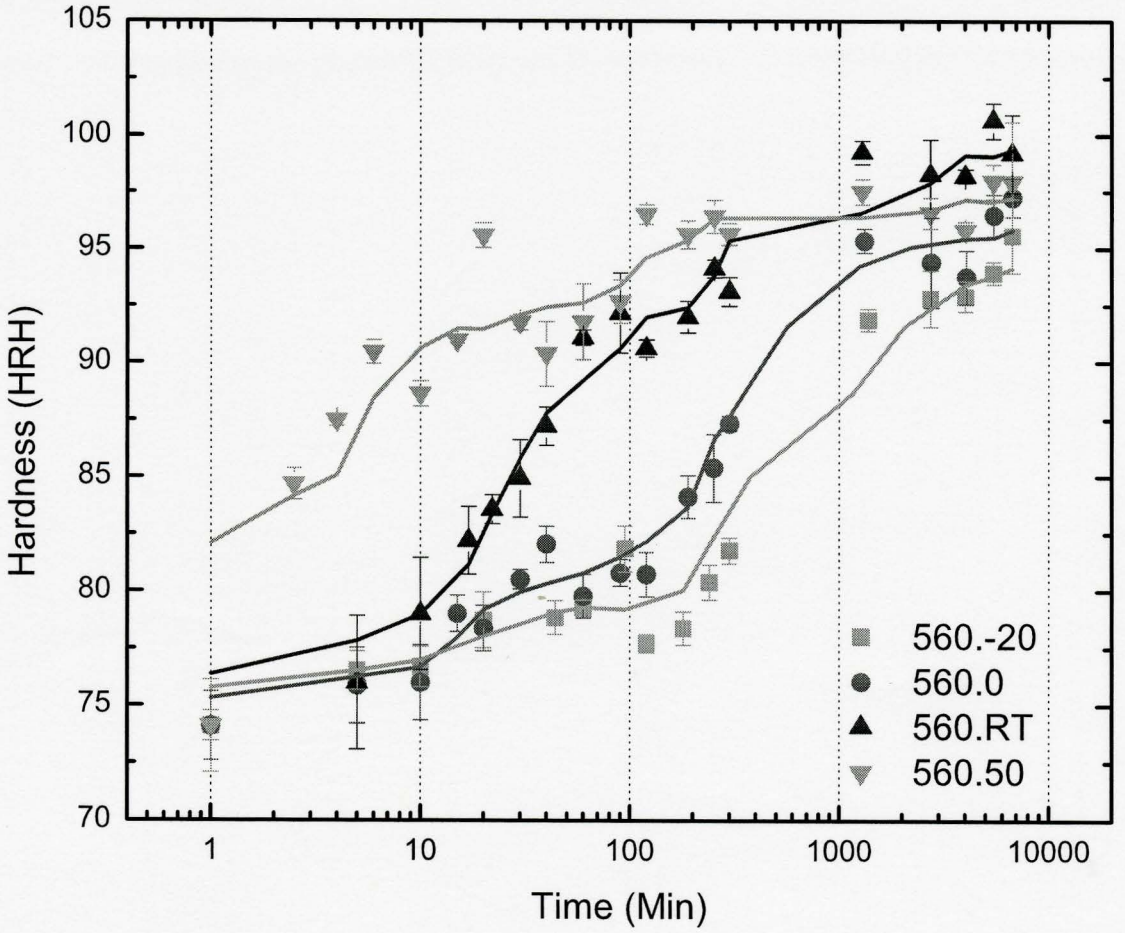

Figure 5.4: Hardness evolution of 560°C samples during long ageing times. Note that X axis is in the logarithmic scale.

times, the relationship between Hardness in Rockwell H scale (used in figures 5.1, 5.2 and 5.3, 5.4) and yield stress in MPa can be found:

$$HRH = 48.69027 + 0.4412YS \tag{5.1}$$

This will provide a mean of changing hardness values to yield stress and therefore makes the application of a mechanical model to the clustering data possible. This will be done in chapter 6, section 6.3.1.

5.4 Electrical Resistivity Measurements

Similar to the hardness test, the results of electrical resistivity measurements are sorted into two categories: short-term and long-term ageing. The first category includes ageing of up to 300 minutes while the second one consists of ageing of up to 7 days. The short-term results (figures 5.6 and 5.7) are plotted in linear scale and the long-term results (figures 5.8 and 5.9) are plotted in logarithmic scale. The plotted lines in all of these figures are the average moving lines from the actual experimental points. For all samples, the resistivity is increasing with ageing time. By plotting the resistivity values versus logarithm of time, linear relationships can be fitted onto the data with a very high accuracy. The interesting feature is the appearance of three different stages of ageing in the electrical resistivity results (for example see 0°C in both 525 and 560 samples). This needs further discussion and explanations which will be given in chapter 6, section 6.2.3.

Each stage of resistivity change in figures 5.8 and 5.9 can be expressed by a simple relationship of:

$$\rho = K \ln t + C \tag{5.2}$$

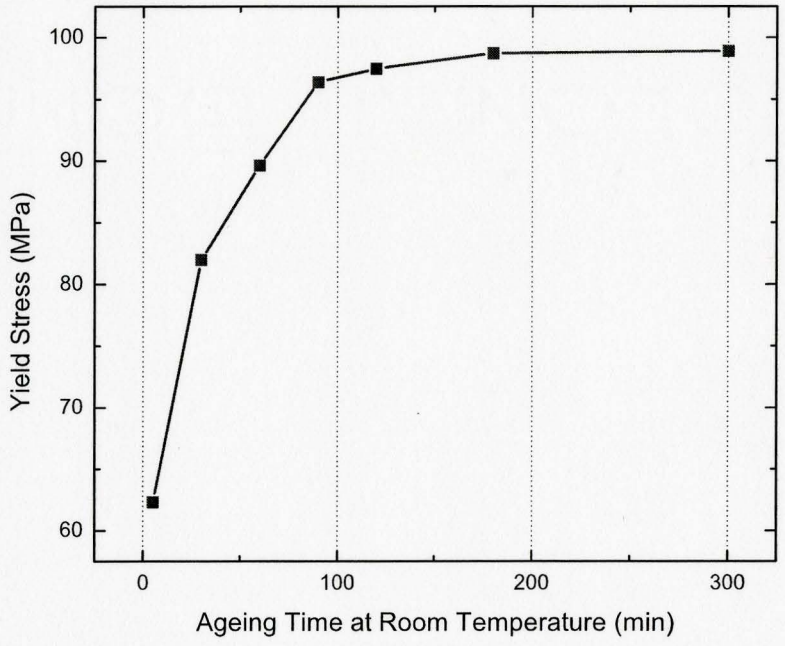

(a)

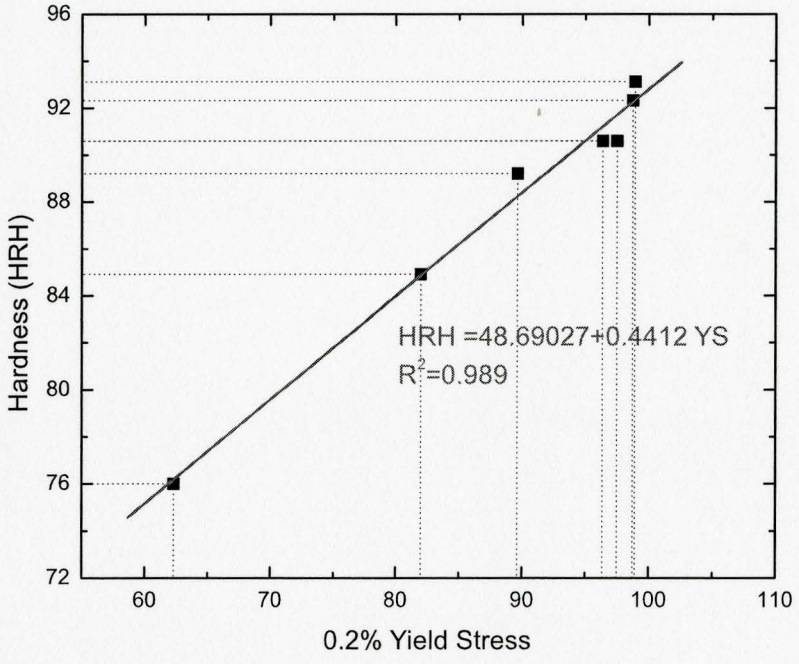

(b)

Figure 5.5: (a) 0.2% Proof yield stress evolution versus ageing time at room temperature. (b) Relationship between Hardness and yield stress.

where K and C are constants. The logarithmic fitting can be explained by the concepts of effective diffusion during precipitate growth. This will be done in the section 6.2.3 of chapter 6.

5.5 Positron Annihilation Lifetime Measurements

The average annihilation lifetime of positrons (τ_{Avg}) for the 560.RT samples are plotted in figure 5.10. The lifetime increases with time at the beginning of ageing and then reaches a constant value at long ageing times. Discussion about these results will be given in chapter 6, section 6.2.4.

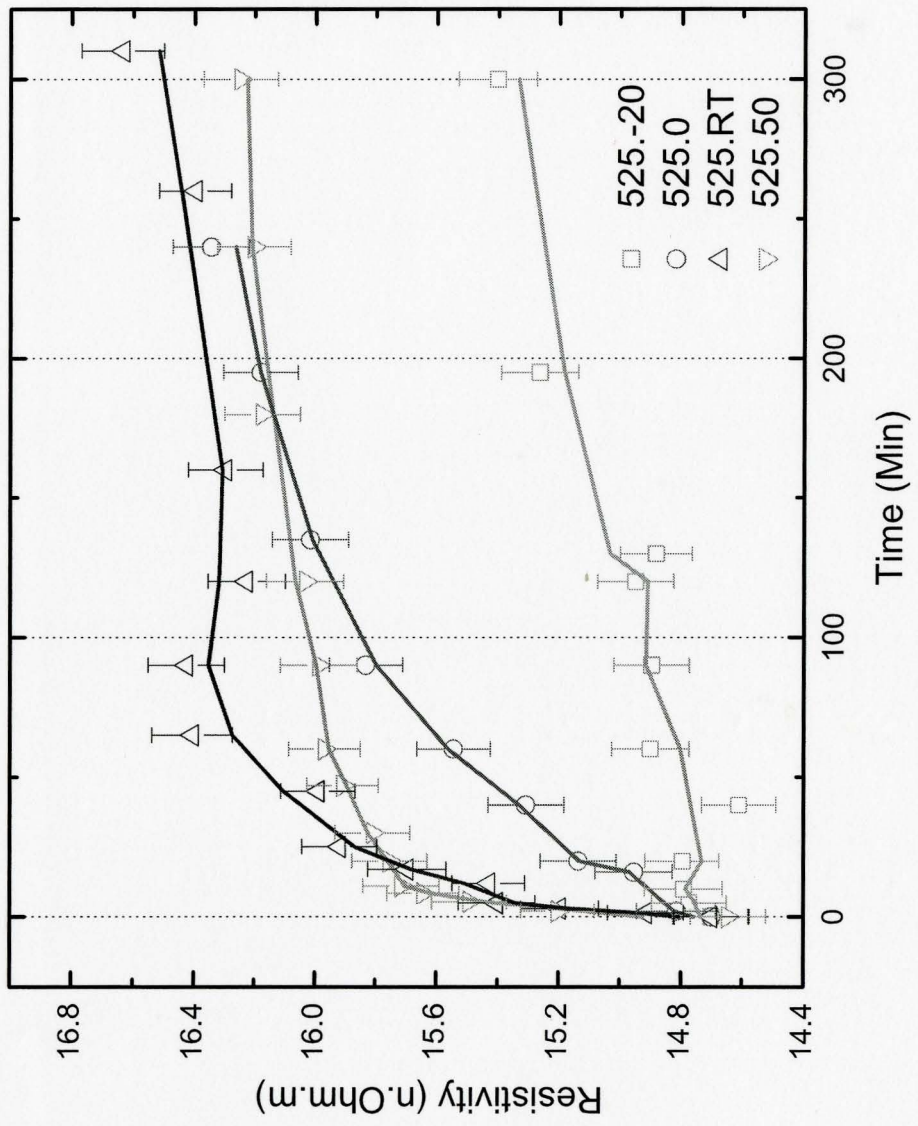

Figure 5.6: Electrical resistivity evolution of 525°C samples during short ageing times. Note that X axis is in the linear scale.

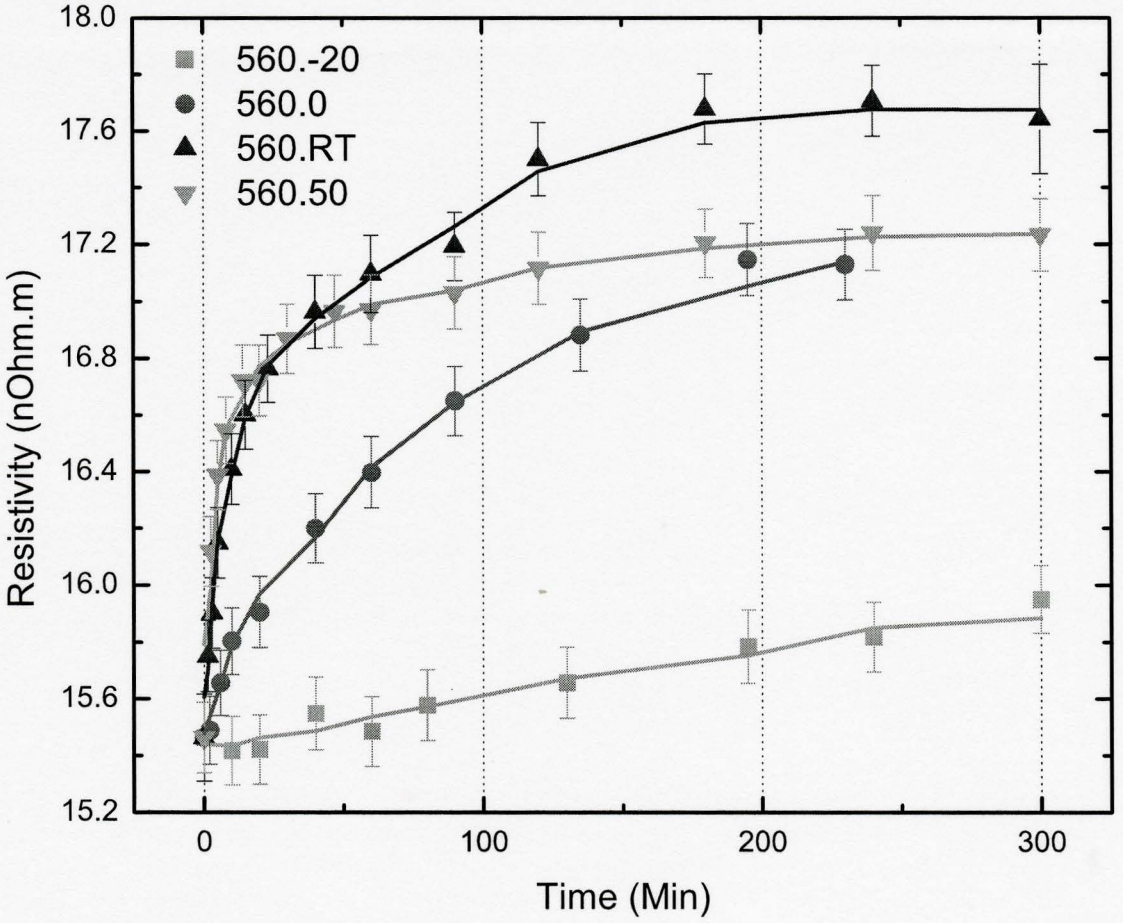

Figure 5.7: Electrical resistivity evolution of 560°C samples during short ageing times. Note that X axis is in the linear scale.

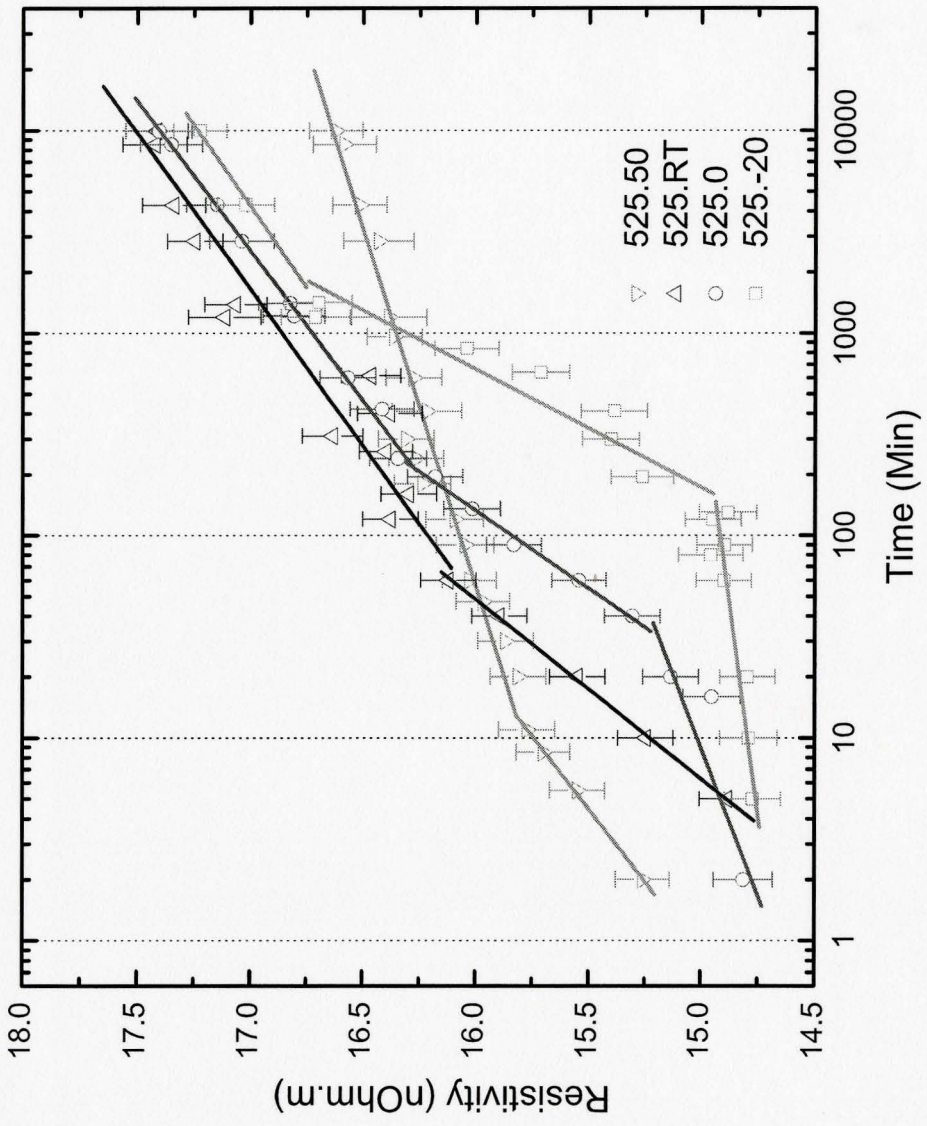

Figure 5.8: Electrical resistivity evolution of 525°C samples during long ageing times. Note that X axis is in the logarithmic scale.

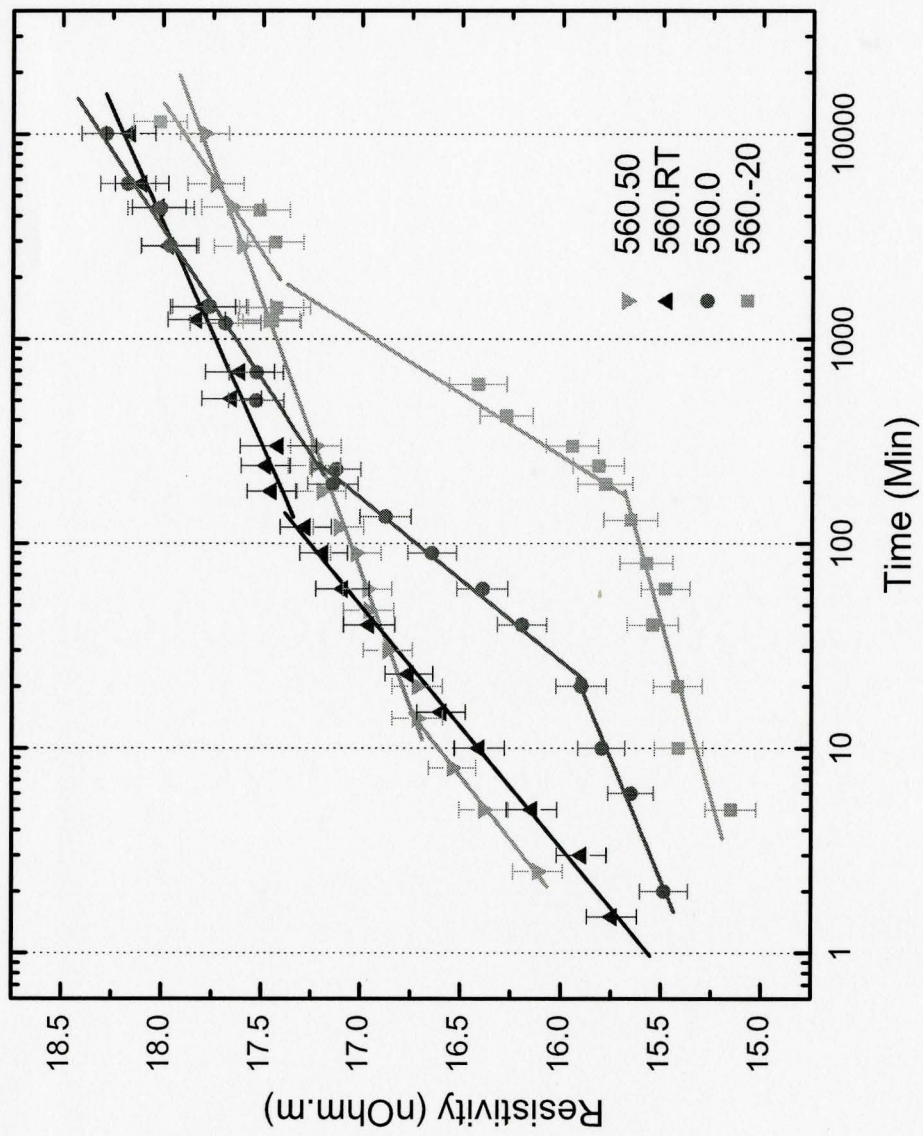

Figure 5.9: Electrical resistivity evolution of 560°C samples during long ageing times. Note that X axis is in the logarithmic scale.

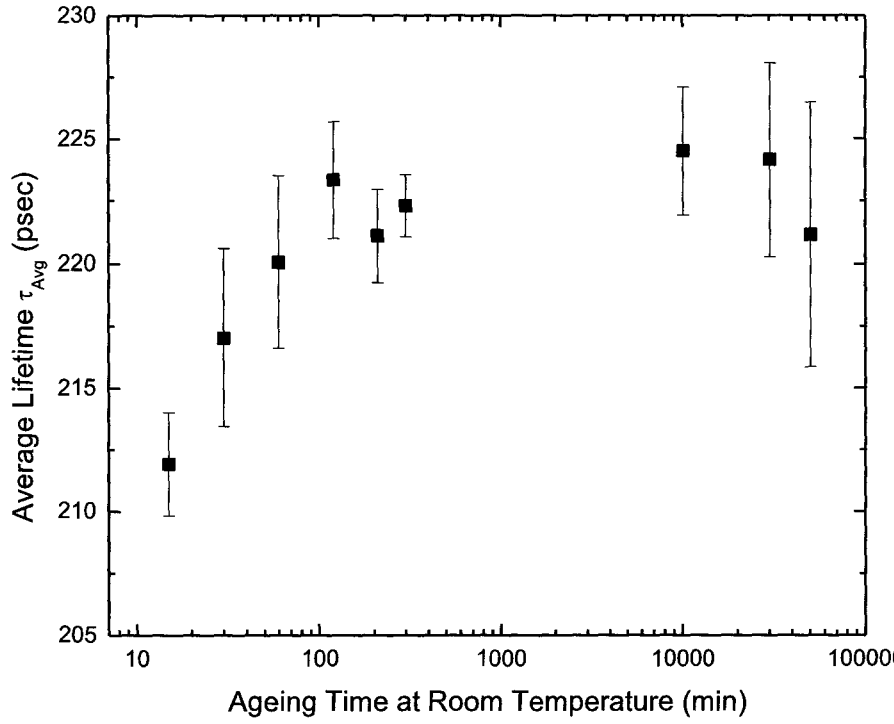

Figure 5.10: Evolution of average positron annihilation lifetime by ageing time at room temperature.

Chapter 6

Discussion

6.1 Introduction

In this chapter, the results of experiments (shown in chapter 5) will be interpreted and discussed extensively. This will be followed by a series of analysis on them. Finally a general model for the clustering of solute atoms in Al-Mg-Si alloys will be developed and explained based on the hardness, electrical resistivity and positron annihilation measurements.

6.2 Interpretations and Explanations

The first section of the discussion chapter will be devoted to the interpretation and explanation of results shown in chapter 5. This starts with the hardness test results first, in order to provide the general view of the effect of clustering on the macroscopic properties. Then the electrical resistivity measurements will be discussed. Finally the results of positron annihilation lifetime spectroscopy will be explained.

6.2.1 Hardness Test

Hardness test results are shown in figures 5.1 to 5.4. Generally, as ageing proceeds, hardness increases, however, the rate of increase is not always constant. There are three aspects to investigate here: effect of ageing time, effect of ageing

temperature and effect of solution treatment temperature on the hardness evolution.

Effect of ageing time:

As it was mentioned earlier, the hardness is generally increasing during ageing. At the beginning, the rate of increase is very fast, however, as ageing proceeds, the kinetics of ageing starts to slow down.

To explain the hardness increase, it is required to recall the theoretical background about the contribution of clusters to the overall hardening in 6xxx alloys. This can be written as:

$$\sigma_{cluster} = C_{cluster} \cdot (r \cdot f_{r.cluster})^{1/2} \tag{6.1}$$

where $C_{cluster}$ is a constant, r is the radius of the cluster and $f_{r.cluster}$ is the relative volume fraction of clusters which is defined in equation 2.13. Knowing this, the interpretation of figures 5.1 and 5.2 is trivial: as ageing proceeds, the volume fraction and size of clusters increases and according to equation 6.1, material becomes harder.

Based on the above discussion, it seems that the kinetics of clustering can be found from the hardness results using equation 6.1 and figures 5.1 and 5.2. This will be done later in section 6.3. The reason behind the change in the kinetics of clustering can be best understood by considering the results of the electrical resistivity measurements and positron annihilation lifetime spectroscopy, however at this point, as a hypothesis, this might be explained as the following way:

After quenching the sample, the quenched-in vacancies start to move towards annihilation sinks in order to bring their concentration to the equilibrium value. However due to the existence of strong binding energies between vacancies and solute atoms (Panseri et al. 1963 and Ozawa and Kimura 1970), Mg and Si atoms bind with the vacancies, in other words clusters start to form. While vacancies continue

their way toward sinks, more and more solute atoms attach to them and therefore clusters grow. At the same time this slows down the vacancies (Panseri et al. 1963 and Ozawa and Kimura 1970) and consequently rate of clustering will decrease.

Effect of ageing temperature:

Higher ageing temperatures increase the diffusion rate of vacancies and solute atoms. This should result in a faster kinetics of clustering. Indeed, this is what happened in the hardness results. In the both series of 525 and 560°C samples, increasing the ageing temperature resulted in a faster kinetics of cluster formation, e.g. samples aged at 50°C reached to almost saturated level of hardness after about 300 minutes while -20°C samples barely showed any sign of considerable hardness increase at the same period. Note that during short ageing times the hardness of samples aged at higher temperature is almost always higher than that of the one aged at lower temperature. However at the longer ageing times hardness values of all samples start to get very close to each other and finally after a very long ageing (6 days) they will all have almost the same hardness (see figures 5.3 and 5.4). This can not be simply explained by the results of hardness tests and therefore it will be discussed later in section 6.2.3 along with the interpretation of electrical resistivity measurements.

Effect of solution treatment temperature:

As it was mentioned earlier in chapter 4 section 4.3, the motive behind choosing two different solution treatment temperatures is to produce two different concentrations of excess quenched-in vacancies in the matrix prior to ageing and therefore provide the chance to see the effect of vacancies on the clustering process.

By comparing figures 5.1 and 5.2 two observation can be made for ageing at

short times:

- For the same ageing time and temperature, the hardness of 560°C samples is always higher than that of the 525°C one.
- For the same ageing time and temperature, the ageing kinetics becomes faster for 560°C samples compared to 525°C ones.

From these observations it can be concluded that the solution treatment temperature shifts the hardness of materials to higher level and at the same time accelerates the rate of hardness increase. This can be simply understood by the concepts of quenched-in vacancies mentioned earlier in the discussion about the effect of time on hardness evolution. For the same composition of alloy, when the concentration of vacancies is higher (owing to the higher solution treatment temperature), for the same time and ageing temperature, a higher number of clusters can be formed. However for the same alloy composition with a given ΔH_v^m, formation speed of each of the clusters remains constant since vacancy migration depends on the ageing temperature only. It should be mentioned that the concentration of solute atoms are several orders of magnitude higher than that of the vacancies and therefore the number of vacancies defines the number of clusters that are formed. This will also make the vacancy-vacancy interaction insignificant (at least at short ageing times) since there is a considerably higher number of solute atoms around each vacancy which will result in the entrapment of most vacancies at very short times before they reach other vacancies.

From all of above it can be concluded that in the samples which are solution treated at higher temperature, more clusters will form at the same time (although the speed which each cluster forms remain constant) and therefore the kinetics becomes faster. The reason that the general level of hardness is also higher for 560°C samples

can be understood by considering the concepts of Si and Mg clustering immediately after (or even during) quenching. It was mentioned by Murayama et al. (1998) that during quenching Si and Mg clusters form. Since 560°C samples have higher concentration of vacancies, more clusters can form and this brings the initial hardness of the material to higher values and consequently elevates the overall hardness to higher levels.

In the long ageing time plots (figures 5.3 and 5.4) the general trend of hardness increase by time is observed again. However it is shown that for all of samples, as ageing proceeds, the rate of the hardness increase starts to slow down. The reason behind this is the decrease in vacancies migration speed due to the binding of solutes. This was discussed earlier in "Effect of ageing time" part.

The very interesting point in the results of long term ageing is the case of very long ageing time (6 days) where both series of samples (525 and 560°C), reached to the same hardness value. This can not be explained only with the results of hardness test and required other experiments to provide more information about clusters and vacancies. Therefore the complete discussion of this phenomenon will be given in section 6.2.3 where the electrical resistivity results are interpreted.

6.2.2 Tensile Test Results

Tensile tests were performed on 560.RT samples which were aged for up to 300 minutes. After each test, the yield stress of sample was found by using the 0.2% proof stress technique (see section 4.4.2) and then plotted against ageing time (section 5.3). The result were shown in figure 5.5a. By comparing this figure with the hardness measurmeent results of 560.RT sample (figure 5.2) it can be found that the evolution of yield stress is analogous to that of the hardness. This is not surprising since the mechanism responsible the change in both of these properties is the cluster

formation. The purpose of tensile test in this project however, was not similar to that of hardness measurements. Evolution of yield stress by time was used to find the relationship between hardness and yield stress of samples so that the mechanical modeling of results can be done in order to find kinetics of clustering. This is done in section 6.3.1.

In order to find the relationship between σ_{ys} and hardness values, these parameters are plotted against each other (each point corresponds to the sample with the same ageing history). The results were shown in figure 5.5b. As it was expected there is a linear correlation (with R^2=0.989) between hardness and yield stress which is:

$$\sigma_{ys} = 2.267 \text{ HRH} - 110.359 \tag{6.2}$$

where HRH is the hardness value in Rockwell H scale. Note that the hardness of a sample not only depends on the yield strength of specimen but it is also affected by the work hardening properties of the material. Since all hardness measurements were performed at the room temperature, the effect of work hardening is the same for all samples and consequently equation 6.2 can be used for all of the ageing temperatures.

6.2.3 Electrical Resistivity Measurements

The results of electrical resistivity measurements which were shown in figures 5.6 to 5.9 are very similar to those of the hardness tests. As ageing proceeds, the resistivity increases. This increase is very fast at the beginning and then slows down at longer times.

In this section the resistivity plots are interpreted and explained in a manner similar to that which was used in section 6.2.1 for hardness measurements: first, the

effect of time on resistivity is discussed. Then the influence of ageing temperature and solution treatment temperature on resistivity is interpreted and explained.

In the long term ageing plots, where the time is expressed in the logarithmic scale, it can be seen that a linear relationship can be fitted to the experimental data with an acceptable accuracy. This was also observed earlier by Lloyd and Gupta (1997). This can be explained by making few assumptions:

1. The growth of clusters can be treated in a manner similar to the "Diffusion-controlled growth" of precipitates.

2. The effective diffusion coefficient of vacancies is a decreasing function of number of atoms bound with them (n). If the chance of the vacancy jumping away from a solute atom is proportional to $exp(\frac{-E_b}{R.T})$, where E_b is the vacancy-solute binding energy, then for n atoms the probability becomes equal to $exp(\frac{-E_b}{R.T})^n$ and the effective diffusion coefficient of vacancies can be described as:

$$D^v_{eff} \propto D^v.\exp(\frac{-nE_b}{R.T}) \tag{6.3}$$

The exponential relationship between diffusion coefficient and binding energy was previously mentioned in the literature (for example Fujikawa et al. 1978) which is in agreement with the argument made in this project.

The number of solute atoms in a cluster is proportional to the radius of cluster (r) by:

$$n \propto (\frac{r}{r_0})^3 \tag{6.4}$$

where r_0 is the solute atom radius. However, in order to simplify calculations, equation 6.4 will be approximated into (one dimensional consideration) :

$$n \propto \frac{r}{r_0} \tag{6.5}$$

Now by substituting equation 6.5 into 6.3, it can be concluded that the effective diffusion coefficient of vacancies is an exponentially decreasing function of cluster size (r):

$$D^v_{eff} \propto D^v.\exp(\frac{-E_b}{R.T}.\frac{r}{r_0}) \tag{6.6}$$

The growth rate of a precipitate is equal to: (Cahn and Haasen 1983)

$$\frac{\mathrm{d}r}{\mathrm{d}t} = \frac{D}{r}\frac{C_0 - C_i}{C_\beta - C_i} \tag{6.7}$$

where D is the diffusion coefficient, r is the precipitate size and C_0, C_i and C_β are the concentrations of solute in bulk matrix, interface and precipitate respectively. Assumption (1) leads to C_i=C_{alpha} (where C_{alpha} is the concentration of solute in the equilibrium matrix). Now equation 6.7 can be re-written to:

$$\frac{\mathrm{d}r}{\mathrm{d}t} = \frac{D}{r}.\frac{C_0 - C_\alpha}{C_\beta - C_\alpha} = \frac{D}{r}.\Omega \tag{6.8}$$

where Ω is $\frac{C_0 - C_\alpha}{C_\beta - C_\alpha}$. From equation 6.6, equation 6.8 can be written as:

$$\frac{\mathrm{d}r}{\mathrm{d}t} \propto \frac{\exp(\frac{-E_b}{R.T}.\frac{r}{r_0})}{r}.\Omega \tag{6.9}$$

which can be re-arranged into:

$$\exp(\frac{+E_b}{R.T}.\frac{r}{r_0}).\frac{r}{\Omega}.\mathrm{d}r \propto \mathrm{d}t \tag{6.10}$$

By integrating equation 6.10, relationship between r and t can be found:

$$t \propto \frac{R.T.r_0}{E_b.\Omega}(r - \frac{R.T}{E_b}.r_0).\exp(\frac{E_b.r}{R.T.r_0}) \tag{6.11}$$

or:

$$\ln(t) \propto K + \ln(r - \frac{R.T}{E_b}.r_0) + \frac{E_b.r}{R.T.r_0} \tag{6.12}$$

where K is $\frac{R.T.r_0}{E_b.\Omega}$. Now if the cluster size becomes larger than $2.R.T.r_0/E_b$, then the $\ln(r - \frac{R.T}{E_b}.r_0)$ term in equation 6.12 becomes much smaller than the third term in that equation $(E_b.r/R.T.r_0)$ and therefore it can be neglected. For Mg the solute-vacancy binding energy equals to 0.12ev (Boileau et al. 1981) or ~11560 J/mol. This is also the same for Si atoms (Kim et al. 1974). For ageing at room temperature $2.R.T.r_0/E_b$ is then approximately equal to $0.21r_0$. Consequently this condition is always satisfied and the $\ln(r - \frac{R.T}{E_b}.r_0)$ term in equation 6.12 can be ignored and the equation simplifies to:

$$\ln(t) \propto \frac{E_b.r}{R.T.r_0} \tag{6.13}$$

Equation 6.13 shows that the linear relationship with ln$t$ can be found for cluster growth and therefore the resistivity which is related to clustering can be expressed with $\rho = K\ln t + c$ relationship.

In all of the samples, at least two (sometimes three) different linear fits with a clear transition between them exist. This is due to the complex, multi-factor nature of resistivity signal which will be discussed in the next paragraphs.

Unlike the hardness test, interpretation of resistivity signal is not easy. As it was mentioned earlier in section 4.4.1, the resistivity signal during clustering can be due to various factors which include vacancies, solute atoms and clusters. The concentration of vacancies is generally decreasing during ageing in order to reach

to the equilibrium value. Also as time proceeds, the matrix becomes depleted from solute atoms since Mg and Si atoms are forming clusters. Both of these will result in a resistivity decrease of the sample. However cluster formation can increase the resistivity of material since clusters, although very small in size, can act as scattering centers. Therefore it can be concluded that the clustering signal is a result of these three competing effects and finding the clustering characteristics requires the removal of the vacancies and solute depletion contribution from the overall resistivity signal.

Before proceeding to the interpretation of the data, it is beneficial to list the transition times and resistivities as well as the linear constants (in equation 5.2) for each of the linear fits shown in figures 5.8 and 5.9. This is done in tables 6.1 and 6.2.

Table 6.1: Transition times for different stages of the resistivity change. Time and resistivity values are in minutes and nOhm.m respectively.

Ageing	Sol. Treatment	Stage One	Stage Two		Stage Three	
Temp. (°C)	Temp. (°C)		Time	Resistivity	Time	Resistivity
-20	525	YES	160	14.95	1900	16.78
	560	YES	169	15.66	1942	17.41
0	525	YES	30	15.18	210	16.27
	560	YES	23	15.93	255	17.23
RT(~20)	525	NO	—	—	60	16.2
	560	NO	—	—	75	18.95
50	525	NO	—	—	13	15.8
	560	NO	—	—	14	16.73

Effect of ageing time:

The general trend in resistivity results of all samples is the increase in resistivity over ageing time. The speed of it, however, is not constant. As it can be seen in figures 5.8 and 5.9, three different stages are present in the resistivity plots. The appearance of three stages depends on the ageing temperature. For example in the 50°C samples only the last two steps can be detected. The existence of three stages in resistivity plots is very interesting and has never been reported before in the liter-

Table 6.2: Values of K and C constants for different stages of ageing when the resistivity follows a simple relationship of $\rho = K\ln t + C$. K and C are in the nOhm.m units while time is in minutes.

Ageing	Sol. Treatment	Stage One		Stage Two		Stage Three	
Temp. (°C)	Temp. (°C)	K	C	K	C	K	C
-20	525	0.0528	14.673	0.7443	11.165	0.2713	14.735
	560	0.1268	15.030	0.7104	12.033	0.2936	15.190
0	525	0.1497	14.672	0.5644	13.242	0.2943	14.693
	560	0.1854	15.349	0.5451	14.214	0.2926	15.615
RT(~20)	525	—*	—*	0.49504	14.098	0.2814	14.917
	560	—*	—*	0.3822	15.540	0.2088	16.290
50	525	—*	—*	0.3028	15.046	0.1228	15.506
	560	—*	—*	0.3494	15.807	0.1641	16.297

* This stage was not observed due to its very fast kinetics.

ature. However, it is possible to explain it by using the concept of excess quenched-in vacancies discussed earlier in section 6.2.1.

After quenching from the solution treatment temperature, excess quenched-in vacancies start to move towards the sinks (e.g. grain boundaries and dislocations) in order to bring their concentration down to the equilibrium value. At the very beginning of ageing, vacancies which are located near the annihilation sites (i.e. sinks) are annihilated with/without formation of clusters. At the same time other vacancies which are further away from sinks bind with solute atoms due to the very high binding energy between them (Panseri et al. 1963 and Ozawa and Kimura 1970). The annihilation of near-sink vacancies produces a sharp decrease in a resistivity which cannot be totally compensated by the increase in resistivity due to the formation of very small clusters at short times. Therefore in the first stage, the increase in resistivity is not very fast. However once these near-sink vacancies are annihilated from the matrix, the remaining ones continue to bind with other solute atoms. This results in more extensive cluster formation. So during the second stage, the vacancies annihilation contribution is smaller than stage I because most of the near-sink vacancies were annihilated before in stage I while the remaining ones are still inside the matrix

and they are becoming trapped by solute atoms. So the end result is the increase in the resistivity of sample with faster kinetics than the first stage simply because of the smaller contribution of vacancies annihilation.

It was mentioned in chapter 2 that the electrical resistivity measurements of Chatterjee and Entwistle (1973) and Kovacs et al. (1972) showed an initial decrease in resistivity during ageing at low temperatures (for example the 0°C ageing shown in figure 2.14). This was not observed during ageing at higher temperatures (Above 15°C according to Kovacs et al. (1972)). The interpretation given by both of these research groups was that the initial drop in resistivity is due to the formation of silicon clusters while the following increase is due to the formation of Mg clusters. In this research, however, the decrease in resistivity was not observed. It is possible that since in the research of Chatterjee and Entwistle and Kovacs et al., the concentration of solute atoms was much smaller than that of this research, the fast decrease due to near-sink annihilation of vacancies could not be compensated by limited clustering of Si and/or Mg atoms. However in this project, higher solute contents resulted in more extensive clustering and therefore slower, yet positive slope of resistivity change in stage I. Note that the very fast formation of Si and Mg clusters (even during quenching) was observed by various researchers before. For example using atom probe technique, Murayama et al. (1998) found the appearance of Si and Mg clusters in the as-quenched sample.

In all samples, a transition from fast (stage II) to slow (stage III) clustering was observed. This happens at shorter times when samples are aged at higher temperatures. There are two possible explanations for this transition. In this section, these possible mechanisms are just mentioned while their validity will be checked later in section 6.4 where the results of all experiments are discussed together.

Hypothesis (1): As ageing proceeds in the second stage, vacancies start to

slow down as they are bound with the solute atoms. The more solutes they bind with, the slower they become on their way towards sinks. It is also possible that due to the existence of very strong binding energy between vacancies and clusters (Federighi and Thomas 1962), any vacancy (or vacancy-solute) pair that arrives at the site of other cluster becomes trapped inside that cluster. Eventually a point will be reached when all vacancies would become bound with the solutes and therefore further clustering happens very slowly since mobility of vacancies inside clusters has been severely decreased. At this point the transition from stage II (fast) to stage III (slow) happens. This is in agreement with the model which was proposed by Panseri and Federighi (1966) and used later by Esmaeili et al. (2000).

Hypothesis (2): It is well known that precipitation of one phase, depletes the matrix from solutes. Therefore it is plausible that clustering also results in a Si and Mg depletion from Al matrix. According to equation 6.8, the clustering rate (or cluster growth rate) depends on the concentration of the matrix in addition to the diffusion coefficient (which in the case of vacancy assisted migration of solute atoms in clustering is a decreasing function of time). By assuming the "Diffusion-controlled" mechanism for cluster growth, the solute distribution around one cluster can be found. This was done schematically in figure 6.1.

Now if the diffusion field of one cluster (i.e. the solute depleted area around a cluster) meets that of an another cluster, then obviously these two clusters will interact with each other since now migration of solute decreases the concentration of matrix between the two clusters (to the values of less than C_0). Consequently according to equation 6.8, the growth rate decreases further. So it can be possible that after a certain time, clusters reach to a size that they start to affect each other's growth rate. This will be regarded as the "Soft impingement of clusters" in this project. The validity of these mechanisms will be checked later when the results of

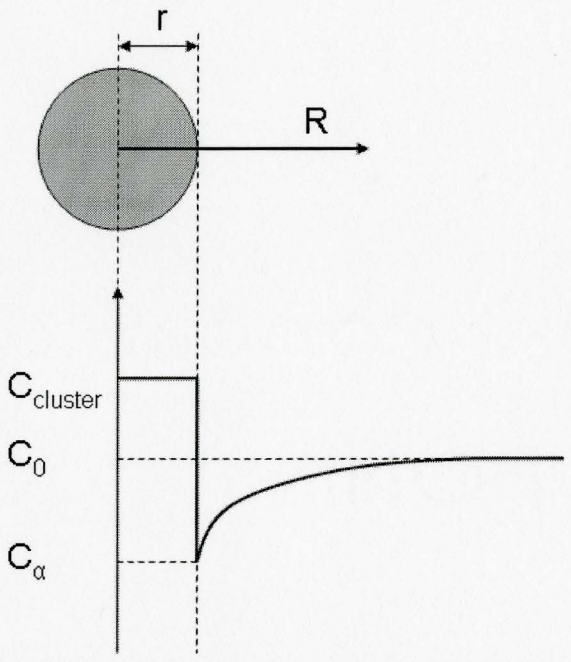

Figure 6.1: The schematic of solute distribution around a cluster (Adopted from Cahn and Haasen (1983).

all experiments are compared together in section 6.4.

Note that the electrical resistivity results of Panseri et al. (1963) showed that in the presence of Mg atoms, excess quenched-in vacancies are retained in the matrix during ageing at temperatures of up to 100°C. This clearly rejects any speculations that the transition from stage II to III happens because of vacancy annihilation. The positron annihilation result of the present research (shown in figure 5.10) also seems to be in agrement with this since during ageing at room temperature, no sign of considerable decrease in lifetime was observed (in stages II and III).

Effect of ageing temperature:

The effect of ageing temperature on the resistivity is rather similar to that of hardness. By increasing the ageing temperature, the resistivity increase becomes higher. This is due to the faster kinetics of cluster formation at higher tempera-

tures (at least during short ageing times) because of the increased migration speed of vacancies.

By looking at tables 6.1 and 6.2, the effect of ageing temperature on clustering can be better understood. There are few points to explain here: First, the transition times are always shorter when ageing happens at higher temperature. The higher ageing temperature results in a higher vacancies diffusion coefficient and their faster migration towards sinks. Since it is well accepted that the clustering process is controlled by vacancies (refer to section 2.3.2 in chapter 2), any transition should happen earlier at higher temperatures.

Second, the resistivity at the stage II to III transition point, in samples with the same solution treatment temperature, is higher when the ageing temperature is lower (see table 6.1). This behavior was also observed in the literature where it was suggested that this is related to the smaller number of clusters formed at higher temperatures (Panseri and Federighi 1966). The smaller number of clusters at higher ageing temperatures seems to be in agreement with the general precipitation theories where the nucleation driving force is expected to becomes larger at lower temperatures. The other point to consider is that if hypothesis (1) for transition from stage II to III is supposed to be valid, then it is expected that due to the slower diffusion of vacancies (and solute atoms) at low temperatures, smaller number of solute atoms will be required to slow down the vacancies. In other words, the onset of stage III starts with smaller clusters (yet more in number) at lower temperature. This also results in less solute depletion from matrix in the case of lower annealing temperature. So it can be concluded that due to the higher number of clusters and lower contribution of solute depletion, the overall resistivity at the transition point is higher for the case of samples aged at lower temperature. This phenomenon can also be explained by another mechanism. It is possible that since the migration speed

of vacancies are faster at higher temperatures, more vacancies can annihilate during first stage of clustering. This can result in less number of clusters (see figure 6.2) in 50°C sample. Consequently, it might be possible that the specimen aged at higher temperature would have lower resistivity than the one aged at lower temperature.

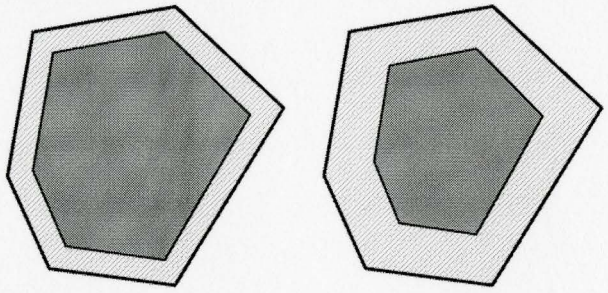

Figure 6.2: Schematic of the vacancies depleted regions (shown with light shade) after the stage I of clustering at (a) -20°C (b) 50°C. The darker areas are where clustering continues to happen during stages II and III.

Effect of solution treatment temperature:

The first obvious effect of the solution treatment temperature on the resistivity data is shifting of the resistivity plots to the higher levels when the solution treatment temperature is increased. The higher concentration of excess quenched-in vacancies in the 560°C sample, will result in larger number of Si/Mg clusters to form immediately after or during quenching and therefore shifting the resistivity plot to higher level. In addition to this, the larger number of vacancies present in the 560°C samples also results in the higher resistivity directly (recall the very high resistivity coefficient of vacancies from table 2.1).

As it can be seen in table 6.1, the transition between stage one and two happens at the same time for both 525°C and 560°C samples. Assuming that no vacancy loss is happening during quenching and according to the calculations done in chapter

4, the concentration of excess quenched-in vacancies in samples solution treated at 560°C should be 1.5 times higher than those solutionized at 525°C. However since the material is solution treated, the distribution of vacancies is homogenous within the matrix and therefore not all of these extra vacancies occupy the near-sink locations. Also note that plenty of annihilation sinks (such as grain boundaries or dislocations) exist within the sample. Consequently the change in the number of vacancies should not result in delay of their annihilation. From all this it can be concluded that the transition time from stage I to II should not change considerably by changing the solution treatment temperature.

The transition times from stage II to stage III, also remain almost constant by changing the solution treatment temperature. Hypothesis (1) for mechanism of transition from stage II to III can explain this. The growth rate of clusters in stage II depends on the migration speed of vacancies which itself depends on the ageing temperature. Therefore at the same ageing temperature, the growth rate remains constant regardless of number of clusters (or vacancies). Note that since the composition of alloy is the same for both solution treatment temperatures, and this concentration is always higher than that of the vacancies, enough solutes are always present in the matrix for clusters to form. Consequently the time which clusters need for reaching a certain critical size (that is required for transition from stage II to III) remains constant with changing solution treatment temperature and therefore the transition happens at the same time. The Hypothesis (2), which assumes that the transition from stage two to three is because of the soft impingement of clusters, can not explain the same transition times for different solution treatment temperatures. In this mechanism it is supposed that when the clusters reach a certain size, their diffusion fields can interact with each other and stage III start. However if there are more clusters inside the matrix (due to higher concentration of excess quenched-in

vacancies), it is expected that the diffusion fields around clusters start to interact with each other earlier since the distance between them is smaller. Consequently the transition should happen much earlier in 560°C samples (where the concentration of vacancies is 1.5 times higher) which is opposite of what it was observed in resistivity results.

6.2.4 Positron Annihilation

The change in mean life time of positrons during ageing of the 560.RT samples is shown in figure 5.10. As it can be seen, at the beginning of ageing, the lifetime starts to increase slightly and then it reaches a constant value after about 60-70 minutes. Note that the lifetimes before 15 minutes of ageing cannot be measured due to the technical constraints in the positron annihilation setup.

The mean lifetime of positrons is always higher than the bulk lifetime of pure aluminum (163psec) but is lower than the mono-vacancy lifetime in Al (244psec) (Sterne and Kaiser 1991).

The increase in lifetime at the beginning of ageing can be understood better by looking back at the 560.RT hardness and resistivity curves shown in figures 5.4 and 5.9 respectively. As it was discussed earlier in sections 6.2.1 and 6.2.3, at the beginning of ageing, vacancies move toward sinks in order for matrix to reach to the equilibrium concentration of vacancies. However due to the existence of high binding energy between the vacancies and solute atoms, vacancies attach to Si and Mg atoms and start to form clusters (stages I and II). This process slows down as ageing proceeds since the mobility of vacancies decreases rapidly by attachment of solute atoms to them. Finally the kinetics of clustering decreases considerably after a short period of time although clustering stills continues (Transition from stage II to III). For 560.RT samples, stage I (rapid decrease in number of vacancies) is so fast

that it can not be detected by resistivity measurements. It is expected that during stage I, the mean positrons lifetime of specimen decreases rapidly and indeed this is what was observed in various Aluminum alloys (Reich et al. 2001 and Dupasquier et al. 2004).

The stage II of resistivity increase remains active until about 60-70 minutes. It is very interesting that the increase in positron lifetime stops at around 100 minutes of ageing which is very close to the time when transition from stage II to III happens in the resistivity plots. This means that almost all of the the increase in positron lifetime happens during the second stage of resistivity change. With this background, the reason behind the increase in lifetime can be understood. In stage II the concentration of vacancies is almost constant and as ageing proceeds more solute atoms attach to the clusters (i.e. clusters grow). When clusters are forming (or growing), the vacancies surroundings become rich in solute atoms. Positrons have higher lifetime near Mg and Si atoms (see table 2.2) so the vacancies trapped inside clusters will also have higher lifetime since the environment is now rich in solutes. Therefore as long as clusters are growing, the lifetime is also increasing. This is in agreement with the results of Bharathi and Sundar (1992) who observed that the positron lifetime in Al-Mg alloys increases by the formation and growth of Mg clusters.

After 60-70 minutes of ageing (stage III of resistivity change), the growth rate of clusters becomes very small. Regardless of the mechanism responsible for this, the vacancies surroundings (i.e. cluster composition) does not change significantly and therefore the lifetime remains constant.

It is also worth mentioning that the fact that the mean lifetime of positrons in the Al-Mg-Si sample is higher than 163psec of aluminum bulk lifetime (although significantly lower than 244psec of aluminum vacancies) proves that the clusters formed during natural ageing contain vacancies and indeed these vacancies play an important

role in their formation. If this was not the case then after a short period of time, the vacancies would have annihilated at the sinks and consequently the lifetime should have gotten closer to the 163psec value. This was also shown previously for the case of Al-Cu-Mg alloys (Dupasquier et al. 2004).

The sensitivity of positron annihilation lifetime to cluster formation was shown before in the literature (for example Reich et al. 2001, Buck et al. 1979 and Dupasquier et al. 2004). The results of this research, however, complement these by showing a correlation between positron lifetimes and resistivity changes during clustering.

6.3 Further Analysis

6.3.1 JMAK Modeling

It was discussed earlier that the hardening contribution of clusters can be explained by means of "Freidel's Statistical model" (refer to section 4.4.2 in chapter 4). In this approach the strengthening factor due to clustering is defined as:

$$\sigma_{cluster} = C_{cluster} \cdot (f_{r.cluster})^{1/2} \tag{6.14}$$

where C is constant and $f_{r.cluster}$ is the relative volume fraction of clusters defined in equation 2.13. Note that in this equation an average size is assumed for clusters which is incorporated in the constant C. This is not a very precise assumption since it will over-estimate the strength of small clusters and under-estimate it for larger cluster sizes. However, in general, a good approximation of cluster strength for qualitative analysis can be obtained by this assumption.

The constant C can be found by measuring the yield strength of a sample

naturally aged for a long time so that $f_{r.cluster} = 1$. The difference between the yield stress of this sample and an as-quenched sample is the approximately equals to C:

$$C_{cluster} = \sigma_{ys.NALong} - \sigma_{ys.AQ} \tag{6.15}$$

The yield stress of the alloy used in this project after 2 months of natural ageing is found to be 132MPa. So C can be calculated:

$$C_{cluster} = 132 - 59.5 = 72.5 \text{ MPa} \tag{6.16}$$

The hardness data can be converted to yield strength values by using equation 6.2. This conversion is valid for all of the samples since all of the hardness measurements were performed at room temperature. For more details refer to section 6.2.2 of this chapter.

Now the relative volume fraction of clusters can be calculated by re-writing equation 6.14:

$$f_{r.cluster} = (\frac{\sigma_{cluster}}{C_{cluster}})^2 \tag{6.17}$$

The Johnson-Mehl-Avrami-(Kolmogorov) equation (JMAK) is often used to describe the kinetics of phase transformation (Porter and Easterling 2001):

$$f = 1 - exp(-kt^n) \tag{6.18}$$

In this equation, f is the degree of transformation, k and n are constants and t is time. k and n are often used to characterize the transformation. If the mechanism of transformation remains the same within a range of temperature, n should remain constant while k should increase as temperature increases (Porter and Easterling

Table 6.3: JMAK constants from fitting the $f = 1 - \exp(-kt^n)$ equation into the experimental data.

Ageing Temp. (°C)	Solution Treat. Temp. (°C)	k	n
-20	525	0.00022	0.927
	560	0.00152	0.671
0	525	0.00247	0.761
	560	0.00204	0.708
RT	525	0.01151	0.578
	560	0.02609	0.461
50	525	0.07915	0.338
	560	0.18237	0.186

2001).

It was shown that the experimental relative volume fractions of clusters can be calculated using equation 6.17. Now if the JMAK relationship holds, then by plotting $ln(ln(\frac{1}{1-f}))$ versus $ln(t)$ a linear relationship should be found. Indeed, it was found that, considering the scattering in data, a line can be fitted into the experimental f_r when they are plotted in $ln(ln(\frac{1}{1-f}))$ versus $ln(t)$ format (see figures 6.3 and 6.4). The values of n and k for all fittings are listed in table 6.3. The JMAK predictions for the evolution of $f_{r.cluster}$ with time are shown in figure 6.5 along with the experimental data.

As it can be seen a relatively good fit can be observed between most of the experimental data and the JMAK model predictions. Note that the hardness data used in the calculation of volume fractions were very scattered and this might account for some discrepancies in the fits. From table 6.3 it is obvious that the k factor is generally increasing with ageing temperature. This is exactly what is was expected. However the values of n are not constant. This can be explained by the fact that the original JMAK model is based on the nucleation, growth and impingement phenomena

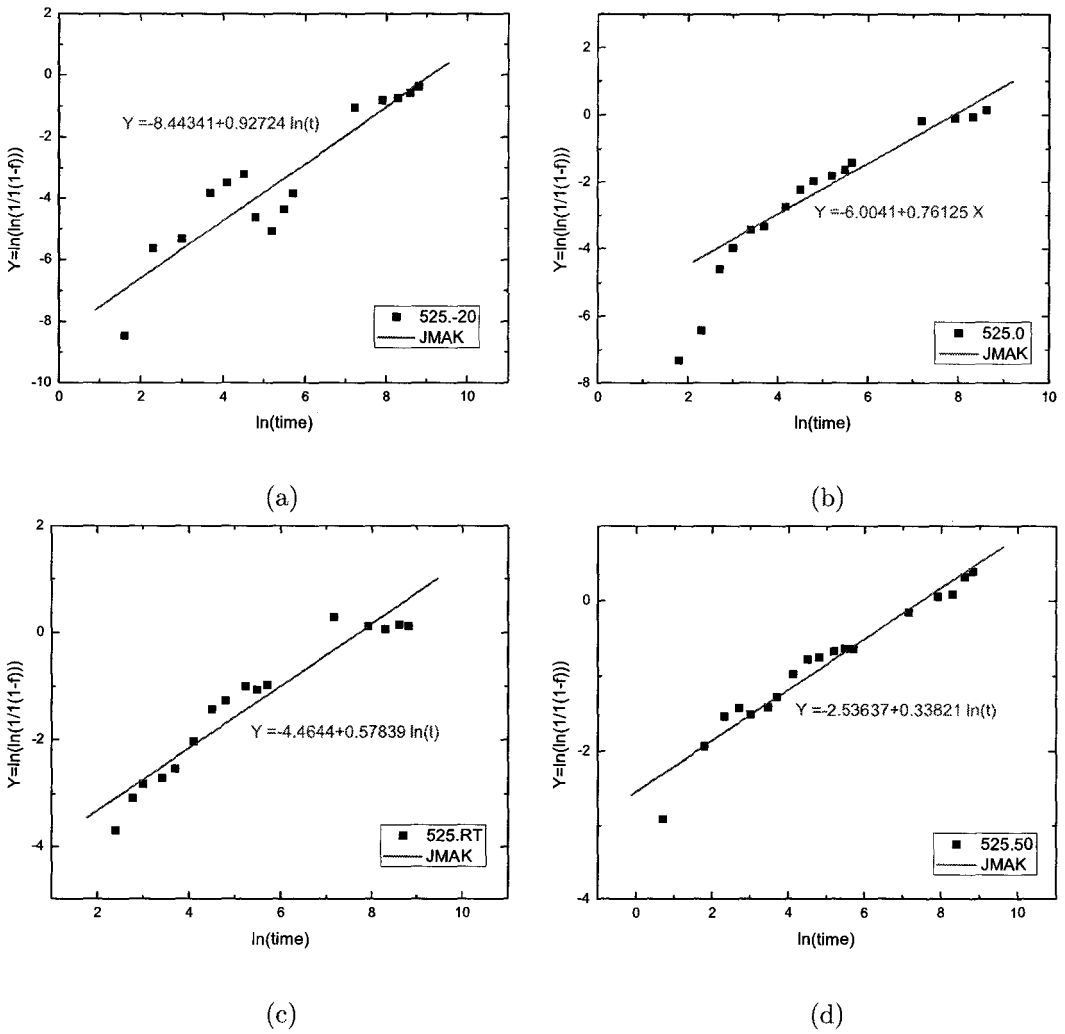

Figure 6.3: $\ln(\ln(\frac{1}{1-f}))$ versus $\ln(t)$ plots for (a) 525.-20 (b) 525.0 (c) 525.RT and (d) 525.50 samples. A relatively good linear fit can be made into the data. The slope of the lines equal to n while the y-axis interception equals to ln(k) in the JMAK equation of $f = 1-\exp(-kt^n)$. Note that time is in minutes in all of these figures.

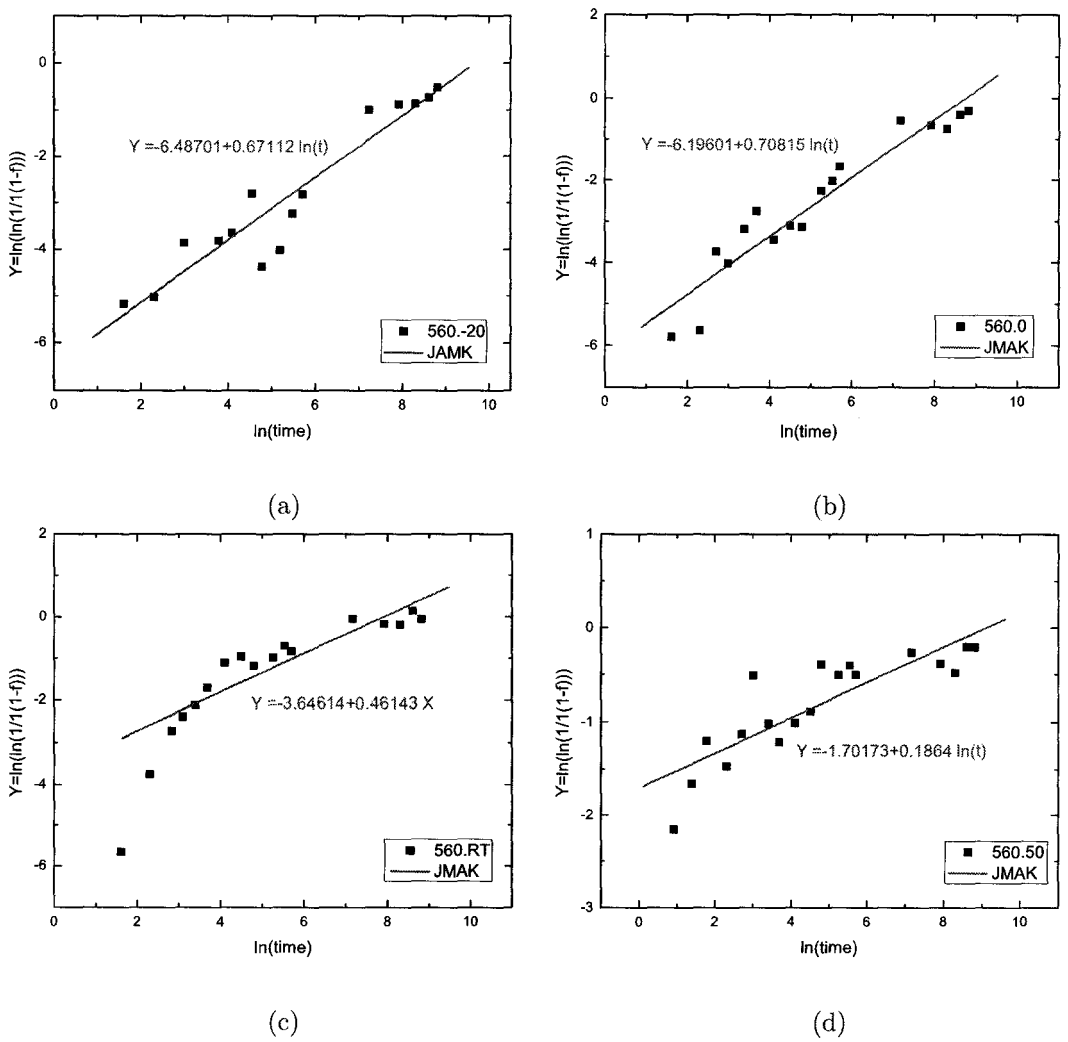

Figure 6.4: $\ln(\ln(\frac{1}{1-f}))$ versus $\ln(t)$ plots for (a) 560.-20 (b) 560.0 (c) 560.RT and (d) 560.50 samples. A relatively good linear fit can be made into the data. The slope of the lines equal to n while the y-axis interception equals to ln(k) in the JMAK equation of $f = 1-\exp(-kt^n)$. Note that time is in minutes in all of the figures.

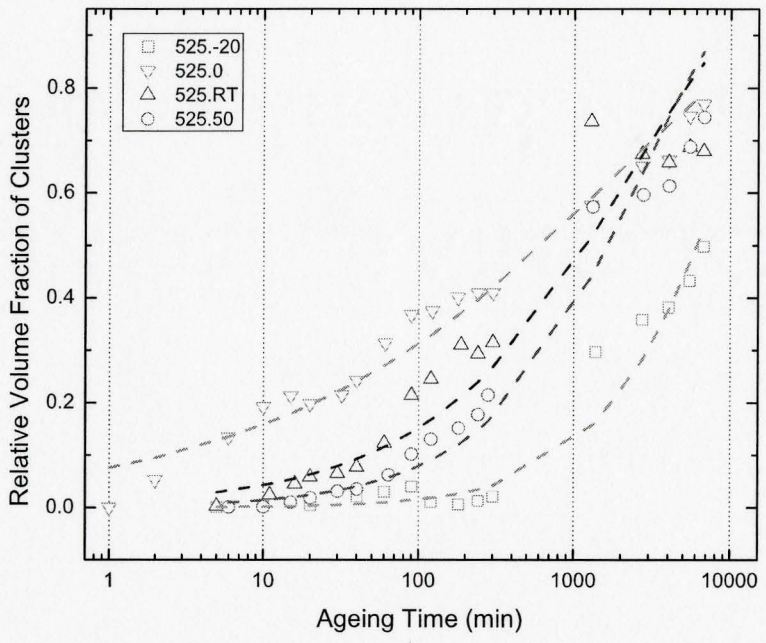

(a)

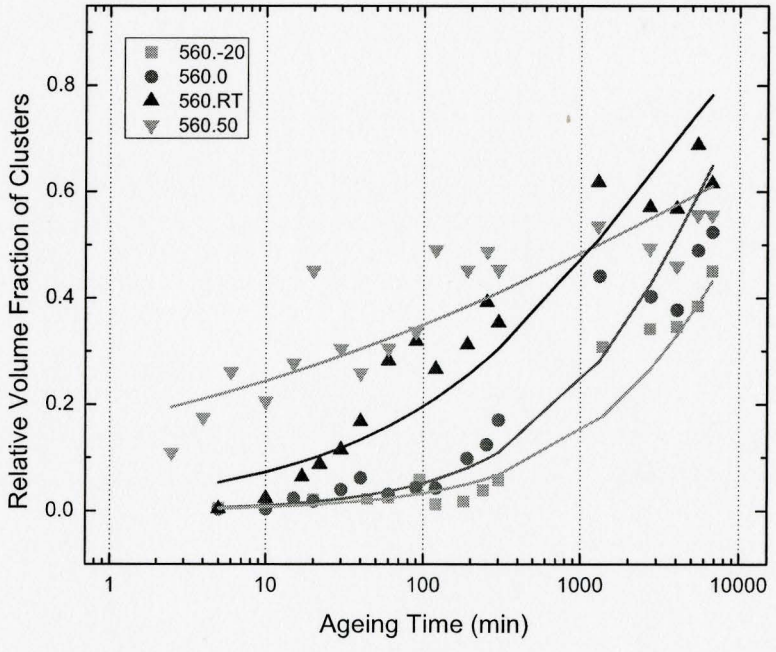

(b)

Figure 6.5: The evolution of clusters volume fraction with time in (a) 525 samples. Dashed lines are the JMAK model fittings. (b) 560 samples. Solid lines are the JMAK model fittings.

of phase transformation (Porter and Easterling 2001). It was shown by Sha (2005 and 2007) that the JMAK model can be used for other phase transformation processes even if it does not satisfy the physical basis of its derivation. So the results shown in this section does not bear any physical meaning and they just show the qualitative evolution of the clusters volume fraction with ageing time.

The JMAK model has been used by other researchers to fit the experimental data (such as Esmaeili et al. 2003a) and this is why it was also utilized in this thesis. However as it was discussed earlier, this modeling is simply a mean of fitting the experimental data and does not bear any other physical meaning.

6.3.2 Clustering Activation Energy Calculation

Several attempts have been made by other researchers to find the activation energy of clustering. For example using the DSC technique and for Al-0.63Mg-0.37Si-0.5Cu (wt%) alloy, Gaber et al. (2004) found the activation energy of clustering to be 53.3 kJ/mol. For Al-0.98Mg-0.58Si-0.33Cu (wt.%) and by using the same technique, (Doan et al. 2000) could not measure the activation energy of clustering due to overlapping peaks observed for cluster formations, however they detected a peak corresponding to the formation of vacancy clusters with an activation energy of 79kJ/mol. As it was mentioned earlier in section 2.3.2, this interpretation of data needs to be considered with extra care since, unlike Al-Si alloys, no evidence of vacancy cluster formation was observed in Al-Mg-Si alloys probably due to the very high binding energy between Mg atoms and vacancies.

Various studies have been done to measure the activation energy by using the electrical resistivity results. For example Sha (2006) tried to find this energy by plotting the change of resistivity for a given time versus temperature. His earlier results showed that this technique is useful in hardness data analysis. However this

was not the case for the resistivity measurements. He attributed this to the existence of more than one thermally activated mechanism during clustering. Indeed as it was shown in figures 5.6 to 5.9 and discussed in section 6.2.3, three different stages of clustering exist and therefore calculation of the activation energy from resistivity data is not possible by simply plotting $\Delta\rho$ vs. 1/T.

In order to find the clustering activation energy in this project, the cross-cut technique is utilized. This methods was used before by various researchers to calculate the activation energy of clusters (e.g. Juhasz et al. 1985) or GP-zones formation (e.g. Murty and Vasu 1971) in other alloys.

The procedure is very simple. The time ($\Delta\tau$) required for a constant increase in resistivity (during a single stage) is found for various ageing temperatures and then they are plotted (in the natural logarithmic scale) versus 1/T (Juhasz et al. 1985). Since the transition time follows the simple Arrhenius-type equation of $t = t_0 exp(-Q/RT)$ (Panseri and Federighi 1966), the slope of $ln\Delta\tau$-1/T curve is equal to the activation energy divided by R.

As it was mentioned earlier in section 6.2.3, three stages are present in the resistivity plots. The first stage is not always present in all of the ageing temperatures, however, stages II and III is observed in all samples. In stage II the concentration of vacancies is believed to be constant and therefore their contribution to the resistivity signal remains unchanged. This is why stage II is the only stage that might provide information about the clustering activation energy.

In order to perform the cross-cut technique, two $\Delta\rho$s of 0.5 and 1 nOhm.m were chosen. The reasons for this choice is as follows: If the increase in resistivity is very small, then, especially for case of the RT and 50°C ageing temperatures, the required time becomes very small (within few minutes). The transition times from stage I to II and II to III are found by simply fitting lines into the data as it was

Table 6.4: Stage II activation energies calculated using the cross-cut method with two different $\Delta\rho$ or 0.5 and 1 nOhm.m.

Solution Treatment Temperature	Activation Energy (kJ/mol)		Average
	$\Delta\rho$=0.5 nOhm.m	$\Delta\rho$=1 nOhm.m	
525°C	44.9	45.1	45.0
525°C	48.5	44.7	46.6
Average	46.7 ± 2.5	44.9 ± 0.3	45.8 ± 1.8

discussed earlier and this process (particularly in log scale) in not very accurate (error of several minutes). In addition to this, the resistivity measurements are also valid within few minutes. Therefore the resistivity change should be chosen as a value which results in a $\Delta\tau$ of higher than the error limit of measurements for all ageing temperatures.

The Plots of $\ln(\tau)$ vs. 1/T for $\Delta\rho$ =0.5 and 1 nOhm.m are shown in figures 6.6.a and 6.6.b respectively. In these figures the effect of solution treatment temperature is also shown. The activation energy can be found by multiplying the slopes of curves by R (8.314J/mol.K). The results are listed in table 6.4 for all four lines.

Within the acceptable range of error, the activation energy of clustering remains almost constant for both series of samples (525 and 560°C samples) and for both values of $\Delta\rho$. The latter finding confirms that the mechanism of resistivity increase during stage II is constant. The former finding, means that the mechanisms responsible for the second stage of clustering does not depend on the number of vacancies, i.e. it is independent of solution treatment temperature.

Using the DSC results, Gaffar et al. (2007) found that for the Si excess alloy, the activation energy of clustering is equal to 41.8 kJ/mol. This is very close to the 45.8 ± 1.8 kJ/mol value which is measured in this research.

Now it is necessary to calculate the activation energy of migration for Mg

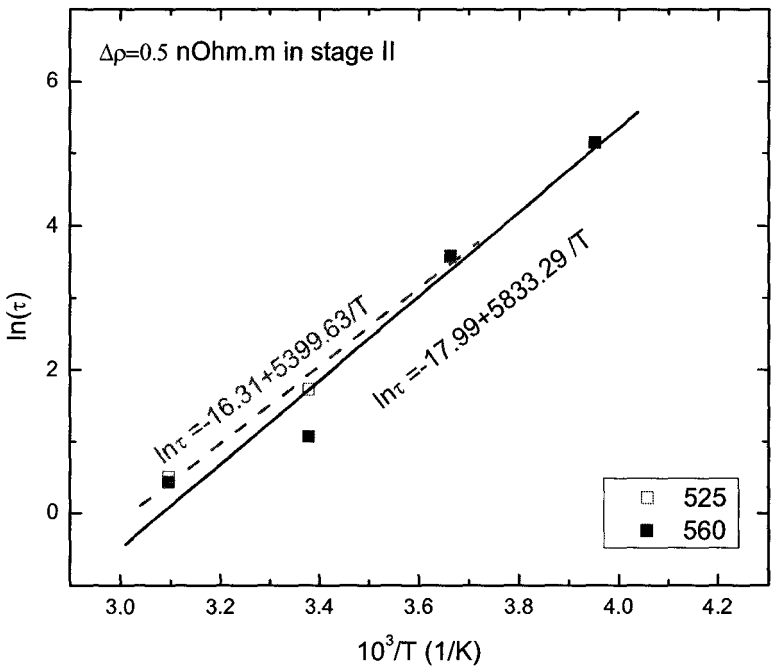

(a)

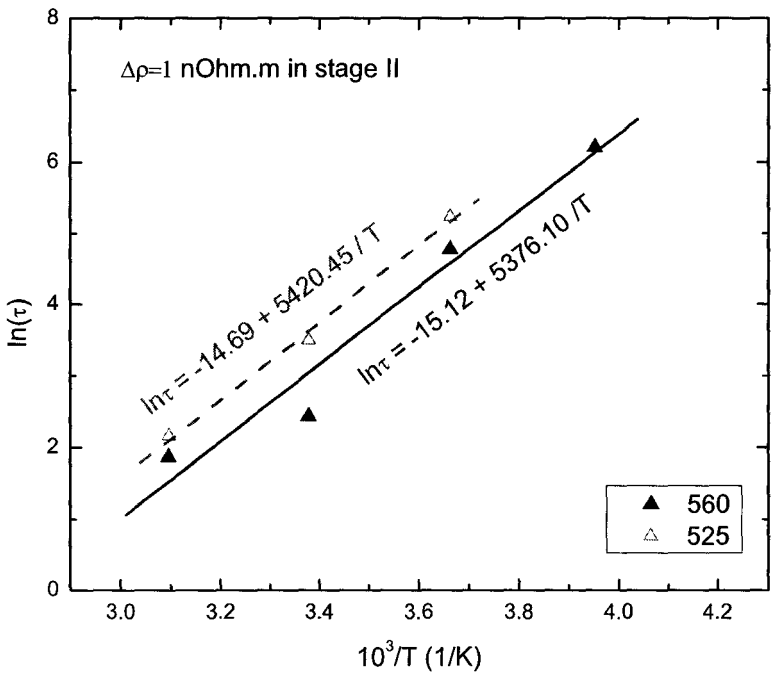

(b)

Figure 6.6: The $\ln\tau$ versus 1/T plots for resistivity change of (a) 0.5 nOhm.m and (b) 1 nOhm.m during stage II. The slopes of the lines are equal to $-Q/R$ where Q is the clustering activation energy in stage II.

Table 6.5: Mg, Si and vacancies migration energies in the aluminum matrix.

Parameter	Value (kJ/mol)
ΔH^m_{Mg}	57.9 ± 16.4
ΔH^m_{Si}	64.0 ± 12.6
ΔH^m_v	58.4 ± 2.5

atoms, Si atoms and aluminum vacancies in the aluminum matrix. These energies can be approximately found by using the following formula (Adopted from Fujikawa et al. 1978):

$$\Delta H^m = \Delta H^D - \Delta H^f_v \tag{6.19}$$

where ΔH^m is the migration energy of a given substance, ΔH^D is the diffusion energy of it and ΔH^f_v is the aluminum vacancy formation energy. The challenge is finding the exact value of these parameters. Various researchers reported different values for each of these which can produce a great uncertainty into the analysis. Table A.1 (Appendix A) lists some of the values found for ΔH^D of Mg and Si in aluminum matrix while table A.2 (Appendix A) provides various reported ΔH^f_v. Finally table A.3 (Appendix A) shows the vacancy migration energies in aluminum matrix (ΔH^m_v).

By assuming the average values for each of ΔH^m_v, ΔH^D and ΔH^f_v, the migration energy for Mg and Si can be calculated as 57.9 ± 16.4 kJ/mol and 64.0 ± 12.6 kJ/mol respectively. Table 6.5 lists the calculated values of ΔH^m_v, ΔH^m_{Mg} and ΔH^m_{Si}.

Note that the values chosen for latter two parameters are very uncertain since the reported energies in literature differs from each other by more than 20 kJ/mol (for example look at diffusion energy for Mg in table A.1).

It was shown earlier that the activation energy of clustering approximately equals to 46 (45.8 ± 1.8) kJ/mol (table 6.4). Within the range of error, this value is close to the migration energy of Mg and vacancies in the aluminum matrix. This

means that during stage II of clustering, Migration of vacancies and Magnesium atoms inside the matrix controls the process of clustering although the accuracy of the measurements and calculation is not enough to clearly identify which of these parameters is the main rate-controlling factor.

It is also worth mentioning that the migration energy of Si is not very different from that of Mg and vacancies when considering the huge (yet inevitable) inaccuracies present in energies calculations. So Si atoms might also play an important role in stage II of clustering. This was also suggested by Gaber et al. (2004) where by using DSC technique, they found the activation energy of clustering to be 53.3 kJ/mol.

Finally note that the binding energies of vacancies and solute atoms were not considered in these calculations. However as it was mentioned earlier in section 6.2.3, the effective diffusion coefficient of vacancies depends on E_b and cluster size. Including these parameters in the calculations is very difficult since the details about cluster evolution with time (such as number of solutes in it) is not known yet. Equation 6.3 was the simplest approximation in measuring their contribution in D_{eff}. For Mg and Si vacancy binding in aluminum alloy, E_b approximately equals to 11kJ/mol (Boileau et al. 1981 and Kim et al. 1974) which is comparable with the huge uncertainties (around 20kJ/mol) present in the activation energy. Thus it seems that the energy analysis done in this project is acceptable within the range of error. However computer simulations along with the atom probe experiments might also be used to provide more information about the clustering process and particularly changes in the effective diffusion coefficients during the cluster formation and growth.

6.4 Clustering: The General Overview

Now the process of clustering can be described in more details by combining the findings of all experiments:

During solution treatment of specimens at high temperature, large number of vacancies form. By quenching the material to lower temperatures (water at ambient temperature), the vacancies become trapped inside the matrix and therefore their concentration becomes higher than the equilibrium one. In order for equilibrium to be reached, these quench-in vacancies move towards vacancy sinks such as dislocations and grain boundaries. The near-sink vacancies are annihilated very quickly while the further away vacancies bind with other solute atoms (Mg and Si) on their way to the sinks. Annihilation of vacancies decreases the resistivity of the material while cluster formation increases it. At the very beginning of ageing, the annihilation of near sink vacancies happens and this results in a very strong negative factor on the resistivity which will be compensated by the resistivity increase due to the formation of small clusters. If the alloy is not very rich in alloying elements, the overall resistivity might decrease to values which are even smaller than the as-quenched one (see figures 2.16.a and 2.16.b for example). However in the alloy used in this project, no sign of the decrease in resistivity at the beginning of ageing was observed which could be due to the higher solute content of alloy (and therefore more extensive clustering) compared to that used by Kovacs et al. (1972). This is a plausible argument since Kovacs et al. (1972) and Chatterjee and Entwistle (1973) suggested that the drop in resistivity at the beginning of clustering might be due to the clustering of Si atoms and since the alloy used in this project has much higher contents of silicon than those used by Kovacs et al. and Chatterjee and Entwistle, the decreased in resistivity was not observed in the present research. Note that as it can be seen in hardness plots (figures 5.1 to 5.4) the hardness is increasing rapidly during the first stage which means that

clustering is happening very quickly. Thus the slow rate of resistivity increase in stage I (see figures 5.6 to 5.9) is not due to the slow kinetics of clustering but is because of the compensating effects of vacancies annihilation and cluster formation.

After a very short time, the $\rho - \ln(t)$ plots show an increase in resistivity with a faster slope (designated as stage II). This is due to the fact that all near-sink vacancies have been annihilated during stage I (very short ageing time). In this stage vacancies bind with more solute atoms while they are still moving towards the sinks. The more solutes they attach with, the slower they become. They can also become trapped inside clusters due to the very strong interaction between them (Federighi and Thomas 1962 and Panseri and Federighi 1966). This mechanism is confirmed by positron annihilation results which shows an increase (although small) in mean lifetime of positron at stage II of ageing at room temperature (see figure 5.10). This was attributed to the growth of clusters during stage II.

The activation energy of clustering during stage II was found to be equal to 45.8 ± 1.8 kJ/mol which, within the range of error, is close to the Mg and vacancies migration energies (and also Si atoms). This confirms that in stage II of clustering, vacancies, Mg atoms (and maybe Si) atoms are all moving towards sinks. The fact that the solution treatment temperature (i.e. higher number of vacancies) does not affect the clustering activation energy suggests that during the seconds stage, the clustering mechanism is constant.

After a period of time, the transition from stage II into III happens. The interpretation of this transition, unlike the case of the stage I to II, is not easy and requires special attention. Two possible hypothesis were developed in section 6.2.3 to explain this. The first one assumes that during stage II, as vacancies bind with more solute atoms, they become slower. Finally a time will be reached when all vacancies virtually stop moving towards the sinks (actually they become very slow

and not immobile). This is when the transition from faster stage II into slower stage III happens. The second hypothesis was based on the diffusion field around a cluster. In this theory, the transition happens when the diffusion field of one cluster overlaps with that of other one which will result in lower concentration of solutes in the matrix between them. This decreases the cluster growth rate even more due to the smaller supersaturation of the matrix (according to equation 6.8).

Now the validity of these hypothesis can be checked by considering the hardness results:

At the transition times of stage II to III, the hardness of all samples with the same solution treatment is the same. However, at the same point, the resistivity is is larger the lower the ageing temperature. It was mentioned in section 6.2.3 that hypothesis (1) predicts smaller cluster size at the transition point for -20 samples since the migration speed of clusters is minimum at this temperature (compared to other ageing temperatures) and therefore fewer number of solutes is required to slow them down. Also this hypothesis was based on the assumption that lower ageing temperature results in higher number of clusters (Panseri and Federighi 1966). So the microstructure of the alloy at the transition point of stage II to III consists of a larger number of clusters in smaller sizes for the case of lower ageing temperatures. This results in smaller depletion of matrix from solutes. Consequently, hypothesis (1) predicts higher resistivity for samples aged at lower ageing temperature compared to that of samples aged at higher temperatures. Now the higher number of clusters with smaller size could result in almost the same hardness as lower number of larger clusters (which are formed during ageing at higher temperatures) therefore the constant hardness at transition point can be explained.

Hypothesis (2) suggested that the transition from stage II to III happens when the diffusion fields of clusters overlap with each other. This predicts that the same

size of clusters must be reached so that the transition can take place. If the number of clusters formed is assumed to be constant, then the final state of the material after stage II should be exactly the same for all ageing temperatures, i.e. same number of cluster with the same size. This will result in the identical resistivity and hardness of specimens regardless of their annealing temperature. Although this is true for the case of hardness, it is not what it was observed in the resistivity results. Now another possibility should be examined. At the very beginning of ageing the number of vacancies is the same for all samples, however during stage I, since the migration speed of vacancies is much higher at higher temperatures, more vacancies can annihilate. This will leave less number of vacancies (in the area far from sinks) for extensive clustering to happen during ageing at the later stages. Consequently, at the stage III transition point, less number of clusters with the critical size have been formed in the 50°C samples and also the matrix has less number of vacancies. This results in smaller resistivity of samples aged at higher temperature. Note that some smaller clusters might also be formed during stage I and before the annihilation of vacancies. Now, one possible explanation of the same hardness at transition point can be done by considering the existence of larger number of these small clusters (formed at stage I) in addition to the smaller number of clusters with critical size (grew at stage II) in the 50°C samples compared with the -20°C ones.

It was mentioned in section 6.2.3 that hypothesis (1) can also explain the same transition times for samples with the same ageing temperature and different solution treatment temperatures. Again it was shown that hypothesis (2) can not predict such behavior and according to that, all transitions should happen much faster in the 560 samples since the distance between the clusters is smaller in that case. From all of above, it seems that hypothesis (1) can explain the whole experiments better than the second one. This does not necessarily means that hypothesis (2) is wrong however

the incorrect predictions might be simply due to the fact that there are not enough evidences to build a strong basis for this theory. Computer simulation might be able to provide more information about validity of this theory.

It is very important to mention that hypothesis (2) was developed to explain the "sharp" transition from stage II to III in the resistivity results. Hypothesis (1) cannot justify this clear transition since the slowing effect of solutes on vacancies mobility was already taken into account by the concepts of effective diffusion (see equation 6.3) which results in the linear resistivity plots in the logarithmic scale. Thus there should be another reason (soft impingement of clusters) for this sharp transition.

The other case to investigate is the same hardness of all samples (regardless of the ageing and the solution treatment temperatures) at the very long ageing times, regardless of solution treatment temperature. This can be explained by the concepts of matrix depletion from solutes. The speed of clustering (i.e. cluster growth) depends on the degree of matrix supersaturation. By progress in the clustering process finally a point will arrive that the driving force for clustering becomes very small since the matrix supersaturation is not very large anymore. In other words there might be a solubility limit for clustering where after that no more clustering happens. In the case of the 560°C samples with larger number of initial clusters, this limit is reached faster and cluster grows smaller while this time is longer for the 525°C samples, meaning that clusters can grow larger. This will result in almost the same hardness of samples at the very long ageing times.

Chapter 7

Conclusions

Based on the discussion made in chapter 6, the following conclusions can be made from this research:

- Excess quenched-in vacancies play the most important role in controlling the process of cluster formation. After quenching, these vacancies want to reach the equilibrium concentration (at the ageing temperature) by migrating towards sinks. At the same time due to an extremely high binding energy between them and solute atoms they are attached to Mg and Si atoms and therefore clusters form.

- There are three stages present in the resistivity plots of clustering:

  - In stage I, near-sink vacancies annihilate quickly at the sinks, at the same time other vacancies start binding with other solute atoms and therefore form clusters.

  - In stage II, vacancies bind with more solutes and this slows them down on their ways towards sinks. Vacancies might also become trapped inside other clusters due to the high interaction between vacancies and clusters.

  - In stage III, vacancies start to become virtually immobile either due to the extensive binding with solute atoms which can eventually slow them down and transits the process towards the "slow" stage or because of the

soft impingements of clusters. The first mechanism seem more acceptable since it can explain most of the observations.

- All samples reach to the same hardness value after long ageing times, regardless of ageing and solution treatment temperature. This suggests an existence of a solubility limit for clustering which after that cluster formation becomes very slow.

- The activation energy of the clustering process in the stage II of ageing is calculated to be 45.8 $\pm$ 1.8 kJ/mol. Within the range of error this is very close to the migration energies of Mg atoms and vacancies which are 57.9 $\pm$ 16.4 and 58.4 $\pm$ 2.5 kJ/mol respectively. Also it is close to the migration energy of Si which is 64.0 $\pm$ 12.6 kJ/mol. It was suggested that this could mean that the migration of Mg atoms and vacancies inside matrix controls the process of clustering. Si atoms might also play an important role in the process.

- Finally, it was proved by positron annihilation results that all of the clusters contain vacancies inside them since the mean lifetime of positrons is between 163psec of pure Al bulk lifetime and 244psec of aluminum vacancies lifetime, otherwise, at long ageing times the lifetime should have reached to the bulk lifetime of aluminum rather than a constant value of about 222psec.

Chapter 8

Suggested Future Work

There are still few aspects of cluster formation that need to be clarified:

- Positron annihilation studies for samples aged at very short time and especially on samples aged at lower temperatures (-20°C for example) which showed a long stage I in their resistivity plots. This might shed some light on what is exactly happening during stage I of ageing and during the transition point of stage I to stage II.

- More detailed positron lifetime analysis on the data in order to de-convolute the lifetime into three components. This might require more experiments with higher number of counts to provide more accurate data.

- Computer simulations of the clustering process using binding energies and diffusion constants. This can be used to validate any of the two hypothesis mentioned in this thesis. Also it can be used to find the effect of binding energies, cluster numbers and their size on the effective diffusion coefficient of vacancies.

- DSC experiments on samples which are isothermally aged for short, intermediate and long times (especially at low temperatures such as -20 and 0 °C). This can provide better understanding of clustering kinetics such as evolution of the clusters volume fraction.

Appendix A

Activation Energies

The activation energies reported in the literature for diffusion of Mg and Si (table A.1), formation of mono-vacancies (table A.2) and their migration (table A.3) in the aluminum matrix are listed in this appendix. The individual references can be found in the general review papers which are listed for each of the parameters.

Table A.1: Diffusion activation energy (ΔH^D) of Mg and Si in Aluminum matrix.

Parameter	Energy (kJ/mol)	Reference
ΔH^D_{Mg}	113	Yong et al. 2003
	112.1	
	161.1	
	119.7	
	110.9	
	129.7	
	130.4	
	114.7	
	120.5	
average	123.6 ± 15.8	
ΔH^D_{Si}	150.6	Yong et al. 2003
	113.4	
	127.8	
	131.8	
	123.9	
	136.8	
	136	
	117.6	
average	129.7 ± 11.8	

Table A.2: Aluminum mono-vacancy formation energy (ΔH_v^f)

Parameter	Energy (kJ/mol)	Reference
ΔH_v^f	74.19104	Cahn and Haasen 1983
	73.228	
	68.410	
	70.337	
	63.592	
	68.410	
	59.738	
	59.738	
	64.556	
	63.592	
	63.592	
	66.483	
	67.446	
	57.811	
	63.592	
	63.592	
	63.592	
	70.337	
Average	65.7 $\pm$ 4.5	

Table A.3: Aluminum mono-vacancy migration energy (ΔH_m^v)

Parameter	Energy (KJoul/mole)	Reference
ΔH_m^v	62.6288	Cahn and Haasen 1983
	56.848	
	59.738	
	59.738	
	54.921	
	59.738	
	55.884	
	55.884	
	58.775	
	59.738	
	56.848	
	55.884	
	57.811	
	62.629	
Average	58.4 $\pm$ 2.5	

References

Andersen S. J., Zandbergen H. W., Jansen J., Traeholt C., Tundal U. and Reiso O. (1998): Acta Materialia, Vol. 46, pp. 3283–3298.

Bharathi A. and Sundar C. S. (1992): Materials Science Forum, Vol. 105-110, pp. 905–908.

Birol Y. (2005a): Materials Science & Engineering A, Vol. 391, pp. 175–180.

Birol Y. (2005b): Scripta Materialia, Vol. 52, pp. 169–173.

Birol Y. and Karlik M. (2005): Materials Science and Technology, Vol. 21, pp. 153–158.

Boileau F., Geffroy B. and Paulin R. (1981): Applied Physics A, Vol. A26, pp. 107–113.

Bryant J. D. (1999): Metallurgical and Materials Transactions A, Vol. 30, pp. 1999–2006.

Buck O., Tien J. K. and Marcus H. L., eds. (1979): *Electron and positron spectroscopies in materials science and engineering.* New York: Academic Press.

Cahn R. W. and Haasen P., eds. (1983): *Physical metallurgy.* Amsterdam, New York, NY: North-Holland Physics Pub.

Ceresara S., Russo E. D., Fiorini P. and Giarada A. (1970): Material Science and Engineering, Vol. 5, pp. 220–227.

Chakrabarti D. J., Cheong B. k. and Laughlin D. E. (1998): In *Proceedings of the 1998 TMS Annual Meeting*, San Antonio, TX, USA, pp. 27–44. The Minerals, Metals & Materials Soc (TMS), Warrendale, PA, USA.

Chakrabarti D. J. and Laughlin D. E. (2004): Progress in Materials Science, Vol. 49, pp. 389–410.

Chatterjee D. K. and Entwistle K. M. (1973): Journal of the Institute of Metals, Vol. 101, pp. 53–59.

Collins D. L. W. (1958): Journal of the Institute of Metals, Vol. 86, pp. 325–336.

Doan L. C., Ohmori Y. and Nakai K. (2000): Materials Transactions, JIM, Vol. 41, pp. 300–305.

Dupasquier A., Kogel G. and Somoza A. (2004): Acta Materialia, Vol. 52, pp. 4707–4726.

Dutta I. and Allen S. M. (1991): Journal of Materials Science Letters, Vol. 10, pp. 323–326.

Edwards G. A., Stiller K., Dunlop G. L. and Couper M. J. (1996): Materials Science Forum, Vol. 217-222, pp. 713–718.

Edwards G. A., Stiller K., Dunlop G. L. and Couper M. J. (1998): Acta Materialia, Vol. 46, pp. 3893–3904.

El Sayed H. and Kovacs I. (1974): Physica Status Solidi A, Vol. 24, pp. 123–130.

Esmaeili S. and Lloyd D. J. (2004): Scripta Materialia, Vol. 50, pp. 155–158.

Esmaeili S. and Lloyd D. J. (2006): Materials Science Forum, Vol. 519-521, pp. 169–176.

Esmaeili S., Lloyd D. J. and Poole W. J. (2003a): Acta Materialia, Vol. 51, pp. 3467–3481.

Esmaeili S., Lloyd D. J. and Poole W. J. (2003b): Acta Materialia, Vol. 51, pp. 2243–2257.

Esmaeili S., Lloyd D. J. and Poole W. J. (2005): Materials Letters, Vol. 59, pp. 575–577.

Esmaeili S., Poole W. J. and Lloyd D. J. (2000): Materials Science Forum, Vol. 331, pp. 995–1000.

Esmaeili S., Wang X., Lloyd D. J. and Poole W. J. (2003): Metallurgical and Materials Transactions A, Vol. 34A, pp. 751–763.

Federighi T. (1959): Philosophical Magazine, Vol. 4, pp. 502–510.

Federighi T. and Thomas G. (1962): Philosophical Magazine, Vol. 7, pp. 127–131.

Fickett F. R. (1971): Cryogenics, Vol. 11, pp. 349–367.

Fujikawa S. I., Hirano K. I. and Fukushima Y. (1978): Metallurgical Transactions A, Vol. 9A, pp. 1811–1815.

Gaber A., Matsuda K., Yong Z., Kawabata T., Ali A. and Ikeno S. (2004): Materials Forum, Vol. 28, pp. 402–405.

Gaffar M. A., Gaber A., Mostafa M. S. and Zeid E. F. A. (2007): Journal of Alloys and Compounds, Vol. 429, pp. 167–175.

Gupta A. K. and Lloyd D. J. (1992): In L. Arnberg, O. Lohne, E. Nes, and N. Ryum (Eds.), *Aluminium Alloys: Their Physical and Mechanical Properties*, Vol. 2, Trondheim, Norway, pp. 21–25. Norwegian Institute of Technology and SINTEF Metallurgy.

Hirsch P. B., Silcox J., Smallman R. E. and Westmacott K. H. (1958): Philosophical Magazine, Vol. 3, pp. 897–908.

Honma T., Matsumoto K., Nagai Y., Hasegawa M. and Hono K. (2004): Materials Forum, Vol. 28, pp. 494–500.

Hornbogen E., Mukhopadhyay A. and Starke E.A. J. (1992): Zeitschrift fur Metallkunde, Vol. 83, pp. 577 – 584.

Juhasz A., Kovacs I., Lendvai J. and Tasnadi P. (1985): Journal of Materials Science, Vol. 20, pp. 624–629.

Kim S. M., Buyers W. J. L., Martel P. and Hood G. M. (1974): Journal of Physics F, Vol. 4, pp. 343–350.

Kirkegaard P., Pedersen N. J. and Eldrup M. (1989): In *Positron Annihilation*, Gent, Belgium, pp. 642–644. World Scientific, Singapore.

Kovacs I., Lendvai J. and Nagy E. (1972): Acta Metallurgica, Vol. 20, pp. 975–983.

Krause-Rehberg R. and Leipner H. S. (1999): *Positron annihilation in semiconductors: defect studies.* Berlin, Germany: Springer.

Kuhlmann-Wilsdorf D. and Wilsdorf H. G. F. (1960): Journal of Applied Physics, Vol. 31, pp. 516–525.

Lloyd D. J. and Gupta A. K. (1997): In *Proceedings of International Conference on Thermomechanical Processing of Steels and Other Materials (THERMEC 97)*, Wollongong, Australia, pp. 99–107. The Minerals, Metals & Materials Society, Warrendale, PA, USA.

Lynch J. P., Brown L. M. and Jacobs M. H. (1982): Acta Metallurgica, Vol. 30, pp. 1389–1395.

Manninen M., Nieminen R., Hautojarvi P. and Arponen J. (1975): Physical Review B, Vol. 12, pp. 4012–4022.

Maruyama N., Uemori R., Hashimoto N., Saga M. and Kikuchi M. (1997): Scripta Materialia, Vol. 36, pp. 89–93.

Matsuda K., Tada S. and Ikeno S. (1994): Journal of the Japan Institute of Metals, Vol. 58, pp. 252–259.

Matsuda K., Uetani Y., Sato T. and Ikeno S. (2001): Metallurgical and Materials Transactions A, Vol. 32, pp. 1293–1299.

Meyendorf N., Dlubek G. and Surkov A. (2004): In *Testing, Reliability, and Application of Micro- and Nano-Material Systems II*, Vol. 5392 of *Proceedings of the SPIE - The International Society for Optical Engineering*, San Diego, CA, USA, pp. 54–62. SPIE-Int. Soc. Opt. Eng.

Miao W. F. and Laughlin D. E. (1999): Scripta Materialia, Vol. 40, pp. 873–878.

Miao W. F. and Laughlin D. E. (2000a): Journal of Materials Science Letters, Vol. 19, pp. 201–203.

Miao W. F. and Laughlin D. E. (2000b): Metallurgical and Materials Transactions A, Vol. 31A, pp. 361–371.

Murayama M. and Hono K. (1999): Acta Materialia, Vol. 47, pp. 1537–1548.

Murayama M., Hono K., Miao W. F. and Laughlin D. E. (2001): Metallurgical and Materials Transactions A, Vol. 32A, pp. 239–246.

Murayama M., Hono K., Saga M. and Kikuchi M. (1998): Materials Science and Engineering A, Vol. 250, pp. 127–132.

Murty K. N. and Vasu K. I. (1971): Journal of Materials Science, Vol. 6, pp. 39–47.

Nakagawa K., Kanadani T., Anthony L. and Hashimoto H. (2005): Materials Transactions, Vol. 46, pp. 779–783.

Nie J. F., Muddle B. C. and Polmear I. J. (1996): Materials Science Forum, Vol. 217-222, pp. 1257–1262.

Ozawa E. and Kimura H. (1970): Acta Metallurgica, Vol. 18, pp. 995–1004.

Ozawa E. and Kimura H. (1971): Material Science and Engineering, Vol. 8, pp. 327–335.

Panseri C. and Federighi T. (1966): Journal of the Institute of Metals, Vol. 94, pp. 99–107.

Panseri C., Federighi T. and Ceresara S. (1963): Transaction of the Metallurgical Society of AIME, Vol. 227, pp. 1122–1126.

Pashley D. W., Rhodes J. W. and Sendorek A. (1966): Journal of the Institute of Metals, Vol. 94, pp. 41–49.

Polmear I. J. (2004): Materials Forum, Vol. 28, pp. 1–14.

Porter D. A. and Easterling K. E. (2001): *Phase transformations in metals and alloys*. 2nd ed. Cheltenham, UK: Nelson Thornes Ltd.

Raeisinia B. and Poole W. J. (2006): Materials Science Forum, Vol. 519-521, pp. 1391–1396.

Raeisinia B., Poole W. J. and Lloyd D. J. (2006): Materials Science & Engineering A, Vol. 420, pp. 245–249.

Reich L., Suvegh K., Lendvai J. and Vertes A. (2001): Philosophical Magazine Letters, Vol. 81, pp. 145–151.

Rossiter P. L. (1991): *The Electrical Resistivity of Metals and Alloys.* Cambridge, UK: Cambridge University Press.

Sato T., Hirosawa S., Hirose K. and Maeguchi T. (2003): Metallurgical and Materials Transactions A:, Vol. 34, pp. 2745–2755.

Seeger A. (1973): Journal of Physics F, Vol. 3, pp. 248–294.

Sha W. (2005): Physica Status Solidi A, Vol. 202, pp. 1903–1908.

Sha W. (2006): Physica Status Solidi A, Vol. 203, pp. 1927–1933.

Sha W. (2007): Materials & Design, Vol. 28, pp. 528–533.

Silcox J. and Whelan M. J. (1960): Philosophical Magazine, Vol. 5, pp. 1–23.

Starink M. J., Gao N., Davin L., Yan J. and Cerezo A. (2005): Philosophical Magazine, Vol. 85, pp. 1395–1417.

Starink M. J., Gao N. and Yan J. L. (2004): Materials Science and Engineering A, Vol. 387-389, pp. 222–226.

Starink M. J. and Zahra A. M. (1997): Thermochimica Acta, Vol. 292, pp. 159–168.

Sterne P. A. and Kaiser J. H. (1991): Physical Review B, Vol. 43, pp. 13892–13898.

Van Rooyen M. and Mittemeijer E. J. (1989): Metallurgical Transactions A, Vol. 20A, pp. 1207–1214.

Yamada K., Sato T. and Kamio A. (2000): Materials Science Forum, Vol. 331-337, pp. 669–674.

Yong D., Chang Y. A., Baiyun H., Weiping G., Zhanpeng J., Honghui X., Zhaohui Y., Yong L., Yuehui H. and Xie F. Y. (2003): Materials Science & Engineering A, Vol. A363, pp. 140–151.

Zhen L. and Kang S. B. (1997): Scripta Materialia, Vol. 36, pp. 1089–1094.

Zhen L. and Kang S. B. (1998): Materials Letters, Vol. 37, pp. 349–353.